Lawrence Berkeley Laboratory
UNIVERSITY OF CALIFORNIA

CHEMICAL BIODYNAMICS DIVISION

PHOTOVOLTAIC PROPERTIES OF METAL-MEROCYANINE-TiO_2 SANDWICH CELLS

Terje Asbjörn Skotheim
(Ph. D. thesis)

August 1979

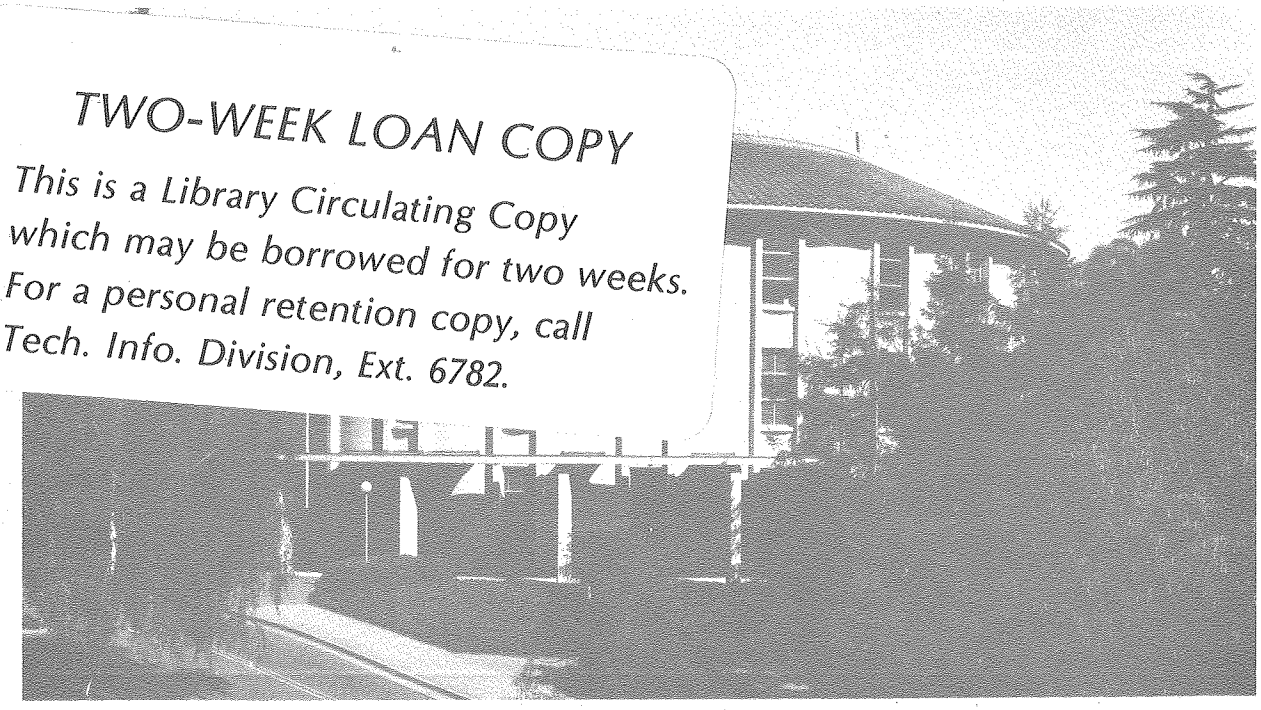

Prepared for the U.S. Department of Energy under Contract W-7405-ENG-48

DISCLAIMER

Photovoltaic Properties of Metal-Merocyanine-TiO_2 Sandwich Cells

By

Terje Asbjorn Skotheim

Abstract

Photocurrent generation in thin films of merocyanine photosensitizing dyes sandwiched between an n-type semiconductor and a metal overlayer has been studied using photovoltaic techniques. In the system analyzed in detail TiO_2 single crystal, doped n-type, was used as the semiconductor and a semitransparent Au film as a metal overlayer.

A comprehensive theoretical model was developed to explain the observed photovoltaic properties. The model assumes that the principal route for the formation of charge carriers is via singlet excitons diffusing to the merocyanine-TiO_2 interface followed by dissociation of the excitons into electron-hole pairs, the electrons being injected into the TiO_2 conduction band and the holes into the merocyanine. The model also incorporates field dependence of the quantum efficiency for charge generation and is strongly supported by a variety of steady state and kinetic measurements. An exciton diffusion length of 79 angstroms was determined by analyzing the short circuit action spectra using the theoretical model developed.

Dark current voltage measurements revealed that the current is space-charge limited at high current densities with an electron trapping density of approximately $10^{17} cm^{-3}$. This was determined by using TiO_2 as an electron injecting contact with the cell in the forward mode.

Interpretation of the kinetics of rise and decay of the photocurrent suggests that the mobility of holes, the majority carrier in

Acknowledgements

I wish to thank Dr. Melvin Klein and Dr. John Otvos for their support and advice during the completion of this work.

I also thank Professor Melvin Calvin for stimulating my interests in artificial photosynthesis and thereby changing the course of my scientific education.

To my wife Ellen I owe a special debt. Her unfailing support and confidence in me have sustained me during the more trying periods of my graduate career.

I thank Drs. Mark Spitler and Kevin McGregor for many stimulating discussions and Jerming Yang for his aid in carrying out a number of experimental measurements.

Many thanks are due the support staff of the Laboratory of Chemical Biodynamics for their cooperation in the construction of apparatus as well as aiding in the preparation of this thesis.

Table of Contents

Chapter 1

Introduction

There have been a number of reports in the literature of studies of organic photoconductive compounds in the photovoltaic mode[1-11]. It typically involves sandwiching a thin (0.1 - 1μm) layer of a p-type organic material between a high work function and a low work function metal. The high work function metal forms an ohmic or injecting electrode and the low work function metal forms a barrier contact. Fedorov and Benderskii investigated Mg-phthalocyanine films sandwiched between Al and Ag contacts.[5] They proposed a p-n junction model formed by replacing Mg with Al in the dye-metal complex during heat treatment. They also reported dramatic changes in the photoconductive and photovoltaic properties when the films were doped with oxygen. The observed efficiency increases one to three orders of magnitude for doped cells. Ghosh et al. later reported studies of similar devices.[4] Their results indicated the formation of a Schottky barrier at the low work function metal. The same mechanism has been given support by the results of Tang and Albrecht,[2] Merritt and Hovel,[6] Kampas and Gouterman,[8] and Fan and Faulkner[9] working on sandwich devices incorporating Chlorophyll-a, 8-hydroxysquarylium, porphyrin derivatives, and phthalocyanines respectively. Morel et al.[10] and Ghosh and Feng[11] in sandwiching merocyanine films between Al and Ag electrodes found higher efficiencies for cells where the cells were exposed to air to enable an oxide layer to form prior to the deposition of a dye film. Their cells therefore had many characteristics of metal-oxide-semiconductor cells.

The main advantages of using organic photoconductive compounds for solar cell materials are that these materials are readily available and potentially inexpensive and device fabrication is comparatively simple. The overwhelming barrier to successful deployment of such devices has been their poor conversion efficiencies even under the best laboratory conditions. The highest efficiencies achieved to date have been 0.7% under solar spectrum radiation for merocyanine cells.[11] In general, these low power conversion efficiencies are attributable to low quantum efficiencies for charge generation, low carrier mobilities, high bulk resistivities and trapping effects. Intentionally doping semiconductive materials to alter electronic properties is well known in inorganic solar cell technology, but this approach has rarely been pursued with organic compounds. Besides Fedorov and Benderskii's results with oxygen doping of phthalocyanines, the only other report in the literature was that of Merritt[7] where, by doping squarylium dyes with bromine and a pyrazoline compound, he achieved an increase in the conversion efficiency of approximately a factor of five.

Although the progress to date is encouraging for organic photovoltaic materials, the question that still remains to be answered is whether the low efficiencies merely represent device limitations rather than fundamental limitations inherent in organic materials as a class.

I have chosen a somewhat different approach in employing organic compounds in photovoltaic cells. It lies more in the tradition of photosensitization and the device could perhaps be called a dye-sensitized photovoltaic cell. Dye sensitization of semiconductors is well known from the photographic science literature.[12-16] In recent

years, a considerable amount of work has been done on photosensitization of wide band gap semiconductors by organic dyes adsorbed to the surface of the semiconductor.[17,18]

The basic process of photosensitization we are concerned with in the present work consists of the generation of a photocurrent on absorption of photons of energy less than the band gap energy of the semiconductor by monolayers or multilayers of dyes adsorbed onto the surface. A dye molecule adsorbed onto the surface of a semiconductor such that its highest occupied molecular orbital (homo) lies somewhere in the bandgap of the semiconductor and the lowest unoccupied molecular orbital (lumo) lies somewhere above the bottom of the conduction band of the semiconductor, has the ability to photosensitize the semiconductor. This occurs via tunneling of an electron from the photoexcited dye molecule into the conduction band of the semiconductor, where it can be drawn away by an electric field (Fig. 1). If this process takes place in an electrolyte a reducing agent can be provided to regenerate the photooxidized dye molecule.

Alternatively, if the dye molecule has a homo below the top of the valence band and a lumo somewhere in the bandgap, the excited dye molecule can be reduced by the semiconductor by tunneling of an electron from the valence band into the vacancy in the homo, which can be described as injection of a hole from the dye into the valence band of the semiconductor. In an electrolyte acceptor molecules can be provided to oxidize the photoreduced dye molecule and thereby regenerate the molecule (Fig. 1). In both of these cases one may be able to observe a photocurrent in a spectral region where the dye absorbs and the semiconductor itself is transparent. In this manner one may be able to extend the

Figure 1. Dye sensitized charge transfer at semiconductor electrodes.

a) Photo-injection of electrons from the excited dye molecule into the conduction band of the semiconductor.

b) Photo-injection of hole from the dye into the valence band of the semiconductor.

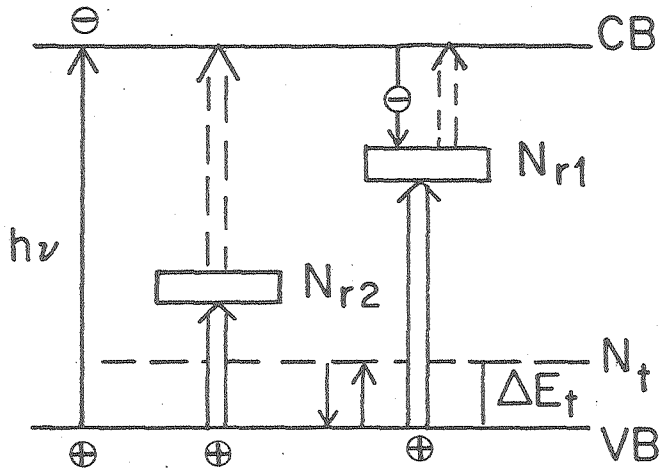

Recombination scheme

$$\begin{cases} S_{p2} > S_{n2} \text{ and } S_{p1} \cong S_{n1} \\ S_{n2} < S_{n1} \\ S_{p2} > S_{p1} \end{cases}$$

Channel N_{r1}: $p_{r1} + \ominus \longrightarrow n_{r1}$ fast

$n_{r1} + \oplus \longrightarrow p_{r1}$ slow

Channel N_{r2}: $n_{r2} + \oplus \longrightarrow p_{r2}$ fast

$p_{r2} + \ominus \longrightarrow n_{r2}$ slow

XBL797-4889

photosensitivity of the semiconductor to longer wavelengths. If one then couples a semiconductor which absorbs in the blue end of the solar spectrum with a dye absorbing in the red end of the spectrum, one achieves an absorption covering a larger part of the solar spectrum with a system based on two energy levels. The main advantage of a two-level system for electricity generation lies in minimizing the thermal losses which inevitably occur with using a one-band gap semiconductor junction. Since the dye will be transparent in the region where the semiconductor absorbs, the light could impinge directly on the semiconductor-dye junction with no losses. One would thereby be able to utilize the high efficiency of the semiconductor depletion region as in a Schottky barrier cell. The effieincy of a solar energy converter composed of two photochemical systems is substantially increased over that of a single photochemical system.[19-21]

I have chosen to investigate one such system, a merocyanine dye sandwiched between a TiO_2 single crystal doped n-type and a gold electrode. Gold was chosen both because it is a high work function metal and therefore forms a Schottky barrier with the n-type TiO_2, and because it does not form oxide layers which would complicate the basic system. The goal was to investigate whether thin films of organic dyes could become efficient enough for charge generation to be serious candidates for practical solar energy devices. It is hoped that the present work represents some progress towards that end.

Chapter 2

Experimental

2.1 Cell Fabrication

The merocyanine dye used in these experiments (Fig. 2) was purchased from Gallard-Schlesinger Company, Carle Place, New York, and was used as purchased. The TiO_2 rutile single crystals used as a substrate were purchased from Nakazumi Crystals of Osaka, Japan. The crystal came as a long boule grown along the c-axis. Slices 250μm with a cross section of about $1.5cm^2$ were cut with a string saw such that the (001) basal plane was exposed. The crystals were made semiconductive by heating in a vacuum oven for two hours at 650°C and 5×10^{-6} toor. This treatment creates oxygen vacancies which act as donors.[22] The crystals were slightly grey in color and were found to have a conductivity of 0.8 $ohm^{-1}cm^{-1}$. With an electron mobility of 1 $cm^2V^{-1}sec^{-1}$,[23] we obtain a carrier density of $5 \times 10^{18}cm^{-3}$ from the solution of $\sigma = ne\mu$,[24] where σ is the conductivity, n the carrier density, e the electronic charge, and μ the electron mobility.

The sandwich cell used in these experiments is diagrammed in Fig. 3. The TiO_2 crystals were polished with 1 micron alumina and etched 15 minutes in 50% sulfuric acid before the dye was deposited. This left a glassy smooth surface. The merocyanine and Au layers were sequentially deposited onto the TiO_2 substrate by resistance heated thermal evaporation at a pressure of about 10^{-5} toor in a vacuum evaporator bell jar diagrammed in Fig. 4. The vacuum evaporator was model VE10 made by Midros, Inc. of Portland, Oregon. The merocyanine dye was sublimed from a molybdenum basket heated by a tungsten wire

Figure 2. Chemical structure of the merocyanine dye used in making the photovoltaic cells.

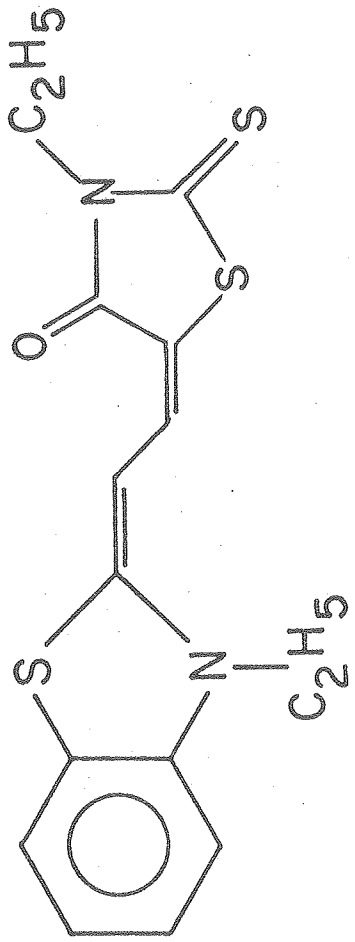

XBL796-4875

Figure 3. Diagram of sandwich cell structure.

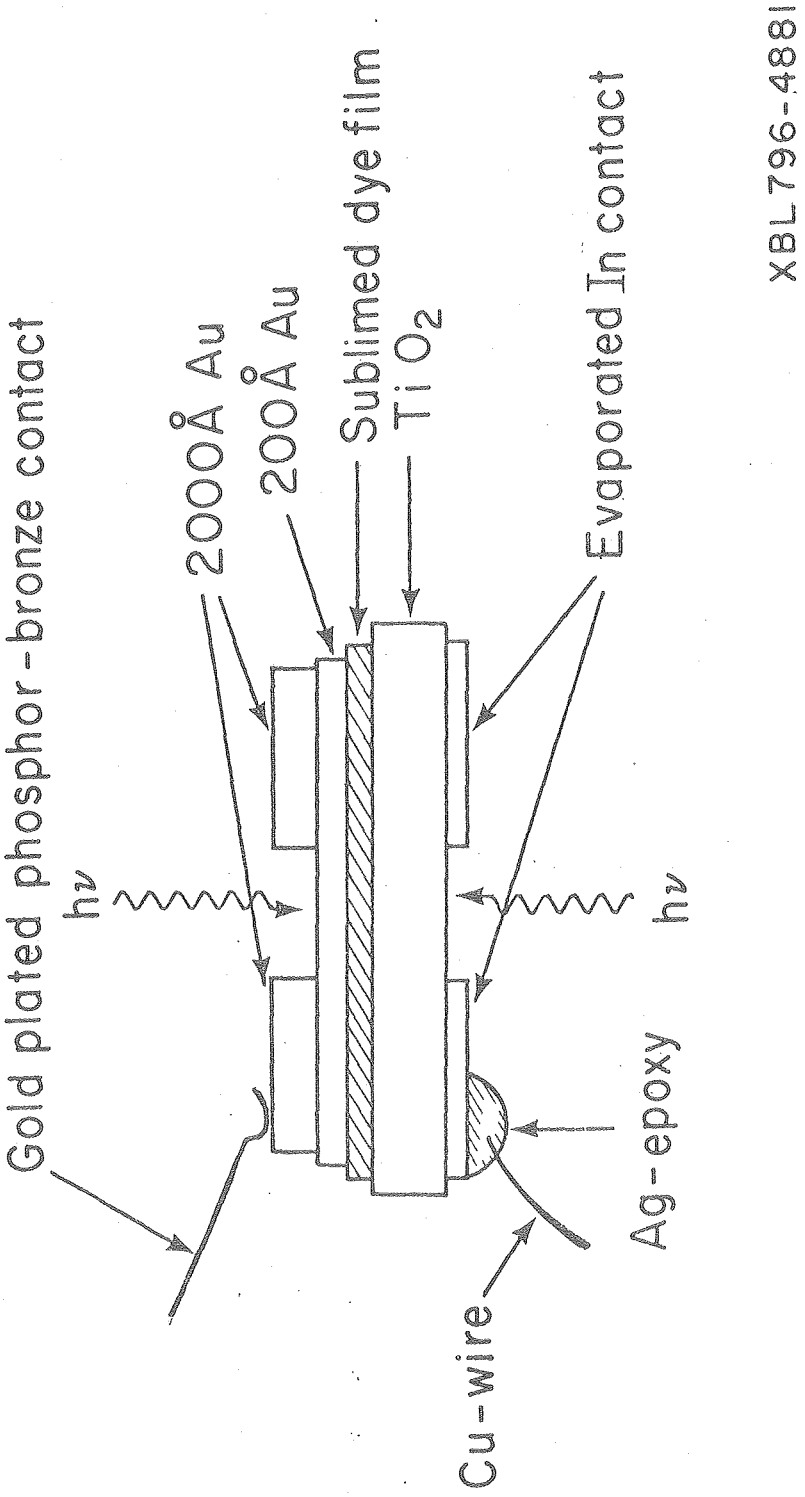
Gold plated phosphor-bronze contact
hν
2000Å Au
200Å Au
Sublimed dye film
Ti O2
Evaporated In contact
hν
Ag-epoxy
Cu-wire

XBL796-4881

Figure 4. Vacuum sublimation apparatus used to prepare sandwich cells.

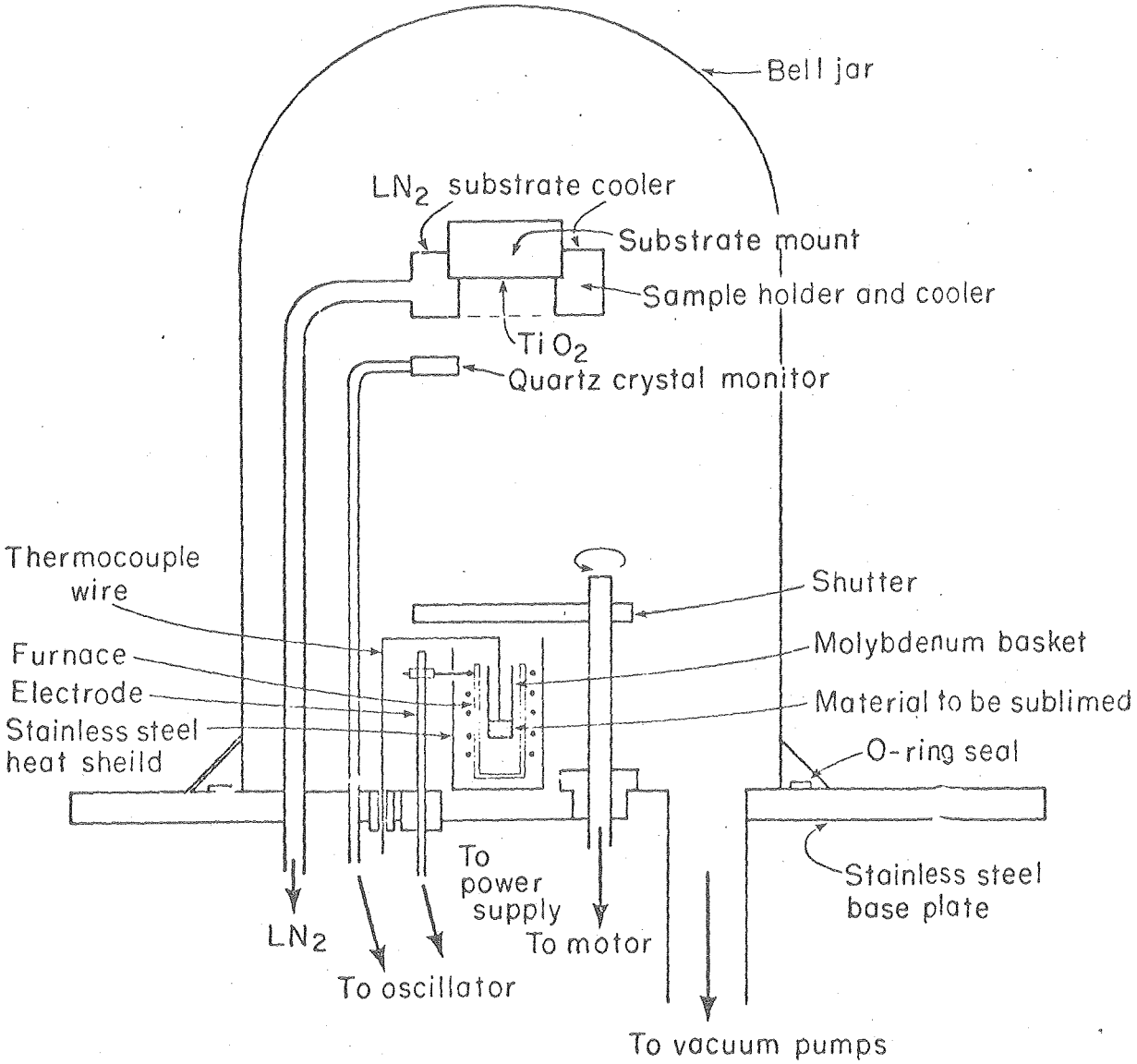
Bell jar
LN_2 substrate cooler
Substrate mount
Sample holder and cooler
TiO_2
Quartz crystal monitor
Thermocouple wire
Furnace
Electrode
Stainless steel heat sheild
Shutter
Molybdenum basket
Material to be sublimed
O-ring seal
Stainless steel base plate
To power supply
LN_2
To oscillator
To motor
To vacuum pumps

XBL796-4879

crucible heater. The sublimation rate was about 2 angstroms per second and was monitored with a Kronos model QM 311 quartz crystal oscillator which was calibrated with a Varian model 980-4020 A-scope multiple interferometer. The temperature of the merocyanine powder was maintained at about 200°C and was monitored with a chromel-alumel thermocouple. The temperature of the substrate could be maintained at room temperature or liquid nitrogen temperature by pumping liquid nitrogen into the substrate holder. A 200 angstrom gold film with approximately 50% transparency in the dye absorption region was evaporated on top of the merocyanine from a molybdenum boat (not shown in Fig. 3). The gold had a purity of 99.9%. A contact ring of 2000 angstrom thickness was subsequently deposited with a circular mask of 3mm diameter leaving a 7.1mm^2 circular area as the effective cell area. The gold could be deposited on top of the merocyanine without breaking the vacuum, although in most cases the dye film was exposed to air for about five minutes before the Au was deposited. No substantial difference in performance between the two types of cells were noticed. A quartz dummy cell was positioned next to the TiO_2 substrate in order to record the absorption spectrum of the dye film for each cell.

2.2 Measurement Apparatus

The transmission and absorption spectra were measured with a Cary 118 spectrophotometer. The extinction coefficient for the dye films were determined by measuring the absorption of various thicknesses of the dye films on quartz and assuming the same reflectivity for films of not too different thickness. The photovoltaic measurements were carried out with the cell mounted on a plexiglass holder

Figure 5. Block diagram of photovoltaic measurement apparatus.

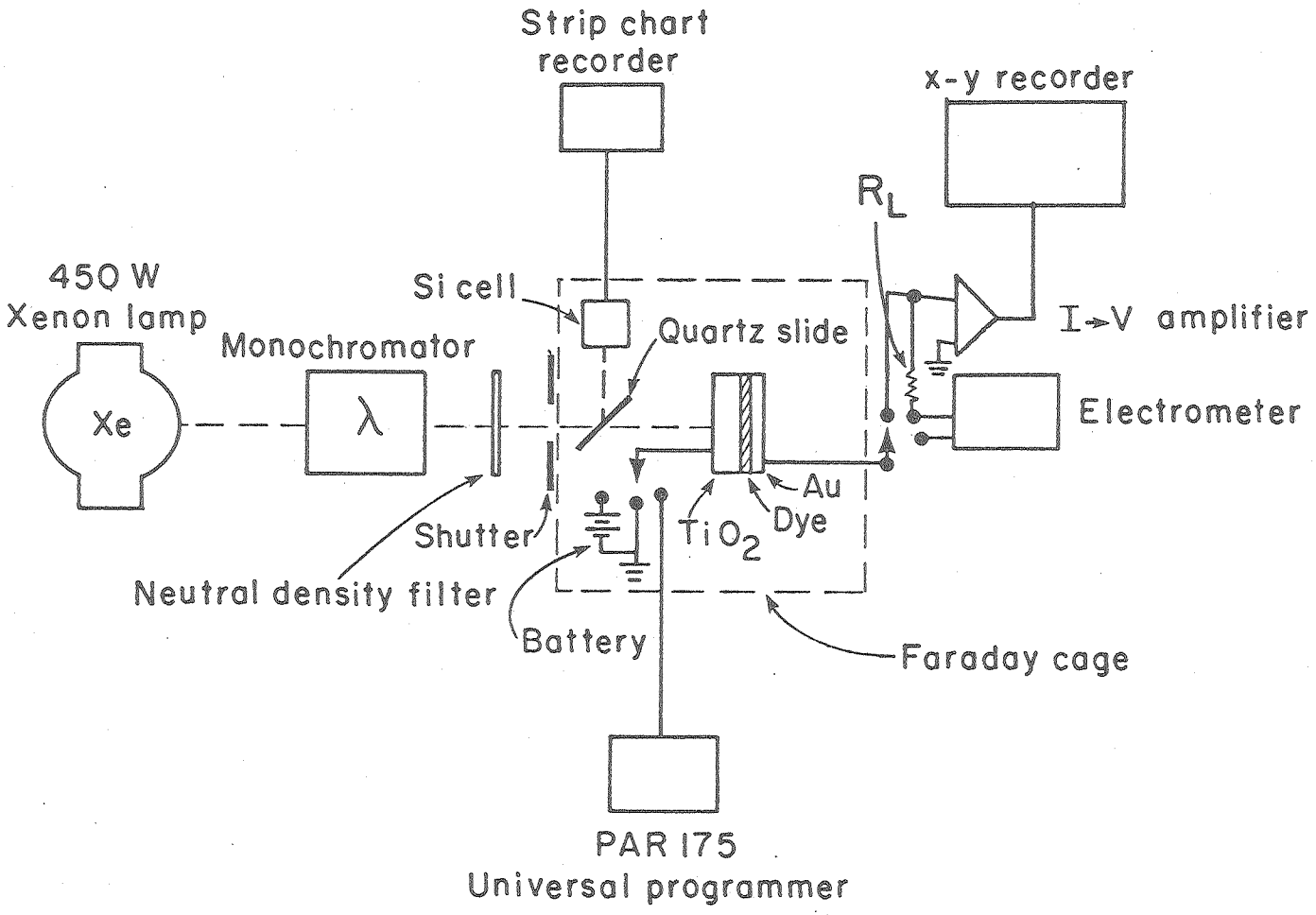
Strip chart
recorder
x-y recorder
R_L
450 W
Xenon lamp
Si cell
Quartz slide
I→V amplifier
Monochromator
Xe
λ
Electrometer
Au
Dye
TiO_2
Shutter
Neutral density filter
Battery
Faraday cage
PAR 175
Universal programmer

XBL796-4878

in a Faraday cage as illustrated in Fig. 5. The cell could be rotated through 180 degrees such that the light could be incident on the semi-transparent metal or the TiO_2 substrate. The light source was a 450 watt Xenon high pressure arc lamp. A Bausch and Lomb high intensity monochromator was used in conjunction with the Xenon lamp for recording action spectra. The band pass was 12nm. Neutral density filters were used in tandem with the monochromator to measure dependence on light intensity. Without neutral density filters the incident monochromatic light intensity was about 10^{14} photons $cm^{-2}sec^{-1}$. The light intensity was measured with a Hewlett Packard 8334A radiant flux detector in conjunction with a Hewlett Packard 8330A radiant flux meter. The intensity of the lamp was monitored with a silicon photodetector whose output was continuously recorded on a strip chart recorder. The dark current and photocurrent were measured with a Princeton Applied Research model 181 current sensitive preamplifier. Various load resistors could be interposed between the cell and the preamplifier in order to measure the photocurrent and photovoltage under load and thereby the fill factor of the cell. The photovoltage was measured with a Keithly model 220 vacuum tube electrometer. To measure the dark current-voltage characteristics, a Princeton Applied Research model 175 Universal Programmer was employed for the voltage scan. The PAR 175 was also sometimes employed to provide reverse bias to the cell to measure photocurrent as a function of applied voltage. The photocurrent as a function of reverse bias was usually measured using a Heath model EUW80A reference voltage source. The temperature of the cell could be varied by housing the ce-l in a styrofoam enclosure with a quartz window and an inlet for cooled nitrogen gas.

The temperature of the cell could thus be varied between +25°C and -100°C. The temperature of the cell was monitored with a chromel-alumel thermocouple.

The capacitance of the cell was measured with a General Radio 1650-A impedance bridge with a 1 kHz internal oscillator or coupled to a Hewlett Packard 3310A function generator if a different frequency was desired. The bias voltage for the capacitance measurements was applied with a Heath model EUW 16 A voltage reference source.

Chapter 3

Results and Discussion

3.1 Absorption Characteristics of Merocyanine Films

The absorption spectra of the merocyanine dye in acetone solution and vacuum deposited onto a quartz slide are shown in Fig. 6. The dilute (10^{-5} molar) solution shows a monomer band at 515nm. The quartz substrate could be held at room temperature or cooled with liquid nitrogen. The films shown were both 1000 angstrom thick. The film deposited onto a cooled substrate had a closer resemblance to the solution spectrum than the one deposited onto a substrate held at room temperature. This is expected, since a cooled substrate would tend to promote a more amorphous and glassy structure with a spectrum more closely resembling the monomer spectrum.[7] The spectrum generated by a room temperature substrate shows additional structure. The peaks at 480 and 560nm could be due to the formation of dimers and larger aggregates respectively.[12,32] It could also be a dichroism effect on microcrystals with differing orientations. Dye films deposited onto room temperature substrates are usually microcrystalline in nature.[7] The shoulder at 550nm in the spectrum with cooled substrate might be the beginning of the formation of larger aggregates.

Action spectra show that the dimer and monomer peaks are approximately equally efficient in the generation of photocurrent, whereas the multiple aggregates are ineffective. The quantum efficiency, measured as the number of electrons produced per photons absorbed, were comparable for amorphous and microcrystalline films. We have chosen to work primarily with the amorphous films because of better

Figure 6. Absorption spectra of the merocyanine dye in acetone solution and vacuum deposited onto quartz slides held at room temperature and liquid nitrogen temperature.

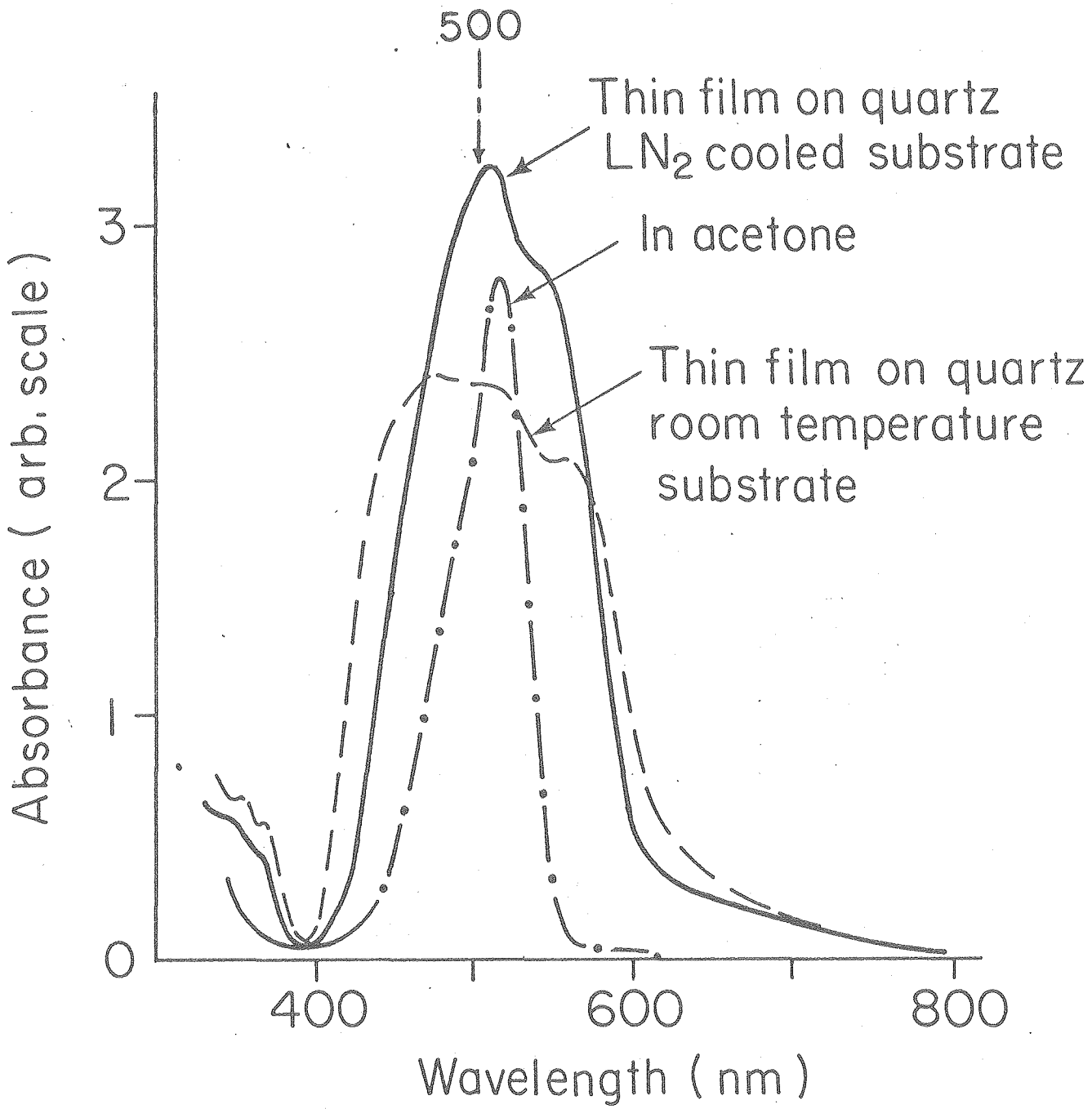
500
Thin film on quartz
LN2 cooled substrate
In acetone
Thin film on quartz
room temperature
substrate
Absorbance (arb. scale)
0
1
2
3
400
600
800
Wavelength (nm)

XBL 796-4876

reproducibility both in the spectral shape and the quantum efficiency. The dye spectra tend to degrade when the films are stored on the shelf overnight. The shape is retained but the absorption is reduced by about 15% in a 24-hour period. This photo-oxidation, which is also noticed in the action spectra, would therefore necessitate careful encapsulation of any practical device.

Figure 7 shows the absorption spectrum of merocyanine and TiO_2 superimposed on the solar spectrum. The dye intercepts about 15% of the solar spectrum for thicknesses of 1000 angstrom or more.[10] In order to get an estimate of the maximum output efficiency one can expect from a device based on absorption by this dye alone, we assume a quantum yield for charge carrier formation of the order of 1 (which is the case for photosynthetic systems[33]) and an output voltage of 0.75 Volts (photovoltages as high as 1.1 volts have been reported for metal-dye-metal structures.[10] We can then get an estimate for the engineering efficiency,

$$\text{Efficiency} \sim 1 \times \frac{0.75}{(2.4)} \times 0.15\% \sim 5\%$$

where the first term represents the quantum yield, the second term the voltage factor (photon energy = 2.4 eV), and the third term the fraction of the solar spectrum intercepted by the dye.

It is clear that this dye must be augmented by other dyes or semiconductors absorbing in other regions of the solar spectrum in order to reach an efficiency of the order of 10% or more which must be attained if the cells are to be economically competitive as solar cells.[7] Dye mixing and multiple layering of dyes as well as coupling dyes absorbing in the red region of the spectrum with semiconductor

Figure 7. Absorption spectra of merocyanine and TiO_2 superimposed on the AM1 solar spectrum filtered through absorption through one atmosphere.

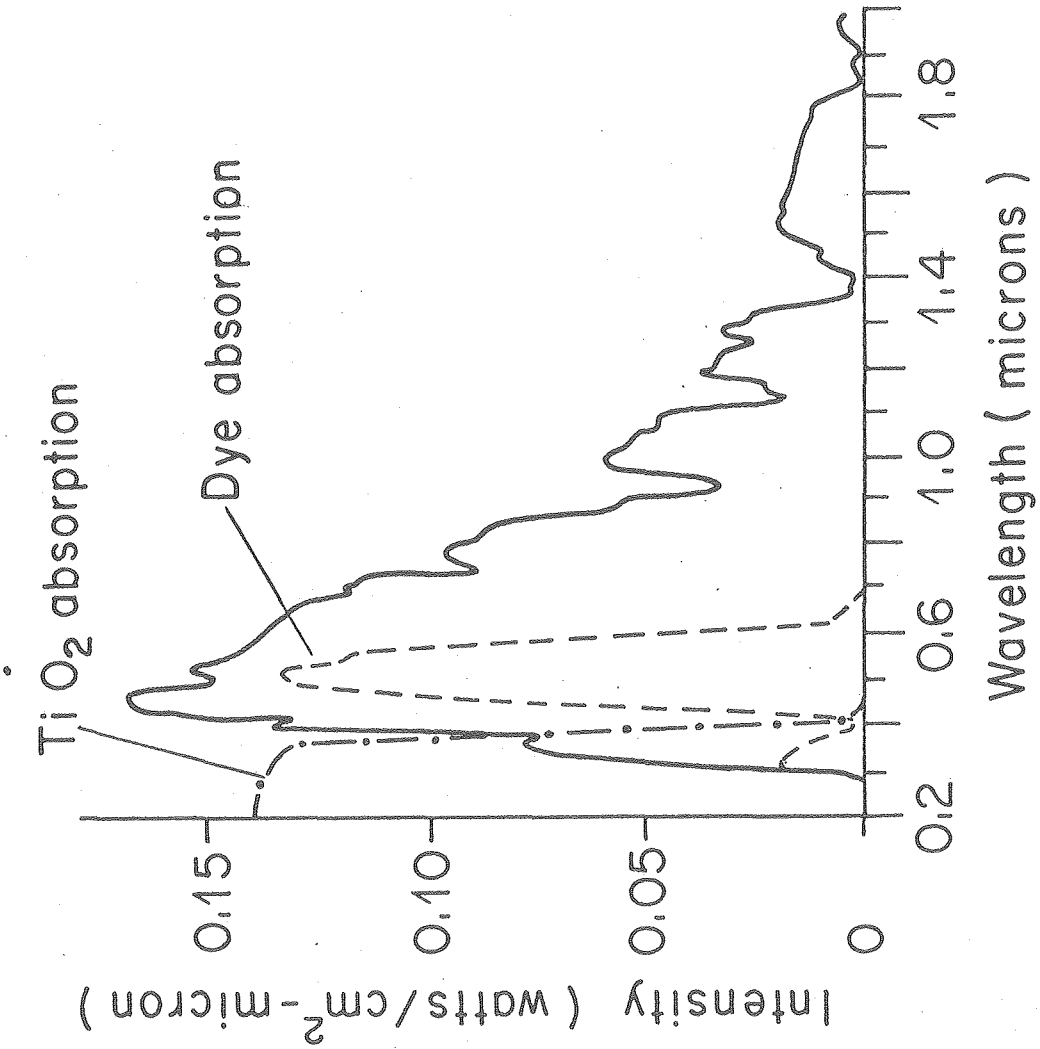
Ti O_2 absorption
Dye absorption
Intensity (watts/cm^2-micron)
0.15
0.10
0.05
0
0.2
0.6
1.0
1.4
1.8
Wavelength (microns)

XBL796-4877

substrates absorbing in the blue region (e.g. CdS thin films) appear promising.

3.2 Dark Current-Voltage Characteristics

Figure 8 shows the dark current-voltage characteristics of a cell with a 2000 angstrom thick dye layer. The cell showed some rectifying behavior with forward bias corresponding to a negative voltage applied to the TiO_2. At 0.4 volts the rectification ratio was about 6. Figure 9 shows a semi-logarithmic plot of the forward current versus applied voltage revealing that the forward current increases exponentially with voltage at low voltages. Figure 10 shows that at higher voltages the current shows a power dependence on the voltage, i.e. $\mathcal{J} \propto V^m$. Between 0.5 volts and 1.3 volts $m \cong 6$ and above 1.3 volts $m \cong 2$. The square law dependence at higher voltages has been observed for films of different thicknesses, but the exponent of the middle range varied from 5.6 to 7.5 with the lower range associated with thinner dye films ($\lesssim$ 1000 angstroms) and the upper range with thicker dye films (3000 angstroms).

The exponential dependence at lower voltages may be attributed to a junction formed between the n-type substrate and the merocyanine which has been shown to exhibit p-type conductivity.[45] The power dependence at higher voltages suggests that the current is space-charge limited in the presence of deep traps.[46,47] According to Rose[46] and Mark and Helfrich[47] the space-charge-limited current (SCLC) for a solid with a trap distribution decreasing exponentially with increasing trap depth is given by (see Appendix):

Figure 8. Dark current-voltage characteristics of a Au-merocyanine-TiO_2 cell with a 2000 angstrom thick merocyanine film. The arrows indicate the direction of the voltage scan. The voltage scan was 10mV per second.

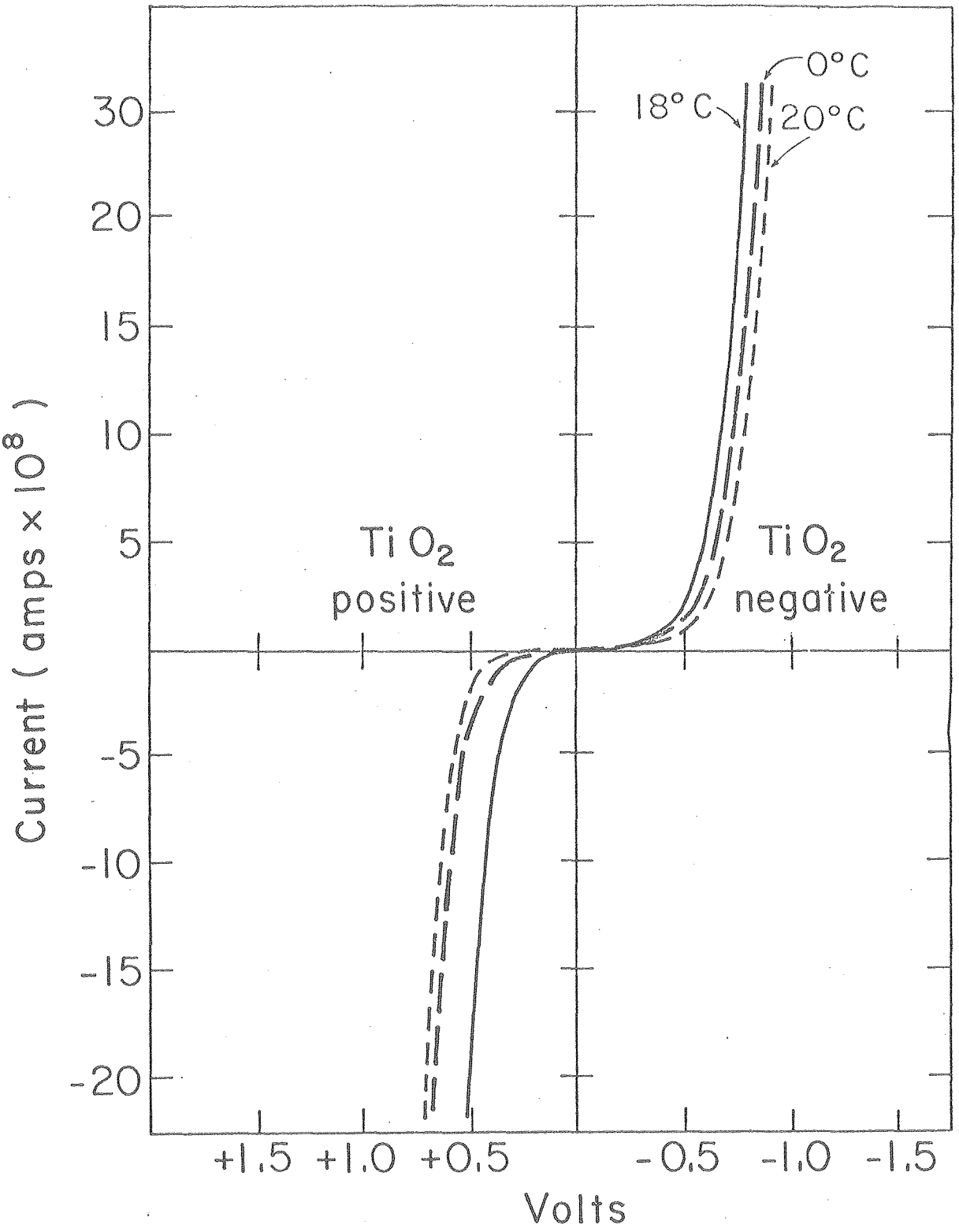
0°C
18°C
20°C
30
20
15
10
5
-5
-10
-15
-20
Ti O2
positive
Ti O2
negative
Current (amps x 10^8)
+1.5 +1.0 +0.5
-0.5 -1.0 -1.5
Volts

XBL797-4912

Figure 9. Semi-log plot of current versus applied forward bias for a cell with 2000 angstrom thick merocyanine film.

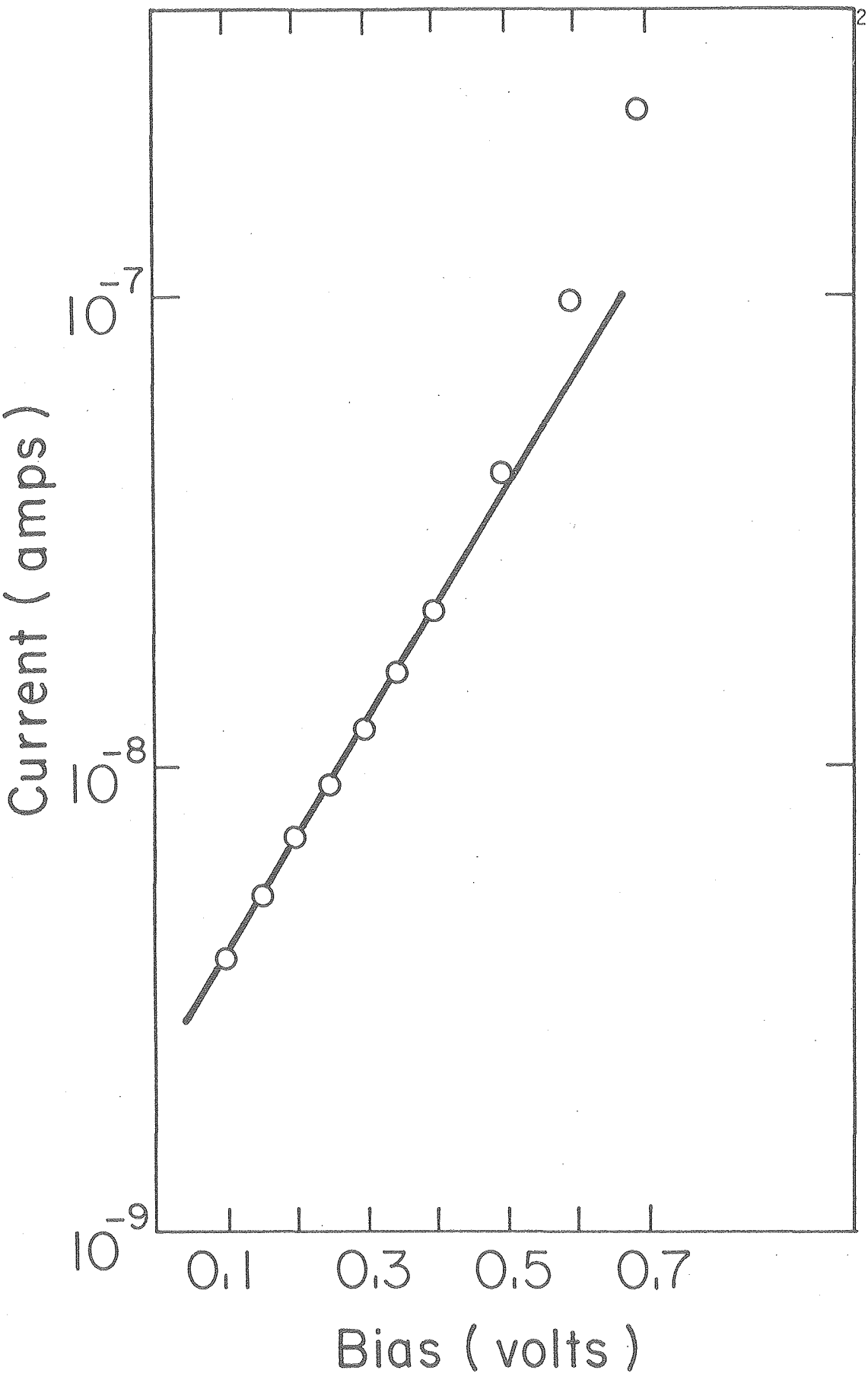

XBL797-4896

Figure 10. Log-log plot of current versus applied forward bias for a cell with 2000 Angstrom merocyanine film. V_{t-c} represents the transition to trapfree Child's law behavior.

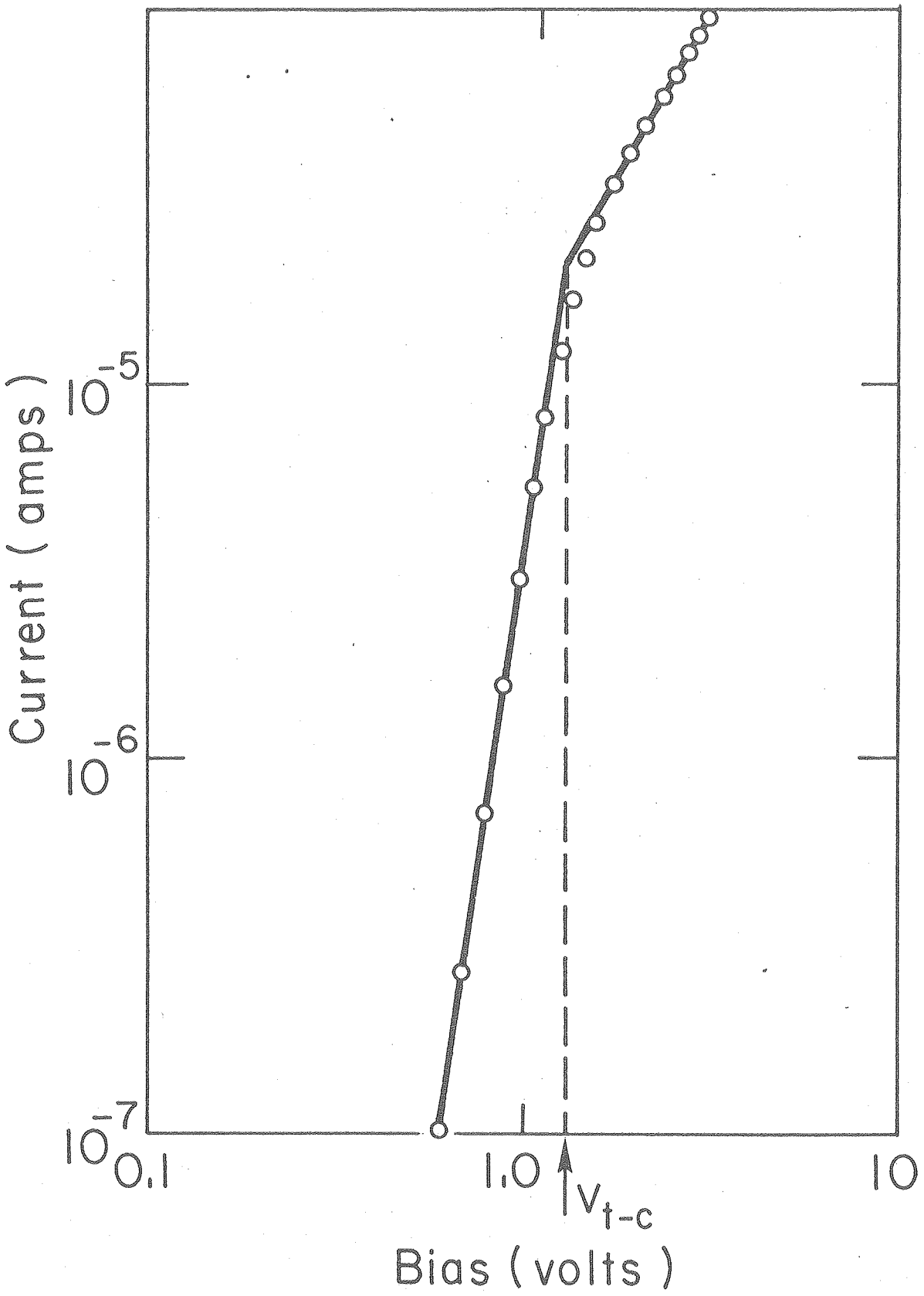

XBL797-4903

$$\mathcal{J} = N_0 \mu q^{(i-\ell)} \left(\frac{\varepsilon\varepsilon_0 \ell}{H(\ell+1)}\right)^{\ell} \left(\frac{2\ell+1}{\ell+1}\right)^{\ell+1} \frac{V^{(\ell+1)}}{d^{(2\ell+1)}}$$

N_0 is the effective density of states in the conduction band or valence band, q is the elementary charge, ε_0 is the permittivity of vacuum, is the merocyanine dielectric constant, d is the thickness of the film, H is the total trap density, and $\ell = T_c/T$ where T_c is a characteristic temperature that describes the trap distribution. One assumes a model with a trap distribution given by

$$N_t(E)dE = A_{exp}[-(E_c - E_t)/kT_c]dE$$

where E_c represent the bottomf of the conduction band and E_t the energy of the trapping level. The parameter T_c is a characteristic temperature used to approximate the rate at which the trap density changes with energy. $T_c \to \infty$ means a uniform distribution in energy. The model also assumes that the density of traps is considerably larger than the density of free carriers. If the converse were true, we can, of course, neglect the traps. An exponential trap distribution is common in imperfect crystals and thin amorphous films with a large density of defects, both for inorganic[55] and organic[47] materials.

The transition voltage to V^2 behavior is indepdnent of μ and $\mathcal{J}$ and is given by the following equation.[47]

$$V_t = \frac{qd^2}{\varepsilon\varepsilon_0}\left[\frac{9}{8}\frac{H^{\ell}}{N_0}\left(\frac{\ell+1}{\ell}\right)^{\ell}\left(\frac{\ell+1}{2\ell+1}\right)^{\ell+1}\right]^{1/(\ell-1)}$$

The dielectric constant for thin dye films typically lie in the range 3 - 4,[48,49] N_0 of the order of $10^{21}cm^{-3}$ is estimated for Cu-phthalocyanine[49] and tetracene[1] films. With the value of $\ell = 5$ and $V_t =$

1.3 volts from our data, and d = 2000 angstroms and assuming $\varepsilon = 3.5$, we obtain $H \cong 10^{17} cm^{-3}$. Such a value is consistent with literature values which range from $\sim 10^{15} cm^{-3}$ for films of phthalocyanines.[49,9a] The trap density was found to increase with decreasing thickness of the dye film. This dependence on thickness indicates that a large fraction of the trapping states are associated with the interfaces between the dye and the semiconductor and/or the dye and the metal. The trap density determined by the SCLC in the forward biased mode (TiO_2 negative) is the density for electron traps since the TiO_2 is assumed to be an electron injecting contact as data presented below will show.

Reverse Breakdown. The large increase in conductance with applied voltage in the reverse direction beyond the 'breakdown' voltage of about 0.7 volts (Fig. 8) is similar to that of a Zener diode[40] for semiconductor devices. The reverse current does not increase exponentially at low voltages. In semiconductor diodes, two distinct breakdown mechanisms are known to occur, avalanche breakdown and tunneling or Zener breakdown. The Zener tunneling in semiconductors is a band-to-band tunneling under reverse bias.[40] Tunneling can also be observed in metal-insulator-semiconductor structures under reverse bias involving surfaces states at the semiconductor-insulator interface.[40, 51] A more common mechanism in semiconductor junction breakdown is avalanche multiplication or impact ionization.[40,52] When a sufficiently large reverse bias is applied to a p-n junction or a metal-semiconductor junction electron-hole pairs will be generated by the electron impact with the lattice. In the strong electric field of the reverse biased junction region the electron-hole pair production

continues in an avalanche fashion. The two processes may be operationally separated since the temperature coefficients of the breakdown voltages are of opposite sign in the two cases. For avalanche multiplication the breakdown voltage increases at higher temperatures. A simple explanation for this increase is that the hot carriers passing through the high electric field in the junction region lose part of their kinetic energy to optical phonons. Since the mean free path of the optical phonon decreases with increasing temperature, the carriers would lose more energy to phonons along a given distance at constant field. The carriers would therefore need a greater potential difference to acquire the energy necessary for electron-hole pair production. Hence, the breakdown voltage will increase with increasing temperature.[53]

The breakdown voltage for tunneling, on the other hand, has a negative temperature coefficient, i.e. the voltage decreases with increasing temperature in most semiconductors because the energy band gap decreases with increasing temperature.[40]

In Figure 11 we show the current-voltage curves taken at three different temperatures on a film of 2000 angstroms. The decrease of the breakdown voltage at higher temperatures suggests a tunneling mechanism. The curves can be retraced many times reproducibly. The current surge is therefore not a destructive breakdown. This phenomenon has also been observed in bimolecular lipid membranes with electrolytic contacts.[54]

3.3 Photoeffects

3.31. Transient Response. The photocurrent and the photovoltage

Figure 11. Current-voltage curves recorded at three different temperatures with a cell with a 2000 angstrom merocyanine film.

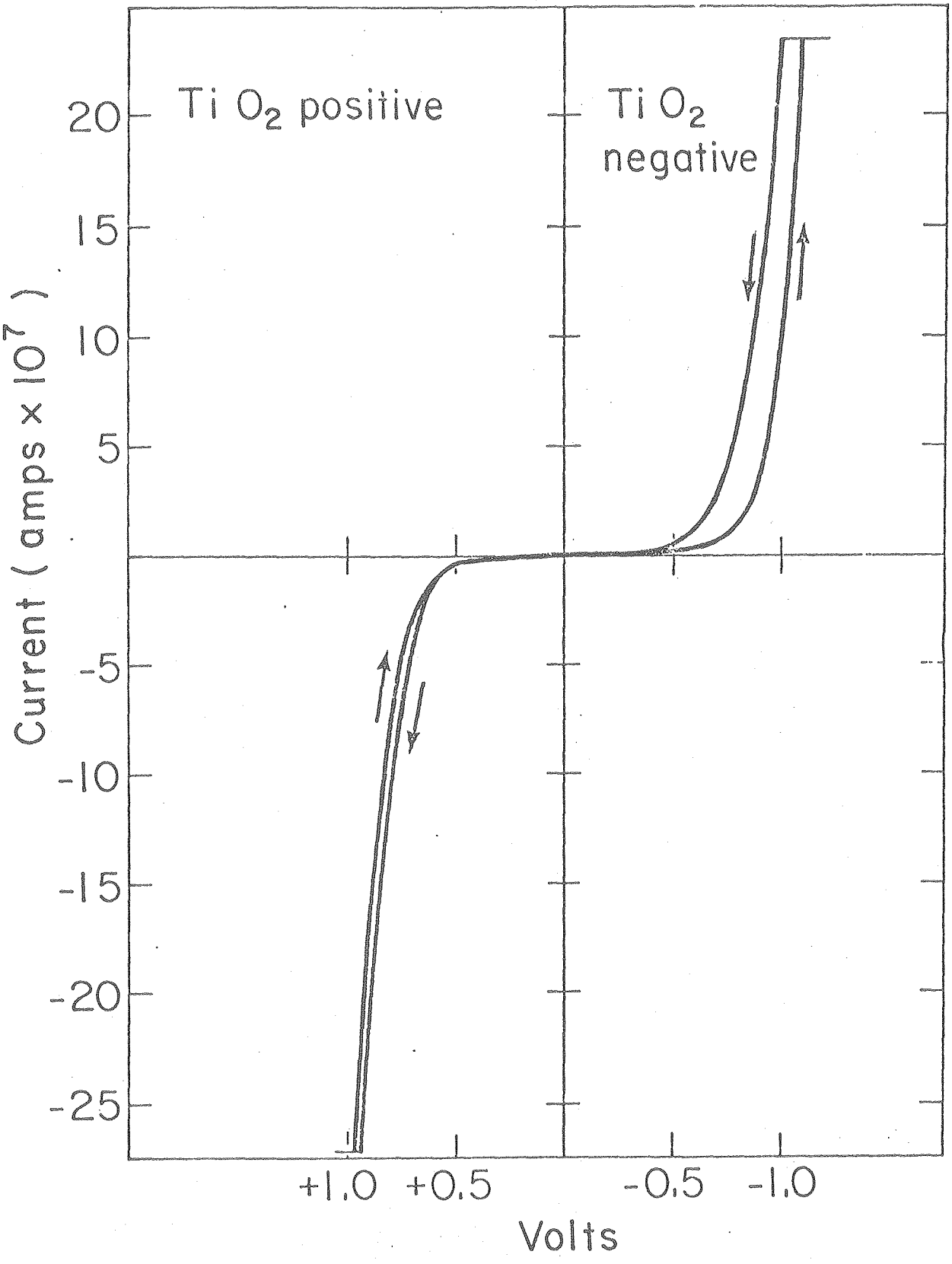
Ti O_2 positive
Ti O_2 negative
20
15
10
5
-5
-10
-15
-20
-25
Current (amps x 10^7)
+1.0
+0.5
-0.5
-1.0
Volts

XBL797-4913

of the Au-merocyanine-TiO_2 cells exhibit a rather slow rise and decay time of the order of seconds (Figs. 12A and 12B). The rise time of Au-TiO_2 Schottky barrier cells on the same time scale is only limited by the response of the recorder. The rise and decay times in the following discussion are therefore to be attributed to the merocyanine film. Although rise times of 10^{-5} - 10^{-6} sec have been observed with suitable experimental arrangements with metal-free and copper-phthalocyanines,[56] long transient times are known to occur for photoconductors with large densities of traps.[57,45]

Most cells reach a steady state level in a few seconds and can generate a photocurrent for more than an hour with no appreciable decline. Some cells show a slightly more complicated behavior in that they exhibit a slow decrease in the photocurrent of approximately 20% over about an hour after reaching a peak in a few seconds. The new level is stable for several hours. All cells exhibit long term decay. After being stored under ambient atmospheric conditions for 2 - 3 days the photocurrent is usually lowered to about 60-70% of its initial value. The exact number varies from cell to cell and is dependent on the cell history.

At high light intensities (greater than 10mW-cm^{-2}) the initial slow decay is faster but the long term history of the cell does not appear to be affected. The long term deterioration (of the order of days) therefore appears to be connected to oxygen effects rather than photocurrents. All our reported measurements are taken with low monochromatic intensities ($\sim$ 0.1 mW-cm^{-2} or $\sim 10^{14}$ photons cm^{-2}sec) and only steady state values are reported in this work. We made no attempt to study the system beyond 2-3 days storage or involving

Figure 12A. Time behavior of the dark current transient and the short circuit photocurrent under monochromatic irradiation at 520nm.

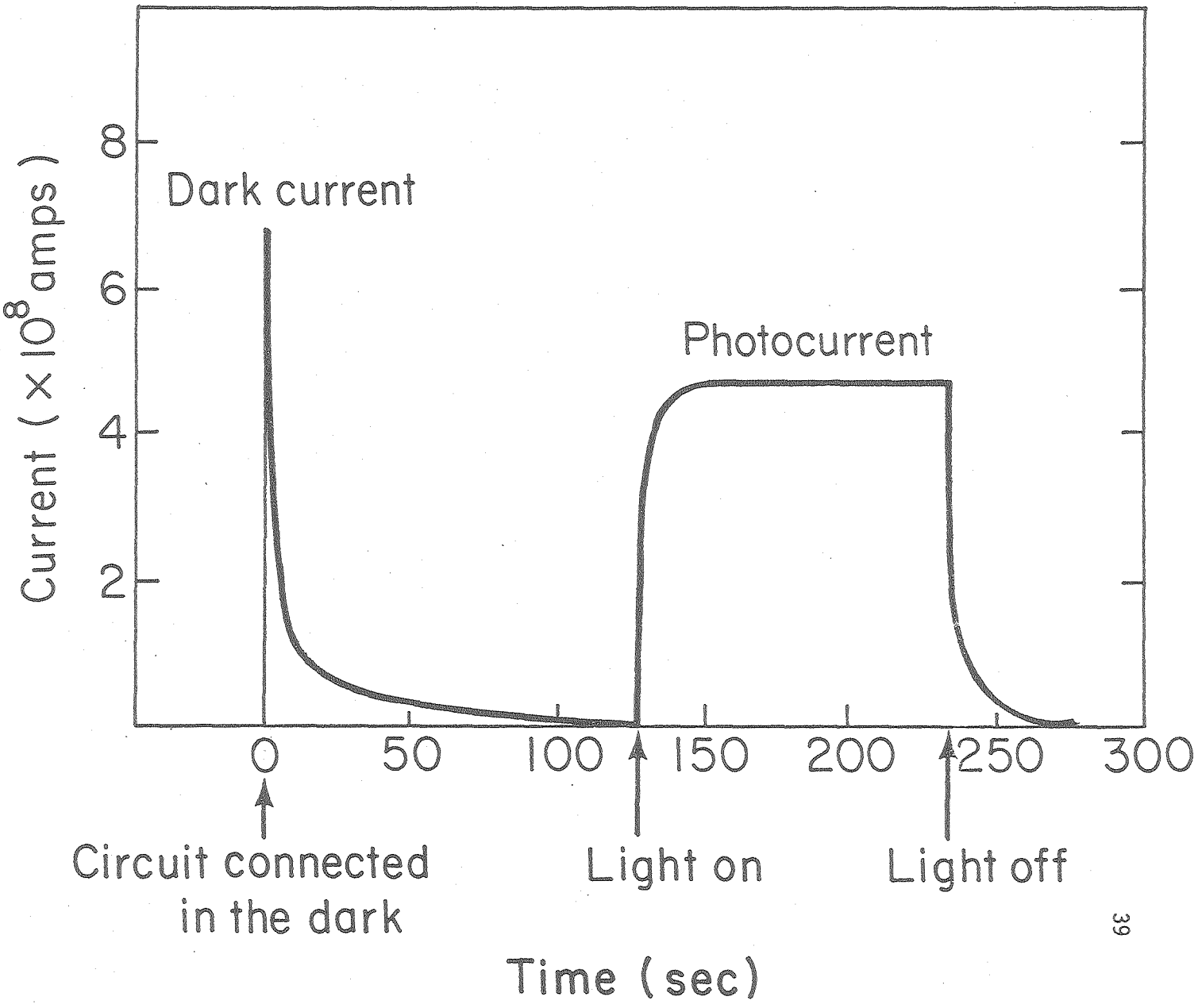
Current (x 10^8 amps)
8
6
4
2
Dark current
Photocurrent
0
50
100
150
200
250
300
Circuit connected in the dark
Light on
Light off
Time (sec)

XBL797-4898

Figure 12B. Time behavior of the open circuit voltage under monochromatic irradiation at 520nm.

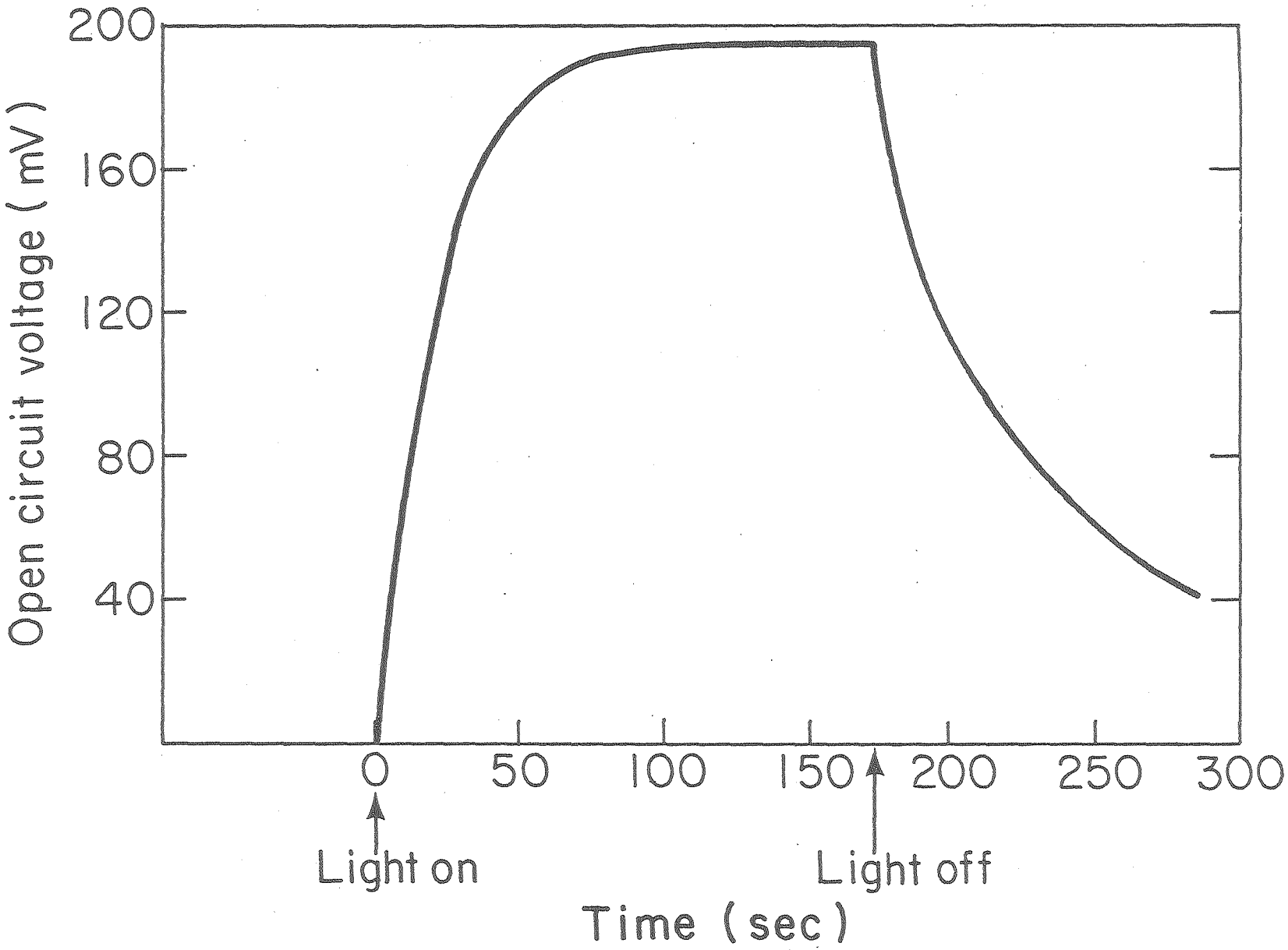
200
160
120
80
40
Open circuit voltage (mV)
0
50
100
150
200
250
300
Light on
Light off
Time (sec)

XBL 797-4905

photovoltaic operation for more than a few hours.

3.3.2 Kinetics of Photoconductivity . Upon bringing the photocurrent to a steady state level there is a rapid initial rise followed by slow rise of the order of seconds (Fig. 12). When the light is turned off and the decay in the dark is followed, it is found that the initial rate of decay is high but that it decreases rapidly during the first few tenths of a second, becoming a constant for the remainder of the process. The decay is slower at a lower temperature (Fig. 13). The initial fast decay is of the first order, i.e.

$$\frac{dn}{dt} \sim \alpha n \tag{3.1}$$

where n is the density of carriers and α is the rate constant. Assuming the photocurrent to be proportional to the density of carriers, we get (Fig. 14)

$$\mathcal{J} \sim e^{-\alpha t} \tag{3.2}$$

For the slow decay process the current obeys the relation

$$\mathcal{J} \sim t^{-1} \tag{3.3}$$

This is the decay one would expect for a process involving the recombination of oppositely charged carriers. In this case, we may write

$$\frac{dn}{dt} = -kn^2 \tag{3.4}$$

where n is the concentration of positively and negatively charged carriers, and k is the rate constant (in units of $cm^3 sec^{-1} carrier^{-1}$). Upon integration we obtain

$$\frac{1}{n} = Kt + \text{constant}$$

and for large t the constant can be ignored. Since the photocurrent is proportional to the concentration of carriers, we arrive at equa-

Figure 13. Long time decay of the photocurrent upon turning off the light at two different temperatures. The decay constant is defined as the slope of the curves.

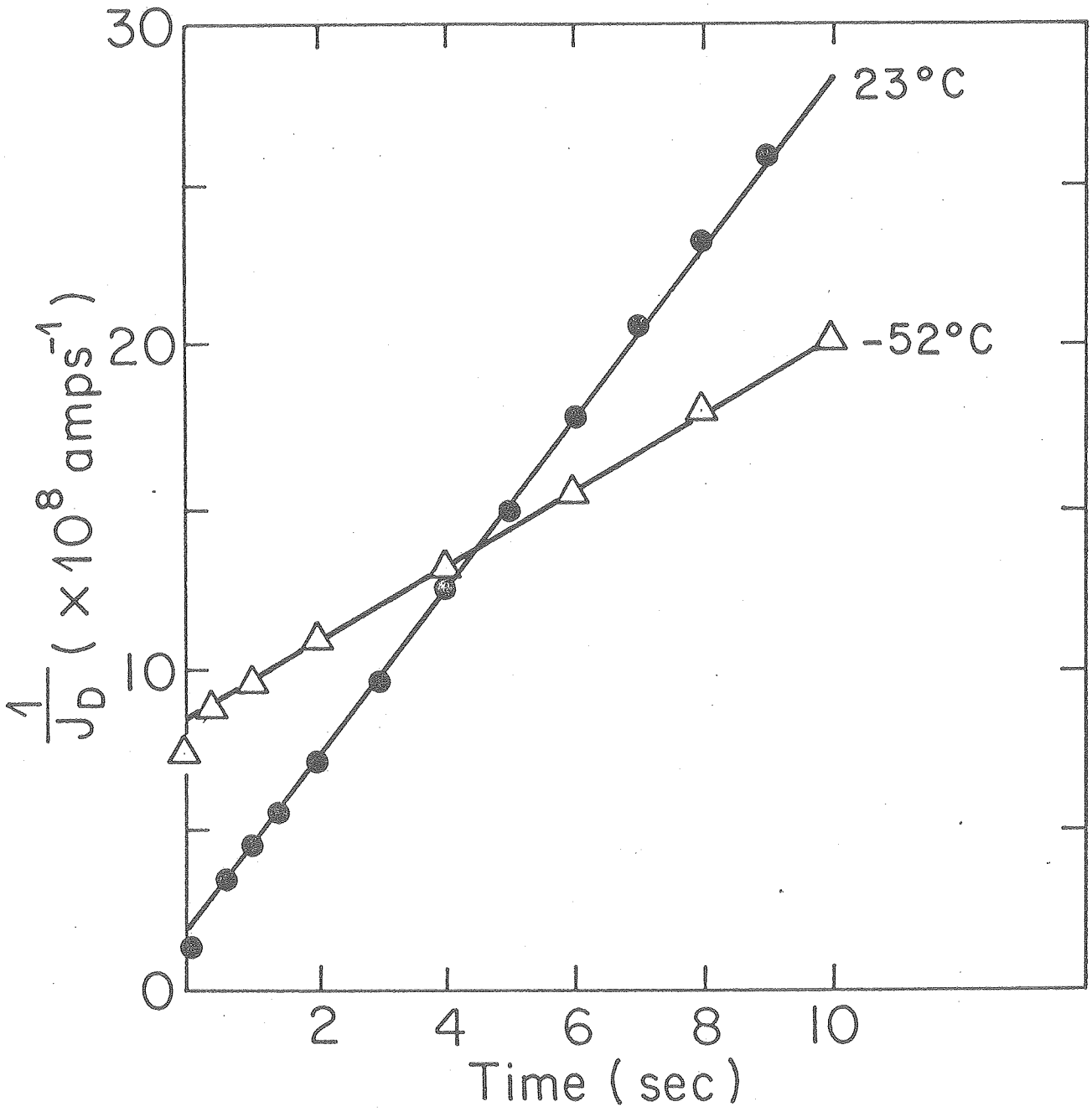

XBL796-4883

Figure 14. Simi-log plot of the initial decay of the photocurrent upon turning off the light.

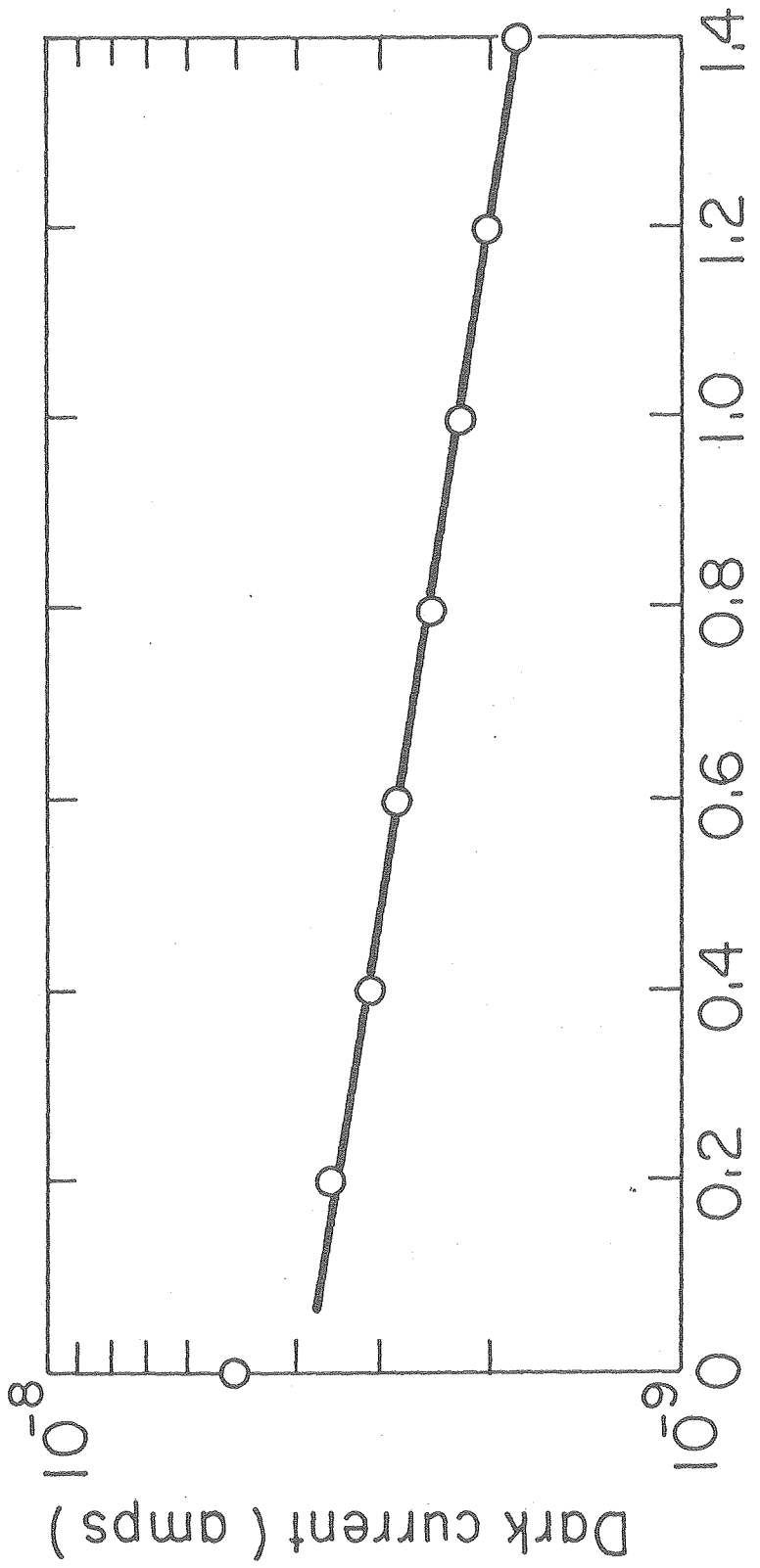

XBL797-4906

tion (3.3). The rate constant, as measured by the slope of the 1/J versus t curve is essentially independent of the magnitude of the initial photocurrent for a reduction of about a factor of two (Fig. 15). It increases slightly for initial photocurrents reduced by an order of magnitude or more.

3.3.3. Temperature Dependence of Photoconductivity. The steady state photocurrent rises with increasing temperature. The growth is given by the equation

$$\mathcal{J}_{photo} \sim \exp(-\Delta E_{ph}/kT) \tag{3.5}$$

Plotting the logarithm of the steady state current as a function of the reciprocal temperature gives a straight line (Fig. 16). Its slope yields the thermal activation energy of photoconductance ΔE_{ph}. The activation energy is found to be 0.11 eV and is the same for films of various thickness. As shown in Fig. 13 the decay constant of the photocurrent in the dark has a temperature dependence and increases with increasing temperature. If the logarithm of the decay constant, as measured by the slope of the decay curves for the slow decay is plotted versus 1/T the resulting straight line gives the activation energy 0.10 eV, close to the value found for the activation energy of the steady state photocurrent (Fig. 17).

3.3.4. Interpretation of Temperature Dependence. The temperature and transient response characteristics of a photoconductor are intimately related to the trapping and release of carriers by trapping imperfections. In general, a photoconductor will have electron and hole traps distributed in energy in the band gap.[46] Deep centers near the middle of the band gap become recombination centers where

Figure 15. Decay plots for a cell at 23°C showing the dependence of decay rate on initial photocurrent.

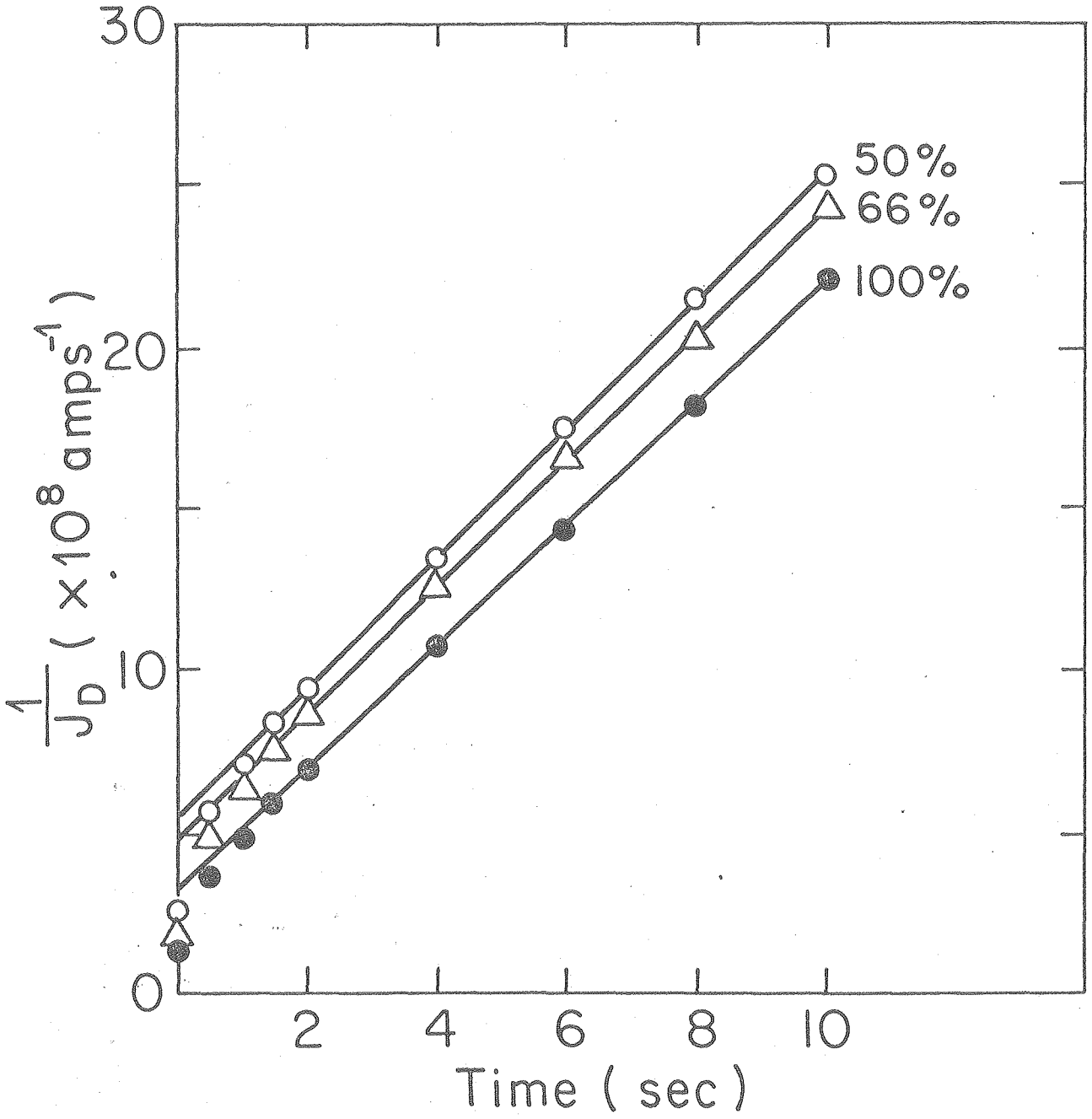

XBL796-4882

Figure 16. Temperature dependence of the steady state short circuit photocurrent.

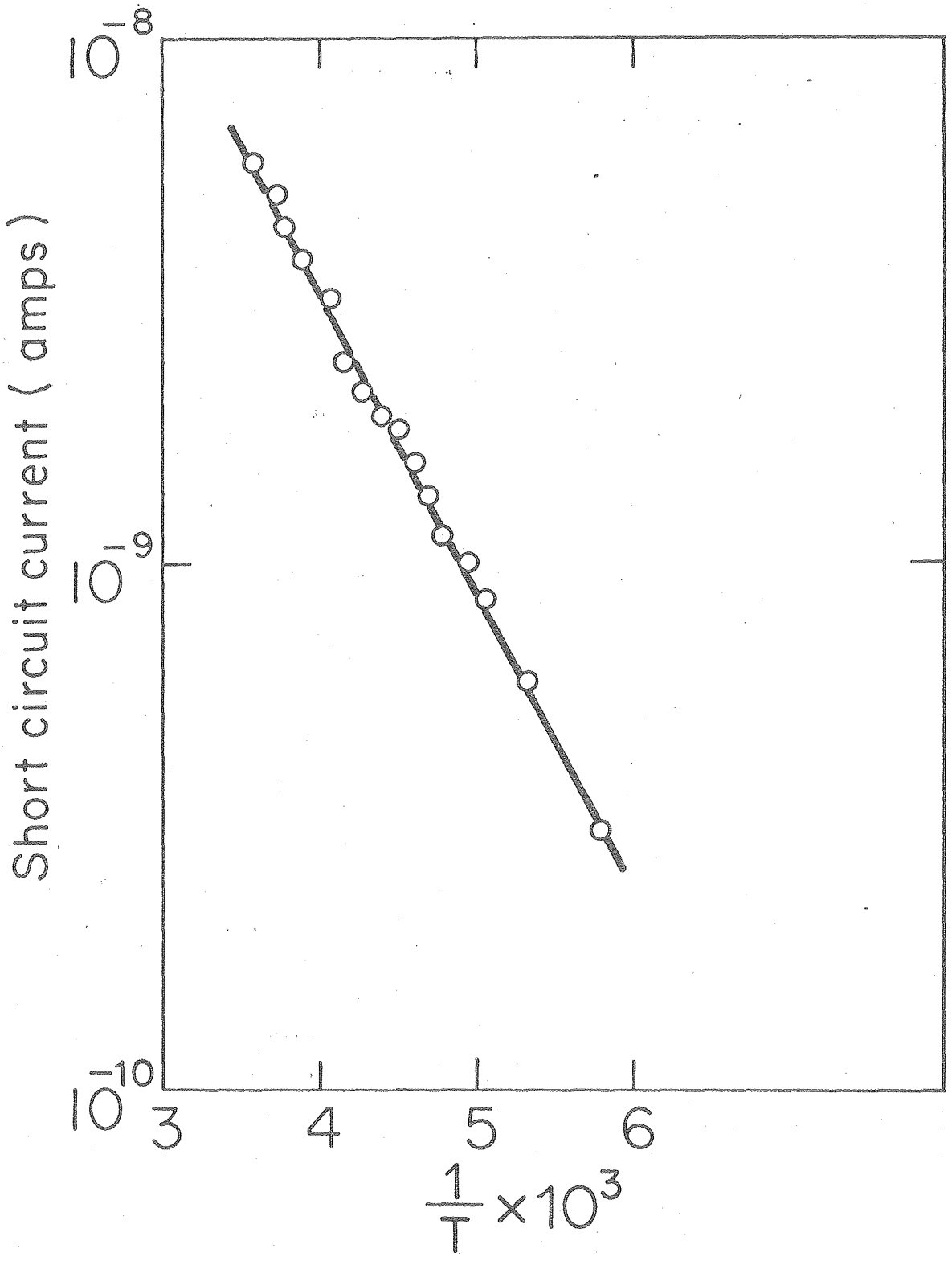
Short circuit current (amps)
10^{-8}
10^{-9}
10^{-10}
3
4
5
6
$\frac{1}{T} \times 10^3$

XBL 797-4888

Figure 17. Temperature dependence of the decay constant.

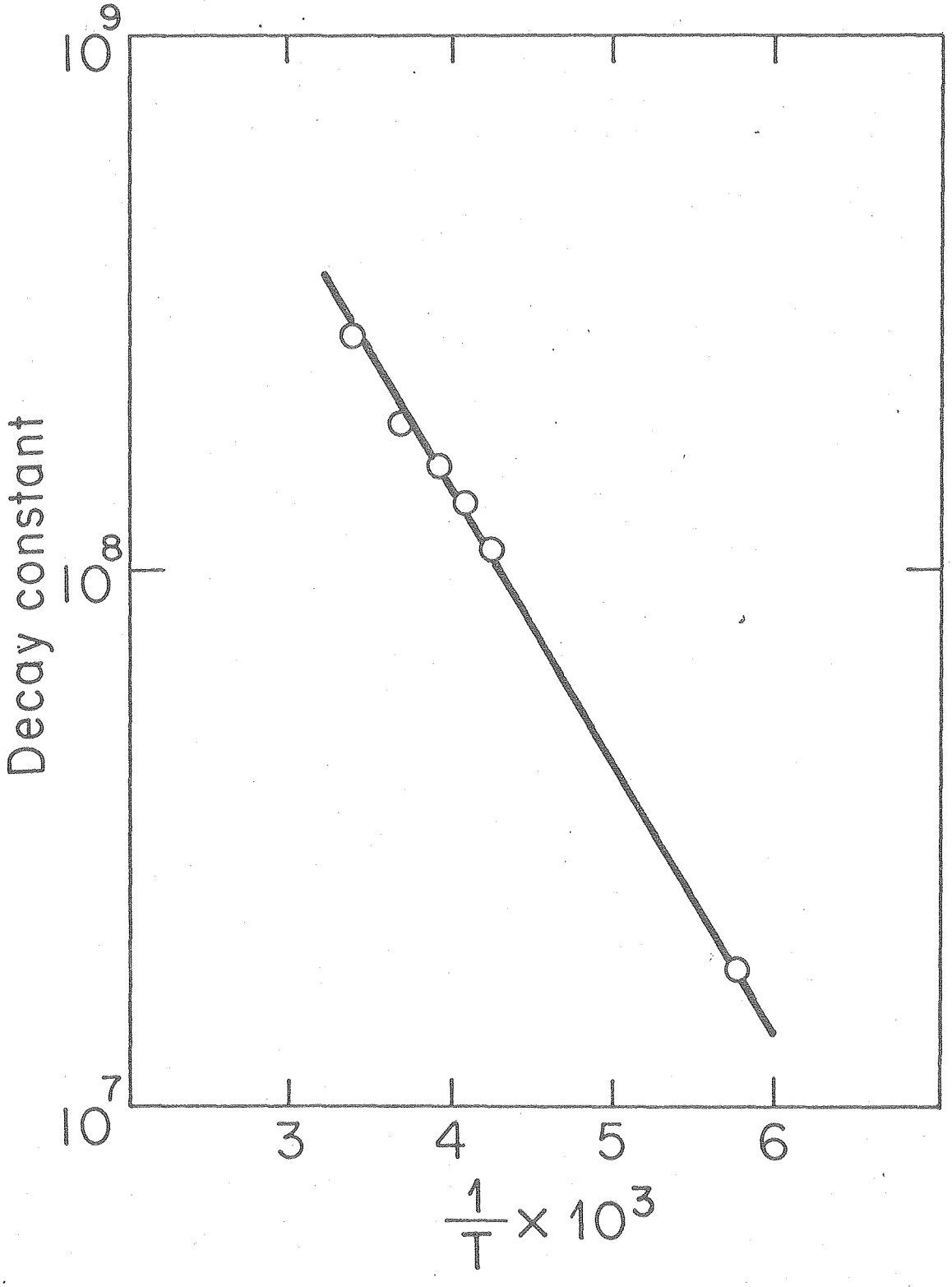

XBL797-4890

a captured electron will recombine with a free hole before it can be thermally re-excited to the conduction band, and similarly for holes. The trapping states are characterized by the fact that a free electron of hole captured into an unoccupied trap will be thermally re-excited into the conduction or valence band respectively before capturing a free charge of the opposite sign. The electron and hole trapping states are in thermal contact with the conduction or valence band, respectively, i.e. their occupancy is determined by the Boltzmann factor

$$\begin{aligned} &\exp[-(E_c-E_t)/kT] \text{ for electrons} \\ &\exp[-(E_t-E_v0/kT] \text{ for holes} \end{aligned} \qquad (3.6)$$

where E_c represents the bottom of the conduction bnad, E_v the top of the valence band, and E_t the trapping level.

The dark current-voltage experiments revealed the existence of an exponential distribution of electron trapping states below the conduction band. With forward bias, only electrons were injected into the dye from the TiO_2. No holes would be injected from the Au electrode since Au forms a blocking contact with TiO_2. The response of the photoconductor was thus dominated by electrons. If both electrons and holes are generated, the response of a photoconductor will be dominated by the majority carriers, the carriers with the longest lifetime. Since the merocyanine dyes are known to exhibit p-type conductivity,[45] it is reasonable to suggest that we can ignore the effect of the electron traps in determining the effect of traps on photoconductivity. Using the relationships in (3.6.) we can then write

$$\frac{P_t}{N_t} = \frac{P}{N_v} \exp[(E_t-E_v)kT] \qquad (3.7)$$

where N_t is the density of trapping states and N_v approximately the number of states in the top kT slice of the valence band. We can write this as

$$P = P_t \frac{N_v}{N_t} \exp(-\Delta E_t/kT) \text{ where } \Delta E_t = E_t - E_v \tag{3.8}$$

With increasing temperature, the number of holes in the traps decrease and the number of free holes in the valence band increases. The photocurrent is proportional to the density of free holes in the valence band

$$J_{ph} \propto p \tag{3.9}$$

For the traps to be effective, we must assume $p_t >> p$. We can therefore write for the photocurrent

$$J_{ph} = A(T) \exp(-\Delta E_t/kT) \tag{3.10}$$

where A(T) is a slowly varying function of temperature. Plotting the logarithm of J_{ph} versus 1/T will therefore give the depth of the dominant traps as an activation energy as seen in Fig. 16.

The response time of the photoconductor will increase because of the filling of the traps. Following the argument of Rose,[46] suppose we wish to double the number of free holes by increasing the light intensity. From equation (3.7) we see that we must also double the number of trapped holes. Hence, an additional time, $(P_t/P)\tau_{po}$, where τ_{po} is the response time in the absence of traps, is required to excite enough holes to double the number of trapped holes, and the total response time is therefore

$$\tau_p = (1 + \frac{P_t}{P})\tau_{po} \tag{3.11}$$

On interruption of light, the decay time will be determined by free holes captured by recombination centers as well as trapped holes emp-

tied into the recombination centers via thermal excitation into the conduction band and subsequent capture. The trapped holes do not normally recombine directly because the discrete states are localized and the trapping and recombination states are in general a few lattice spacings removed from each other. The decay time for the photocurrent will therefore be increased by the factor given in equation (3.11).

As shown in Fig. 13, the photocurrent decays according to a second order reaction for long times. This indicates that a bimolecular recombination determines the decay process after the initial fast decay. The more rapid initial decay is a first order process, as shown in Fig. 14. This separation can be qualitatively understood as follows: The carrier recombination takes place via recombination centers rather than direct electron-hole recombination.[58,46] Trapping centers near the middle of the band gap are the most efficient channels for recombination. Again we are concerned only with the trapping and recombination of holes since they are the majority carriers and dominate the photoconductivity. Consider the recombination scheme in Fig. 18, where we have two separate channels dominating the electron-hole recombination.[57] Channel 1 has a smaller hole trapping cross section than channel 2 and a larger electron trapping cross section. If there is a high concentration of N_{r2} centers, they can dominate the recombination initially. Holes in the valence band and trapping centers N_t recombine with electrons in the N_{r2} recombination center. As the N_{r2} centers become depleted of electrons, the N_{r1} channel becomes dominant and the recombination changes from first order to second order since the electron capture cross section of channel 1 is assumed to be high.

Figure 18. Electron-hole recombination scheme dominated by two separate channels.

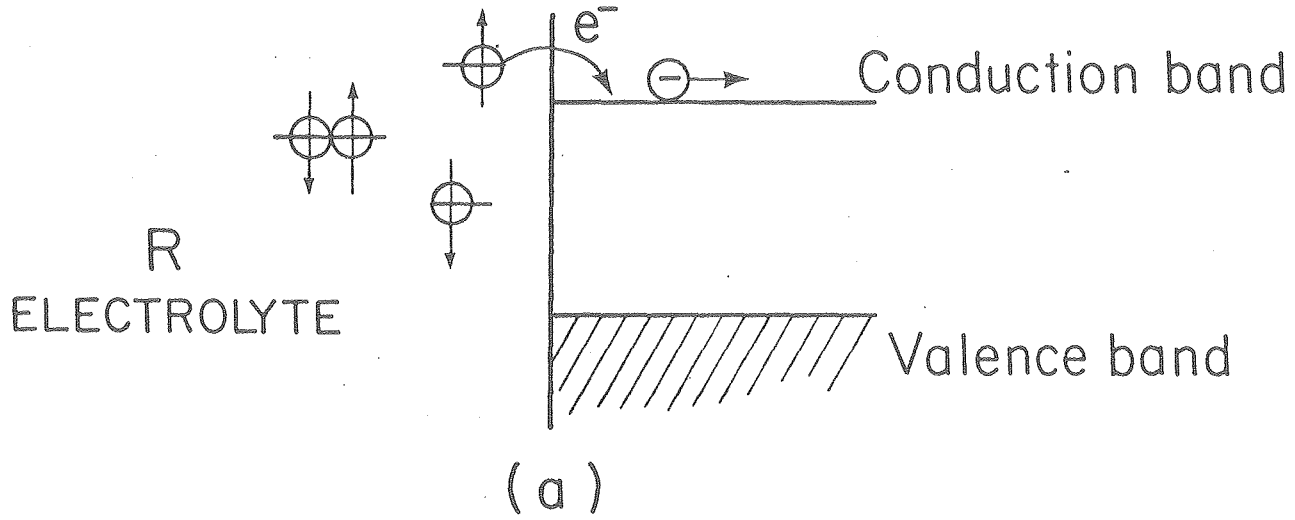

(a)

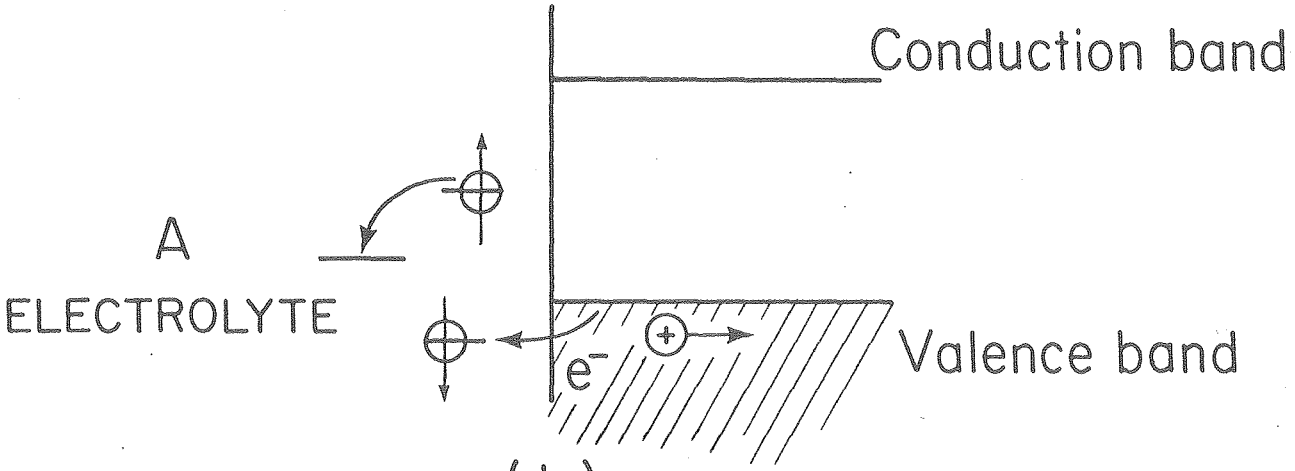

(b)

XBL796-4880

3.4. Photo J-V Characteristics

3.4.1. Light Intensity Dependence of V_{oc} and J_{sc}. Fig. 19 shows the dependence on incident light intensity of the short circuit photocurrent (J_{sc}) and the open circuit photovoltage (V_{oc}) for a cell with a 500 angstrom thick merocyanine film. It shows that the photocurrent varies linearly with the light intensity at least up to intensities of about 10^{14} photons $sec^{-1}cm^{-2}$ or about 0.1 $mWcm^{-2}$. For thicker cells the light dependence of the photocurrent assumes the form $J_{sc} \propto L^m$, L being the light intensity. The light exponent drops from unity to 0.93 for 2000 angstrom thick films. This relationship can be explained using a simple physical picture involving traps and recombination centers.[46] As the light intensity is increased the quasi-fermi level sweeps through trapping states located between the fermi level and the valence band and converts them to recombination centers. As the light intensity is increased, more and more of the trapping states are converted into recombination centers. As the density of the recombination states increases, the lifetime of the charge carriers decreases. This would result in a sublinear dependence of the photocurrent of the light intensity. For very thin films the field across the dye layer is larger and charge separation consequently more efficient, less influenced by traps and recombination centers.

Fig. 20 shows that the open circuit voltage (V_{oc}) increases logarithmically with the intensity, and therefore also with J_{sc}. The behavior follows that expected for an abrupt junction,[40]

$$V_{oc} = \frac{mkT}{q} \ln(J_{sc}/J_o + 1)$$

where m is an empirical coefficient which is equal to 1 for an ideal

Figure 19. Light intensity dependence of short circuit current and open circuit voltage.

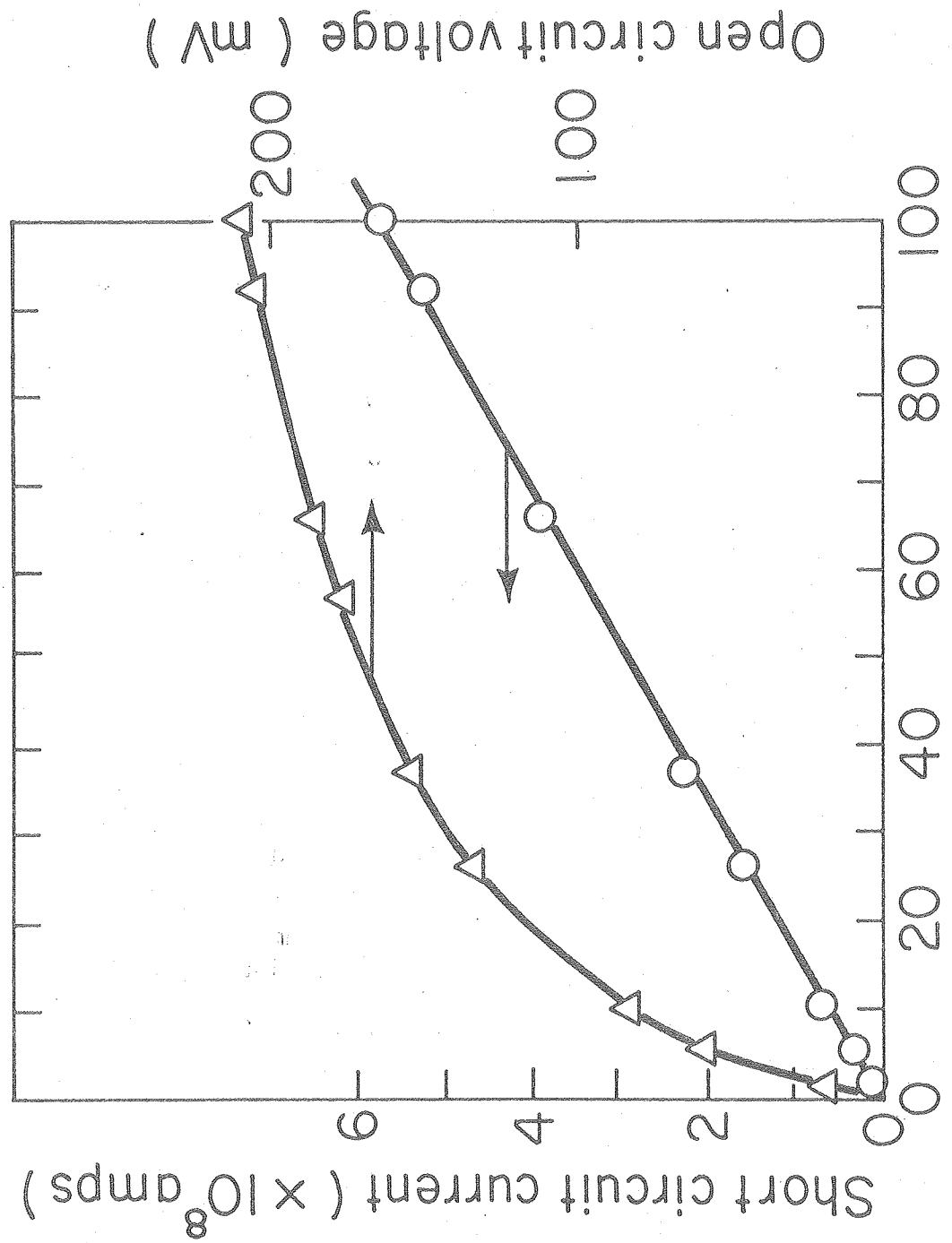
Short circuit current (x 10^{8} amps)
0
2
4
6
Relative light intensity
0
20
40
60
80
100
Open circuit voltage (mV)
100
200

XBL797-4887

Figure 20. Semi-log plot of the light intensity dependence of the open circuit voltage.

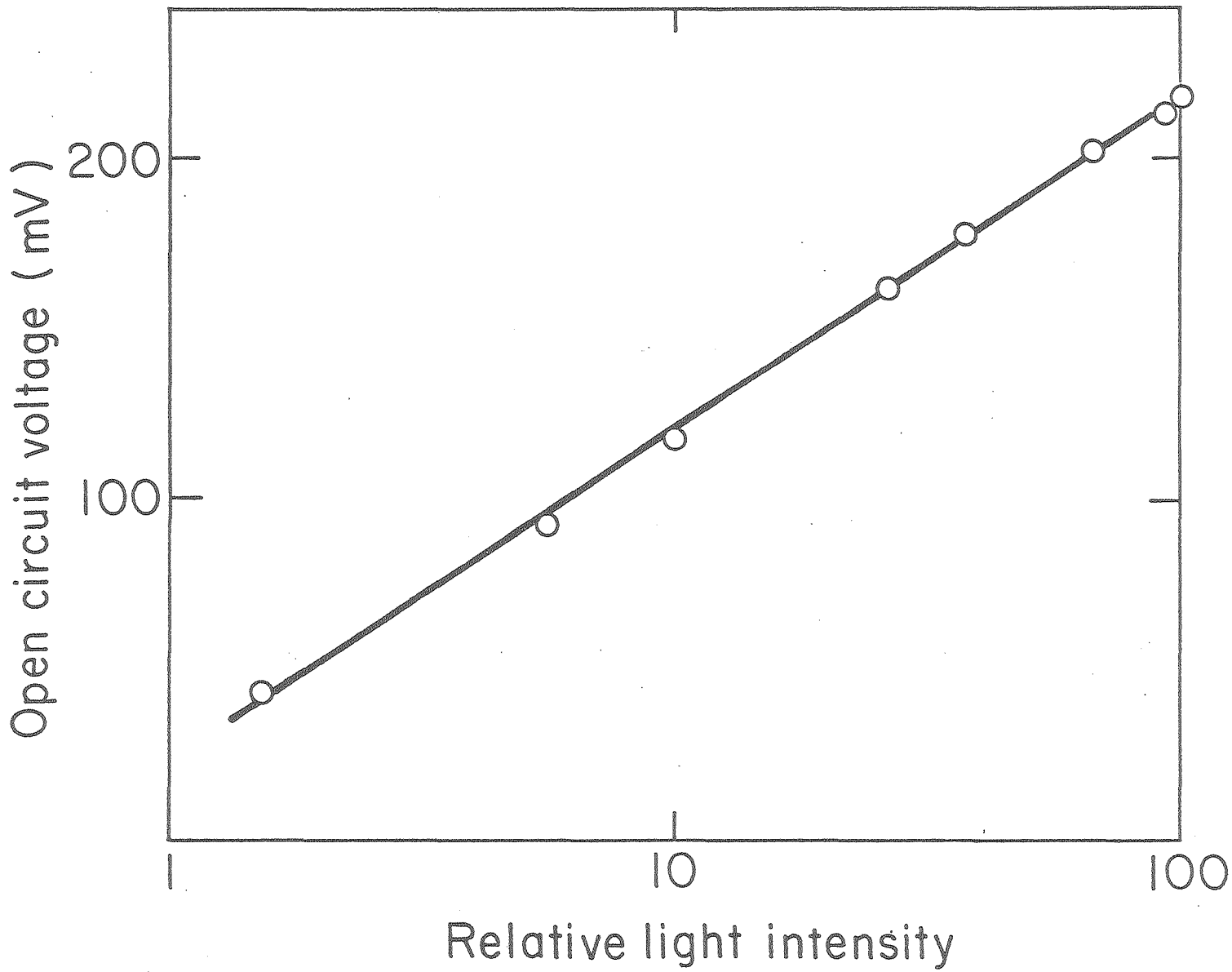
Open circuit voltage (mV)
200
100
1
10
100
Relative light intensity

XBL797-4891

junction and greater than 1 for non-ideal junctions with interface states, and J_o is the reverse saturation current. For a 500 angstrom merocyanine cell, m = 1.71.

3.4.2. Photovoltage-Photocurrent Characteristics. The sign of the photovoltage of the Au-merocyanine-TiO_2 cells is such that the TiO_2 is always negative. Fig. 21 shows the current-voltage characteristics of a cell with a 500 angstrom thick dye film in the photovoltaic mode. The curve is obtained by varying the load resistance at a constant light intensity. The wavelength of the irradiation is 520nm. The maximum power that can be extracted from a photovoltaic device is at the point for which the largest rectangle can be inscribed into the current voltage curve. The maximum power output from this particular cell occurs with a load resistance of about 5×10^6 ohms and is about 5×10^{-9} W. The incident light power on the active cell area is about 5×10^{-6} W, corrected for the O.D. of the TiO_2 crystal. The power conversion efficiency at this light level is therefore about 10^{-3} or 0.1%.

The fill factor is defined as the ration of maximum output power to the product of V_{oc} and J_{sc} and gives a measure of how close the cell is to an ideal solar cell. The fill factor for this cell is 0.35 compared to 0.75 - 0.8 for Si and GaAs solar cells.[38] The low fill factor is probably due to two separate effects. High series resistance will lower the fill factor by lowering the output voltage for a given output current.[39] In addition, the field dependence of the photocurrent would lead to a lowering of the output current for a given output voltage, since the photovoltage would work against the built-in charge separating field. At low quantum yields the second effect is probably dominant.[11]

Figure 21. Photocurrent-photovoltage characteristics for a cell with 500 angstrom merocyanine film.

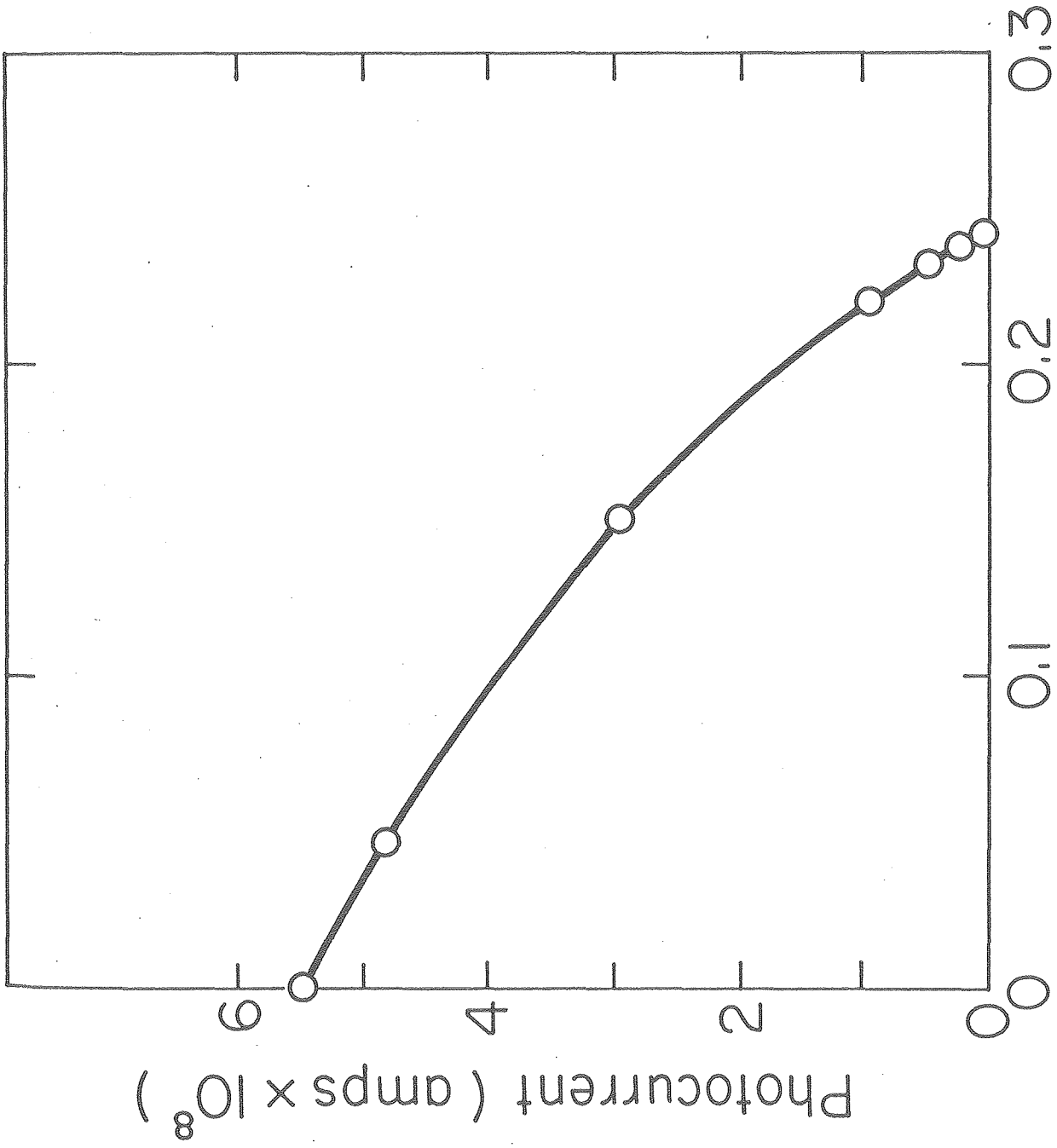

XBL796-4885

3.5. Capacitance-Voltage Measurements

Associated with a depletion layer in a p-n junction or a Schottky barrier there is a capacitance varying with the voltage applied across the junction. Applying a reverse bias across the junction increases the width of the junction and therefore decreases the capacitance. The dependence of the capacitance on applied voltage is obtained by solving Poisson's equation and takes the following form:[40]

$$\left(\frac{A}{C}\right)^2 = \frac{2}{q\varepsilon\varepsilon_o N}\,(V_B - V)$$

where N is the donor or acceptor density, A the surface area, ε the semiconductor permittivity, ε_o the permittivity of free space, q the electronic charge, V_B the barrier height and V the applied voltage.

If we are dealing with a heterojunction formed between two semiconductors having different energy band gaps we obtain[40]

$$\left(\frac{A}{C}\right)^2 = \frac{2(\varepsilon_1 N_{D1} + \varepsilon_2 N_{A2})}{q N_{D1} N_{A2} \varepsilon_1 \varepsilon_2 \varepsilon_o}\,(V_B - V)$$

where N_{D1} is the donor density in semiconductor 1 and N_{A2} is the acceptor density in semiconductor 2. If one plots the experimentally obtained values of $1/C^2$ *versus* reverse bias we would expect a straight line where the slope and the intercept on the abscissa determine the dopant density and the barrier height respectively. Fig. 22 shows the variation of capacitance with reverse bias measured with an impedance bridge coupled to an external oscillator at 200Hz. The capacitance is independent of applied voltage up to and beyond 0.8 volts. This means that the junction region is completely depleted of mobile charges and the cell behaves as a simple capacitor with the dye as a dielectric. Measurements with 1 kHz oscillator frequency produce similar results.

Figure 22. Capacitance as a function of reverse bias for a cell with 1000 angstrom merocyanine film. The oscillation frequency was 200Hz.

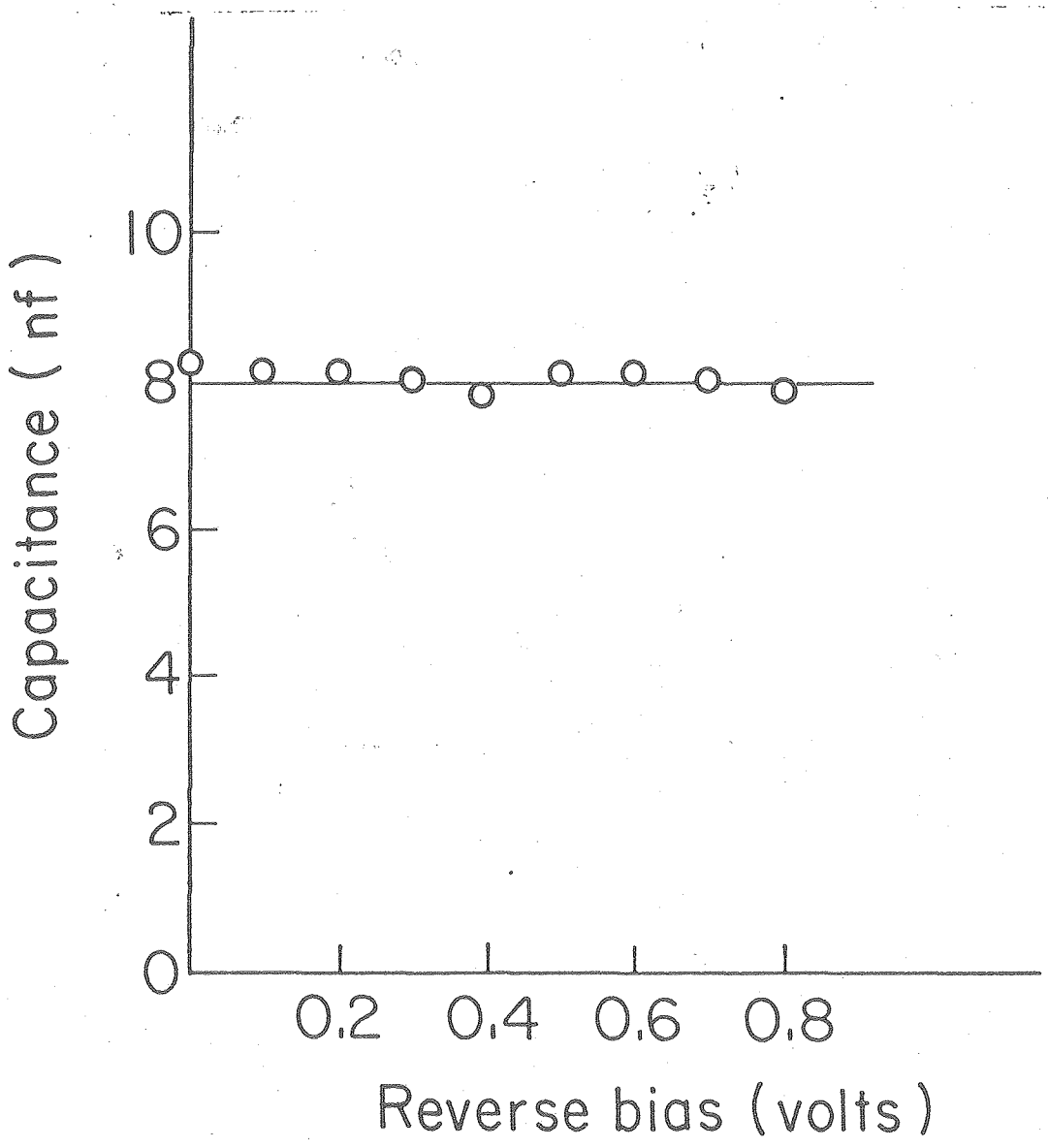

XBL796-4838

This result favors a model where all of the built-in voltage falls across the dye film and there is a virtual absence of band bending in the TiO_2 crystal as well. However, capacitance measurements at low frequencies, down to 10^{-1}Hz, on tetracene, Mg-phthalocyanine, and merocyanine indicate that there might be some band bending in the merocyanine due to a higher density of trapped charges near the interface.[41,11] Our dark J-V characteristics seem to support this model with a higher trap density near the interface than in the bulk but our bridge method did not allow us to measure the capacitance at sufficiently low frequencies.

3.6. Photovoltaic Action Spectrum

Fig. 23 shows the absorption spectrum of a 1000 angstrom merocyanine dye film on quartz and the photovoltaic action spectrum of a Au-merocyanine-TiO_2 cell with a 1000 angstrom film. For the action spectrum the light was incident on the TiO_2 crystal. The value of the photocurrent has been normalized by the relative photon flux at each wavelength and corrected for the optical density of the crystal. It can be seen that the photocurrent action spectrum essentially matches the absorption spectrum of the film.

Fig. 24 shows the absorption and photocurrent action spectra for a cell with a 2000 angstrom film of merocyanine with light incident on the Au overlayer. The spectrum has been corrected for incident photon flux. Illumination through the gold generates peaks in the action spectrum at wavelengths on the shoulders of the absorption spectrum. In addition the quantum yield is more than 2 orders of magnitude less than with illumination through the TiO_2. The polarity of the cell is

Figure 23. Short-circuit photocurrent, normalized to incident photon flux, for light incident on the TiO_2, and absorption spectrum of the merocyanine. The thickness of the merocyanine film was 1000 angstroms.

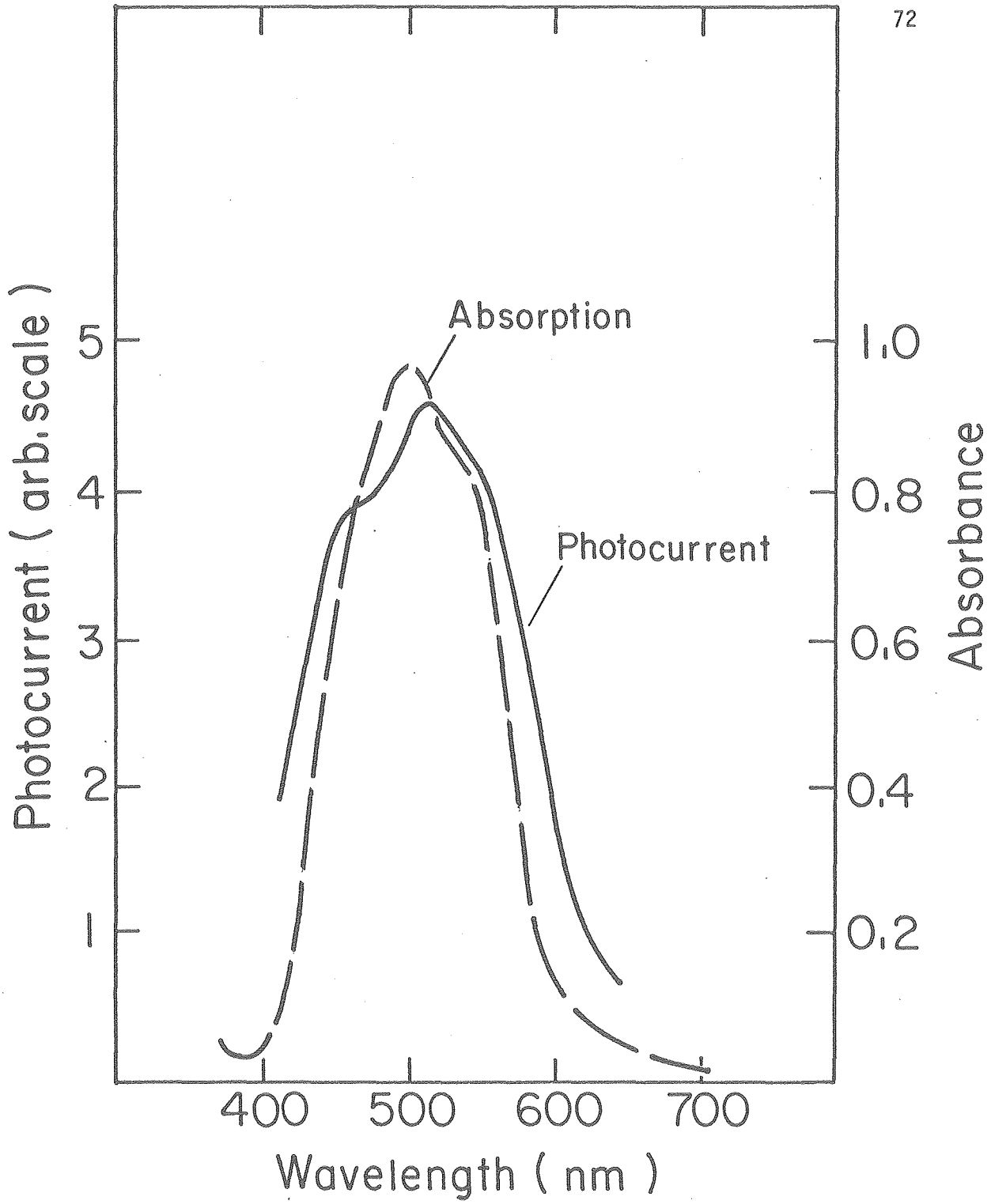
Absorption
Photocurrent
Photocurrent (arb. scale)
Absorbance
1
2
3
4
5
0.2
0.4
0.6
0.8
1.0
400
500
600
700
Wavelength (nm)

XBL797-4899

Figure 24. Short-circuit photocurrent and absorption spectrum with light incident through the Au electrode. The photocurrent was normalized to incident photon flux. The thickness of the merocyanine film was 2000 angstroms.

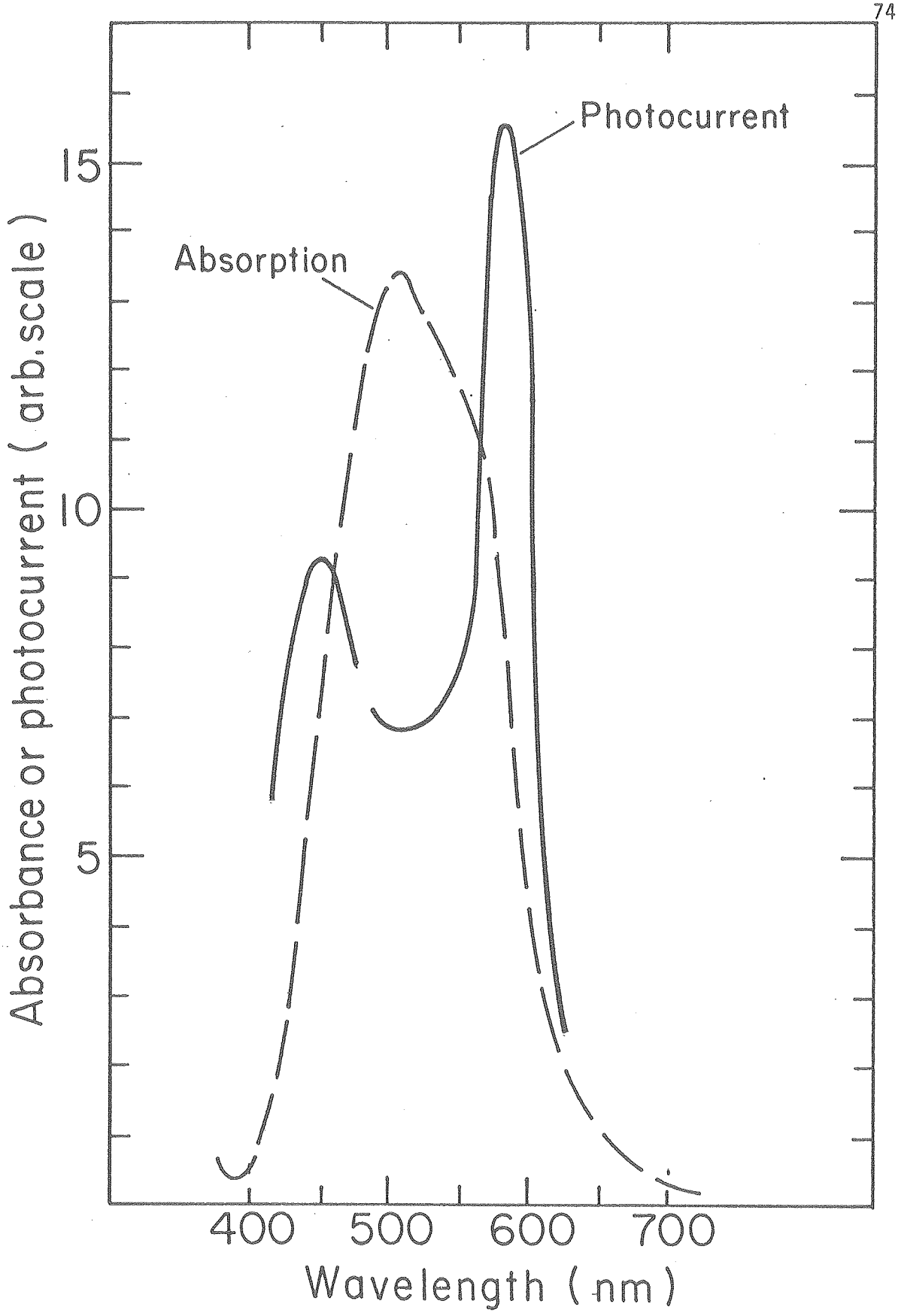
Photocurrent
Absorption
15
10
5
Absorbance or photocurrent (arb. scale)
400
500
600
700
Wavelength (nm)

XBL797-4892

the same regardless of which side is being illuminated. Such photocurrent action spectra where the action spectrum agrees with the absorption spectrum for light incident only through one electrode and with a local minimum near the peak of absorption for light incident through the opposite electrode have been observed for a number of organic systems.[1,2,4,9,11] This effect is not seen for very thin films where the absorption is essentially uniform throughout the dye layer. Fig. 25 shows the absorption spectrum and the action spectrum with light incident on the Au as well as the action spectrum with light incident on the TiO_2 for a cell with a 100 angstrom thick merocyanine film. As can be seen, they both essentially match the absorption spectrum of the merocyanine film. The absorbance was about 0.1 at the peak of the spectrum.

These results are in accord with a theory of the photoconductivity process, which will be elaborated below, where the photovoltaic activity is a surface effect. The photoconductivity is assumed to result from singlet excitons diffusing to the merocyanine/TiO_2 interface where they dissociate into electron-hole pairs which separate in the electric field across the dye layer in competition with geminate recombination. Only those excitons which migrate to the merocyanine/TiO_2 interface contribute to the photocurrent.

For light incident on the Au electrode, the higher the absorption constant the closer to the metal surface the excitons will be generated on the average where the quenching of the excitation is very efficient. For light with lower absorption constant, away from the peak of absorption, the excitons will be on the average generated closer to the merocyanine/TiO_2 interface where the charge separation

Figure 25. -·-· Absorption of merocyanine film. Δ - short circuit photocurrent with light incident through the Au electrode. O - Short-circuit photocurrent with light incident through the TiO_2. The thickness of the merocyanine film was 100 angstroms. The two photocurrent action spectra were normalized to incident photon flux.

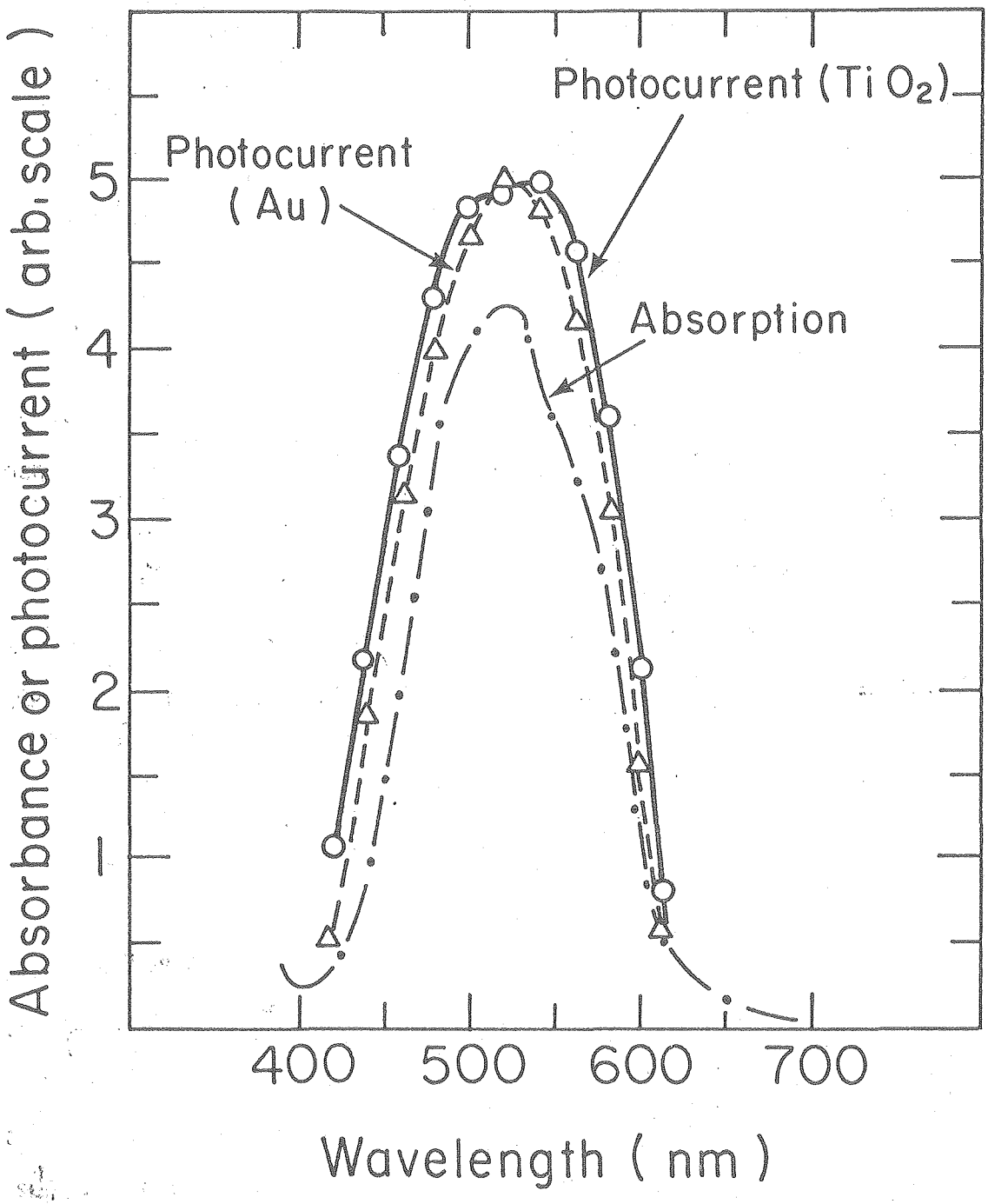
Photocurrent (Ti O_2)
Photocurrent
(Au)
Absorption
Absorbance or photocurrent (arb. scale)
1
2
3
4
5
400
500
600
700
Wavelength (nm)

XBL797-4893

takes place, and consequently a larger photocurrent results. A weak photovoltaic response is also seen for wavelengths of weak absorption because the penetrating light is not effective.

3.7. Photoconductivity of Merocyanines

3.7.1. Theory of Exciton Transport. In most inorganic semiconductors the generation of photocarriers is a simple process whereby the absorbed photon with energy greater than the band gap excites an electron-hole pair directly. In molecular crystals the generation is more complex. In general the photoconduction action spectrum is identical to the absorption spectrum. The absorption spectra of organic molecular solids can be understood in terms of Frenkel excitons which are described in the tight binding approximation.[25] The Frenkel exciton is an excited state of the molecular solid which closely resembles the molecular excited state. It can be a delocalized combination of states or a localized excitation characterized by hopping or 'diffusion' from site to site. The main characteristic of the Frenkel exciton is its correspondence with some molecular state as seen directly in a comparison of absorption and action spectra.

The size of the Frenkel exciton is comparable to lattice constants and is expected to have low mobility. This is what one typically finds in molecular solids where the mobility is usually less than 1 $cm^2V^{-1}sec^{-1}$. Because they are localized they also interact with molecular vibrations as well as lattice vibrations. The original exciton can produce charge carriers via several mechanisms.[26] The possible mechanisms include exciton-exciton interactions, interaction of excitons with free and trapped charges and defect states, and exciton-

surface processes. In addition charges result from direct production of electron-hole pairs.

A. Direct Process

The direct production of electron-hole pairs can be distinguished experimentally by the following properties:[26] (a) the photocurrent spectral response should not have the same general shape and absorption spectrum; (b) the quantum efficiencies for generation of electrons and holes should be equal and should be independent of electrodes and surface preparation. Our spectral response data rule out this process.

B. Exciton-Exciton Interaction

Carrier generation by exciton-exciton annihilation leads to a photocurrent varying as the square of the light intensity since the probability of carrier production increases with the square of the exciton concentration. This has been observed by Silver et al. for anthracene.[29] The light intensity data rule out such a process for merocyanine cells.

C. Interaction with Trapped Charges and Defects

In films which have been exposed to the atmosphere, oxygen will play a dominant role as an electron trap. O_2 molecules diffusing in primarily through defects in the films form O_2^- electron traps. The mechanism by which the O_2 molecule traps the electron is presumably one of direct contact between the exciton and the O_2 molecule leading to dissociation of the exciton and subsequent trapping of the electron by the O_2 and freeing the hole. This mechanism has been used to explain the increased photoconductivity of phthalocyanine films doped with oxygen.[30] In addition to the O_2 chemical traps, charges can also be

trapped at defect centers which are known to be abundant in molecular solids,[31] and contribute to exciton dissociation upon collision.

D. Exciton Surface Processes.

For merocyanine films, we have found that only excitons reaching the merocyanine/TiO_2 interface contribute to the photocurrent. In this section we review the theory of exciton surface processes. Experimental results for the Au-merocyanine-TiO_2 cells will be presented below.

Excitons can diffuse to the surface and dissociate upon collision with adsorbed oxygen, impurities, defects, and/or electrodes. The photocurrent resulting from the exciton dissociation will be linear in the light intensity since the process is monomolecular in nature. An analysis of exciton diffusion and surface interaction was carried out by Stekette and deJonge[27] and Mulder[28] for anthracene crystals and by Ghosh and Feng[11] for merocyanine.

One can obtain a quantitative relationship between the steady state photocurrent and the absorption coefficient by calculating the probability of an exciton reaching the surface by diffusion. It is assumed that the exciton has a certain mean lifetime (due to fluorescence and non-radiative transitions) and that its motion can be described as a free diffusion process. The exciton transport can then be described by the diffusion equation which in this system is essentially one-dimensional.

$$0 = \frac{\partial n(x)}{\partial t} = D \frac{\partial^2 n(x)}{\partial x^2} - \frac{n(x)}{\tau} + \alpha I_0 e^{-\alpha x} \qquad (3.7.1)$$

for the stationary state. Here n is the number of excitons at a distance x from the illuminated surface, D is the diffusivity, τ is

the mean lifetime of an exciton, α is the absorption constant, and I_0 the photon intensity of the incident light. The second term on the right represents recombination due to all processes and the third term generation of excitons. If we assume that all the excitons reaching the surface dissociate there, the boundary conditions become $n(0) = 0$ and $n(d) = 0$ where d is the thickness of the film. Solving equation (3.7.1) with these boundary conditions, we obtain[27]

$$n(x) = \frac{I_0 \alpha \tau}{1-\alpha^2 D\tau} \left\{ \exp(-\alpha x) + \frac{\exp(\frac{x}{L})[\exp(-\frac{d}{L})-\exp(-\alpha d)]-\exp(-\frac{x}{L})[\exp(\frac{d}{L})-\exp(-\alpha d)]}{\exp(\frac{d}{L})-\exp(-\frac{d}{L})} \right\} \tag{3.7.2}$$

where $L \equiv \sqrt{D\tau}$ is the diffusion length of the exciton.

The details of the interaction between the excitons and the surface electrode determines whether the exciton dissociation at the surface will lead to charge separation and a photocurrent. At the charge separating electrode, we assume that the photocurrent is directly proportional to the exciton flux at the surface, i.e. the quantum efficiency for charge generation is assumed constant,

$$\mathcal{J} = A \frac{\partial n(0)}{\partial x} \tag{3.7.3}$$

where the proportionality constant A depends on the nature of the electrode.

If we make the further assumption that $d > L$, then $\exp(d/L) >> \exp(-d/L)$ and we obtain for the photocurrent

$$\mathcal{J} = \frac{A}{D} \frac{I_0}{1/\alpha L + 1} \tag{3.7.4}$$

or

$$1/J = 1/J_{\infty} (1 + 1/\alpha L) = 1/J_{\infty} (1 + 0.434/\varepsilon L) \qquad (3.7.5)$$

where ε is the extinction coefficient defined by $I_x = I_0 10^{-\varepsilon x}$. From equation (3.7.5) we see that a plot of 1/J versus $1/\alpha$ should give a straight line.

3.7.2. Experimental Results. In Fig. 26 the reciprocal photocurrent, which has been normalized by the relative photon flux at each wavelength, is plotted versus the reciprocal absorption constant for wavelengths greater than 420nm. The thickness of the merocyanine film was 2000 angstroms. As can be seen, using a least squares approximation, a well-fitting straight line can be drawn. Using equation (3.7.5) the slope of the line and the intercept on the ordinate yield an exciton diffusion length of 79 angstroms. This is in fair agreement with Ghosh and Feng[11] who calculated a diffusion length of 60 angstroms.

If a similar calculation is performed on merocyanine films deposited on room temperature substrates yielding a photocurrent action spectrum corresponding to the absorption spectrum in Fig. 6, the data do not give a good fit to a straight line. A least squares calculation gives a negative intercept and therefore is of no value for the diffusion length. An explanation can be given in terms of the microcrystalline nature of such films. The microcrystalline interfaces can act as sinks for the excitons and the dissociation therefore generates charges in the bulk of the film. The built-in field which exists across the merocyanine film prevents complete geminate recombination of the electron-hole pair.

Figure 26. 1/J versus 1/α plot of short-circuit photocurrent for wavelengths greater than 420nm. The photocurrent has been normalized by the relative photon flux at each wavelength. The thickness of the merocyanine film was 2000 angstroms.

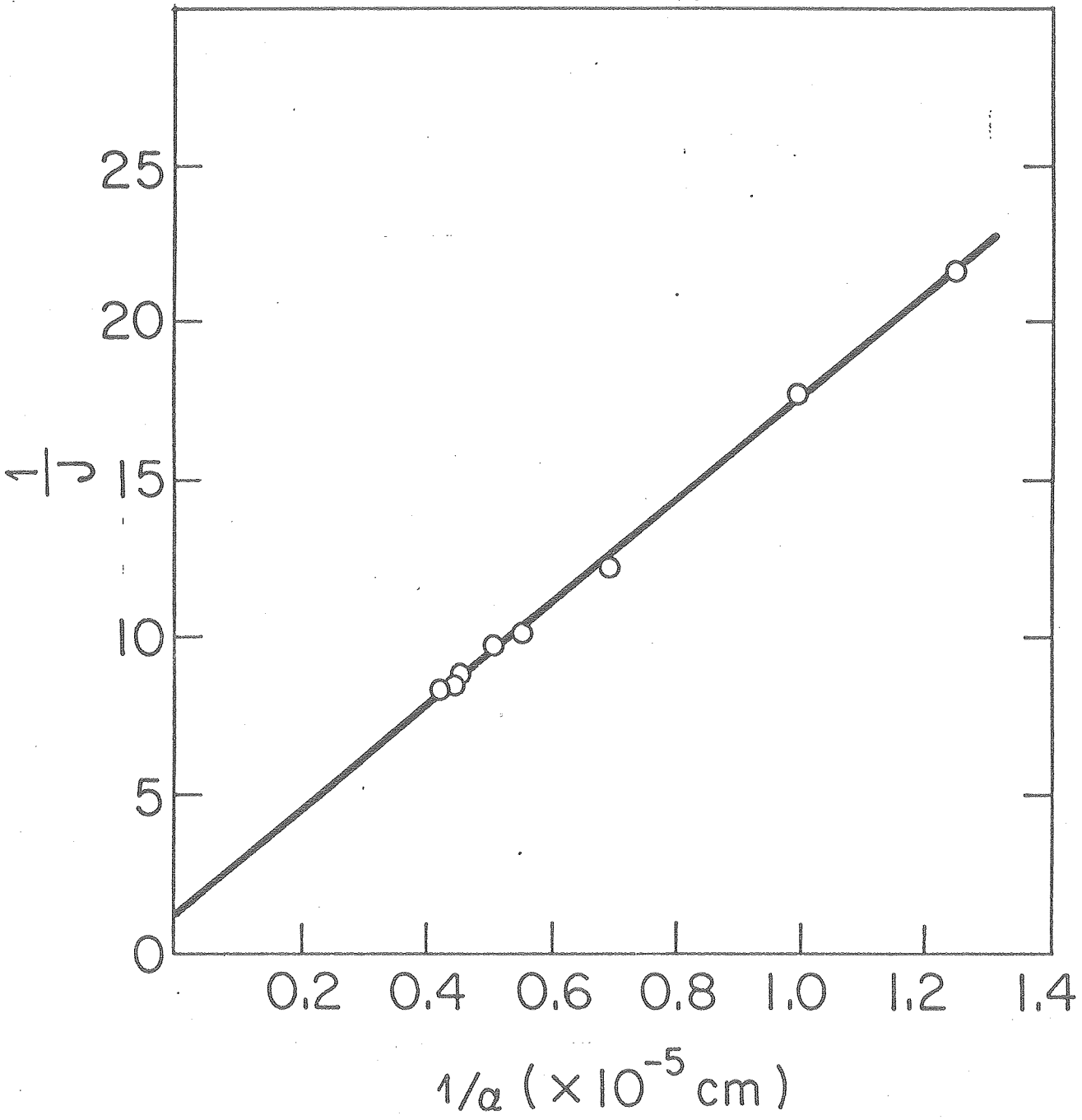

XBL796-4847

3.8. Field Dependence of the Quantum Efficiency

Fig. 27 shows the dependence of the photocurrent on an applied electric field. The cell is reverse biased, i.e. a positive potential is applied to the TiO_2. The dark current has been subtracted from the total current. The curve exhibits a knee followed by a sharp increase at about 0.75 volts for this particular sample with a 500 angstrom thick dye film. The voltage of the transition increases for increasing film thickness. The photocurrent at the knee corresonds to a quantum yield of about 15% where the quantum yield is defined as the number of charges generated per photon absorbed by the merocyanine film. With 1 volt or more applied bias, the quantum yield increases to more than 100%. The sudden increase in photocurrent must therefore be due to secondary charges injected by the electrodes. For thicker films a larger applied voltage would be required to produce the same internal electric field.

Our data support the theory that only excitons that reach the merocyanine/TiO_2 interface produce free charge carriers. The absence of charge generation at the merocyanine/Au interface can be the result of a combination of two different processes. Excited dye molecules in the immediate vicinity of a metal surface can be quenched very effectively via radiative and non-radiative interactions with the metal.[72-75] Secondly, the excitons which do dissociate will be lost to geminate recombination since the dissociation would not be at the surface itself but removed a certain distance corresponding to the effectiveness of the quenching.[75]

Fig. 28 shows the quantum yield as a function of the thickness of

Figure 27. Photocurrent versus applied reverse bias for a cell with a 500 angstrom merocyanine film under 520nm monochromatic illumination. The polarity of the TiO_2 was positive.

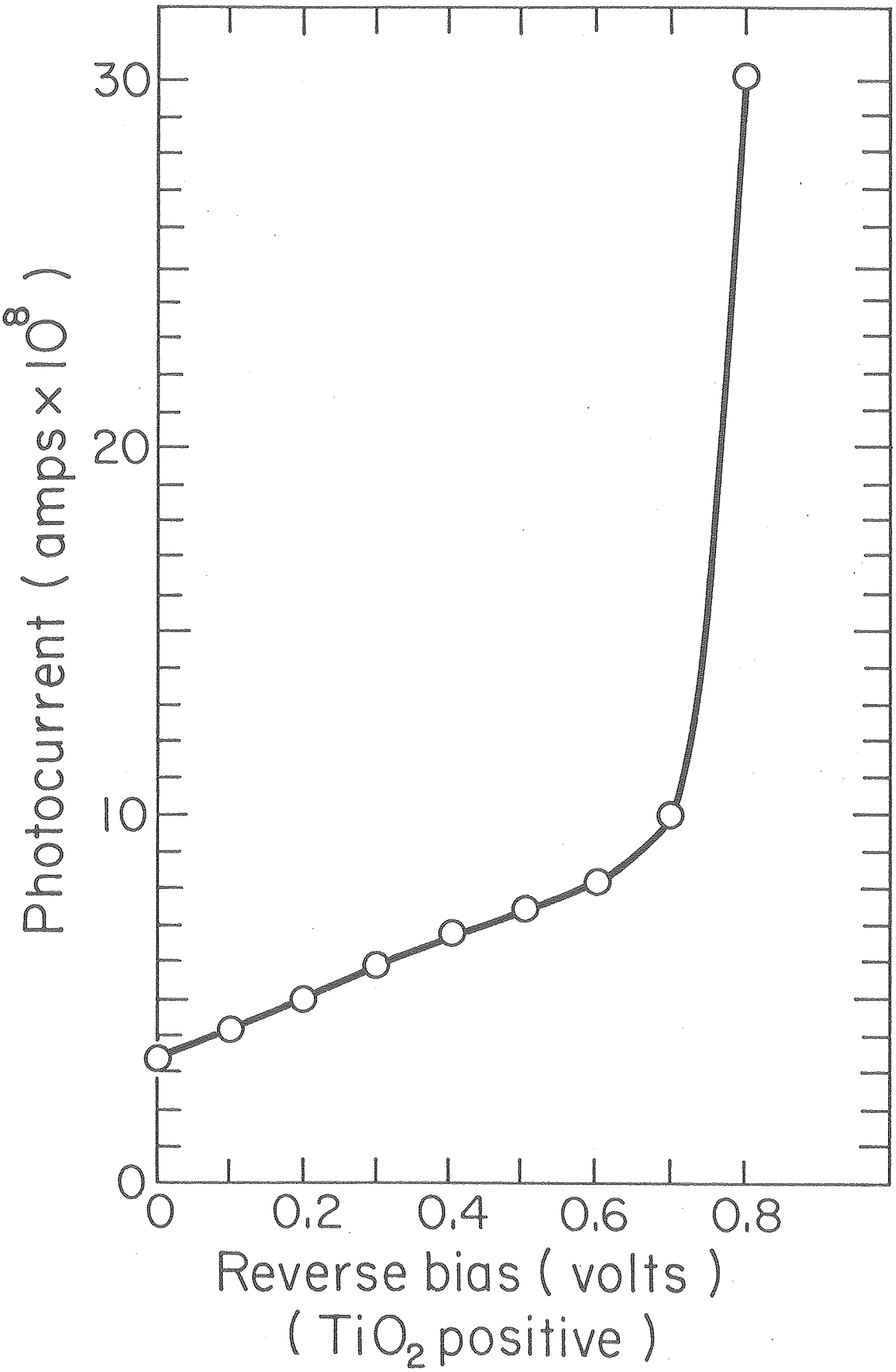
Photocurrent (amps x 10^{8})
30
20
10
0
0
0.2
0.4
0.6
0.8
Reverse bias (volts)
(TiO_2 positive)

XBL 797-4886

Figure 28. The quantum yield, measured as the number of electrons per photon absorbed by the merocyanine, is plotted as a function of the thickness of the merocyanine. The quantum yield was measured with monochromatic illumination at 520 nm in the short circuit mode.

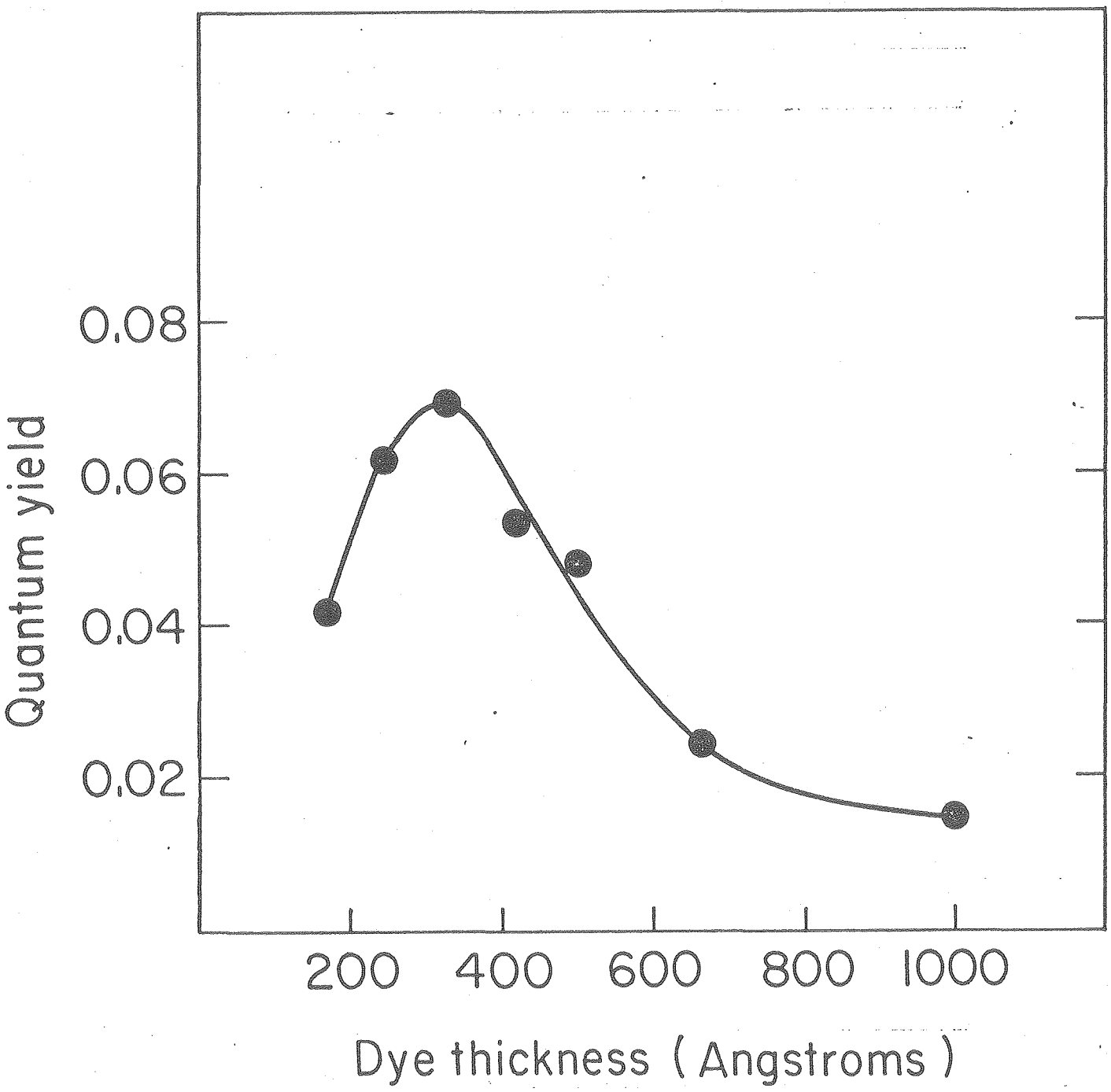
0.08
0.06
0.04
0.02
Quantum yield
200
400
600
800
1000
Dye thickness (Angstroms)

XBL796-4836

the merocyanine film. The measurements are recorded at the peak of the photocurrent action spectrum with light incident on the TiO_2. The decrease in quantum yield for thicker films is mainly due to the decrease of the electric field across the merocyanine as the film thickness increases. The decrease in efficiency when the film is less than about 350 angstroms we believe is due to the quenching of the dye excitation via interaction with the metal surface. This quenching effect takes place over distances typically of the order of 200-300 angstroms and is influenced by the introduction of a second partially reflecting mirror, in this case the merocyanine/TiO_2 interface.[75]

The field dependence of the photocurrent can be understood by application of a one-dimensional solution to the Onsager theory for geminate recombination as applied by Singh and Baessler to the Al-anthracene interface.[34] The Onsager theory considers the brownian motion of a charged partical under the combined action of an external electric field and the coulombic field of its counter charge.[35] In the Au-merocyanine-TiO_2 cells, the dissociation of excitons at the merocyanine/TiO_2 interface results in the injection of a free hole into the merocyanine with a negative image charge in the TiO_2 conduction band. In the course of correlated brownian motion both charges can either recombine or become separated. The orientation of the charge-image charge dipole is in this case always parallel to the direction of the applied field which is the built-in field due to the original difference in fermi levels in addition to any applied bias.

These results also suggest that one way to increase the effi-

ciency of cells of this type would be to choose metal-semiconductor combinations with larger differences between the electrochemical potentials than is the case for Au and TiO_2.

3.9. Open Circuit Voltage

The total potential drop across the junction region is determined by the difference between the work functions of the Au and the semiconductor. If the work function of Au is taken as 4.85 eV[37] and the work function of TiO_2 as 4.33 eV,[36] we get a built-in voltage, V_D, of 0.52 eV. We take the work function of the TiO_2 to be the same as the electron affinity of the crystal since the donor density is high (10^{18} cm^{-3}) and the fermi level consequently lies close to the conduction band. In principle V_{oc} should approach V_D under conditions of intense illumination. The highest open circuit voltage measured under monochromatic irradiation was 375 mV. The incident light intensity was about 0.1 $mW\text{-}cm^{-2}$.

The action spectrum of the open circuit voltage follows the absorption specturm of the merocyanine. Fig. 29 shows the open circuit voltage with monochromatic radiation at 520nm plotted as a function of the thickness of the merocyanine film. The figure also shows the equivalent curve for the short circuit current. As can be seen, the peak of the V_{oc} curve is reached for a larger thickness of the merocyanine film than is the case for the photocurrent.

The open circuit photovoltage is fixed at the point where the dark current caused by the forward biasing photovoltage exactly offsets the photocurrent. Unless some additional barrier against the flow of the dark current is introduced, one would expect the V_{oc} curve

Figure 29. Open circuit voltage with monochromatic illumination at 520 nm as a function of the thickness of the merocyanine film. The normalized short circuit current spectrum is retraced from Fig. 28 for comparison.

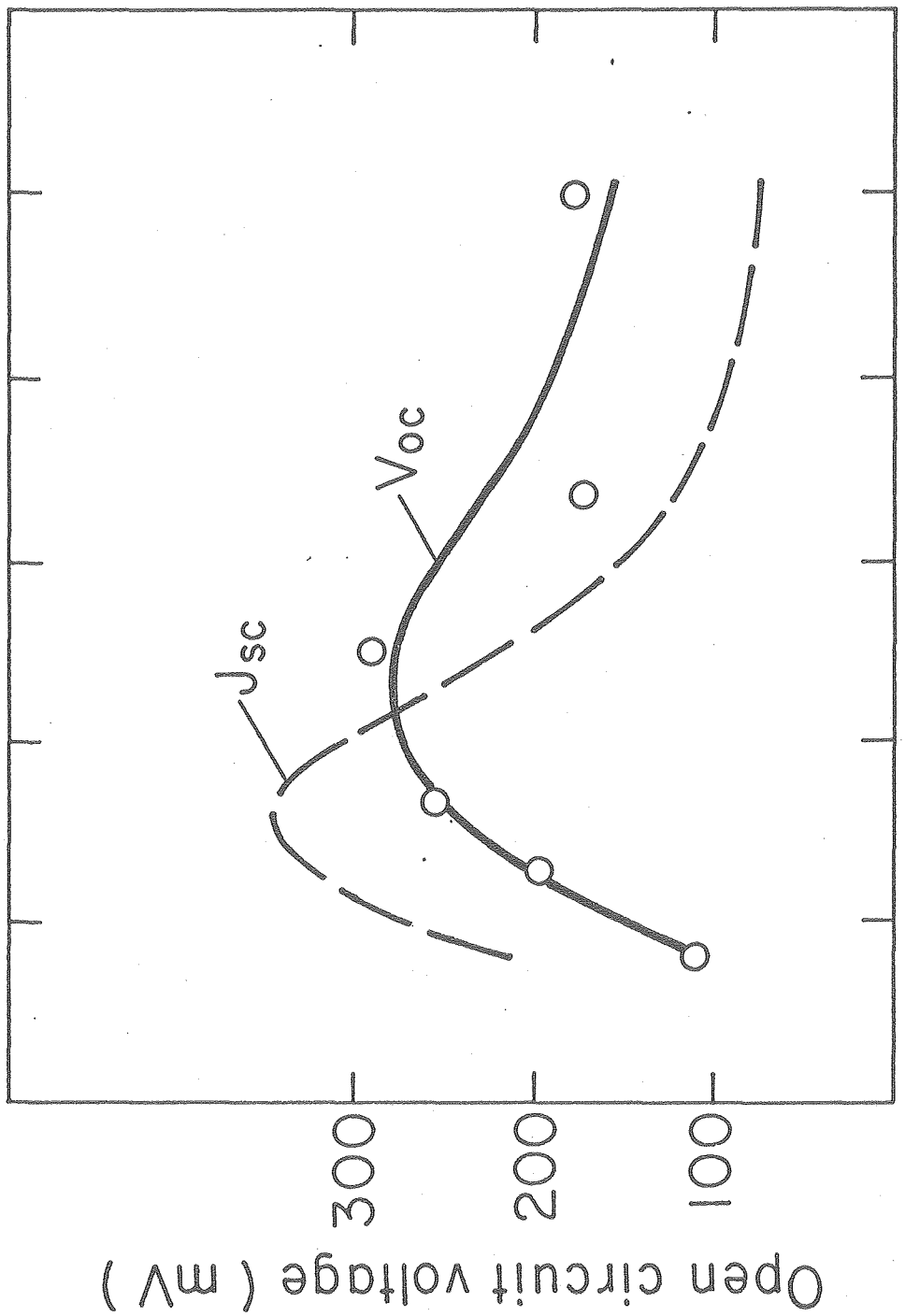
Open circuit voltage (mV)
300
200
100
Thickness of merocyanine (angstroms)
200
600
1000
V_{oc}
J_{sc}

XBL797-4900

to follow the photocurrent curve. The shift to larger thicknesses we believe is due to a barrier against the dark current formed by the introduction of the merocyanine film.

3.10. Energy Level Representation of Au-Merocyanine-TiO_2 Cells

Based on our data and using values for work functions and electron affinities in the literature, we can make a model of the Au-merocyanine -TiO_2 cell as shown in Fig. 30. The work function of Au is taken as 4.85 eV,[37] the electron affinity of the TiO_2 as 4.33 eV,[36] the ionization energy of the merocyanine film as 5.6-5.8 eV[45] and the electron affinity as 3.3-3.5 eV[45] corresponding to a 'band gap' of about 23 eV roughly equal to the energy of the absorption band in the visible end of the spectrum.

Undoped dyes are known to be insulators with resistivities of the order of 10^9 - 10^{13} ohm-cm.[45] Since the TiO_2 crystals have resistivities of the order of 1 ohm-cm we would expect that almost the entire voltage drop due to the difference in electrochemical potential (fermi levels) to fall across the merocyanine film. There would thus be a virtual absence of a depletion layer in the TiO_2 crystal. This is supported by our capacitance-voltage data which show that the cell acts as a simple capacitor with the merocyanine as a dielectric.

Other workers, however, have found a certain bandbending in undoped organic thin films due to higher density of trapped charges near the interfaces by performing capacitance-voltage measurements at low frequencies, down to 0.1Hz.[41] Although our dark current-voltage measurements indicate the presence of a larger density of electron traps near one of the interfaces, we cannot point conclusively to any evidence of "band bending" in the merocyanine phase.

Using this "band model" where the dye is pictured as an insulator depleted of mobile charge carriers, we can get some understanding of why the open circuit voltage as a function of the thickness of the merocyanine film increases beyond the point where the photocurrent begins to decrease. ΔE_c represents an energy barrier against the forward biases dark current (Fig. 30). The electrons flowing from the TiO_2 conduction band due to the forward biasing of the photovoltaic mode, will have to surmount that barrier. There is also the possibility of electron transport via states in the merocyanine "band gap" possibly associated with the triplet level of the dye molecules. As the thickness of the dye film increases, the barrier would become more effective and the open circuit voltage will increase. The competing tendencies of decreasing photocurrent generation which will lead to a lower output voltage, and increasing dye resistance to the dark current which will result in a higher output voltage, produces a maximum beyond which the photon voltage begins to decrease.

3.11. Relevance of Band Model

We have been working with the assumption that band theory is at least approximately applicable to organic semiconductors. Although energy "bands" may not exist in a strict sense, numerous results in the literature attest to the usefulness of an analysis based on narrow conduction and valence bands for describing photoelectric devices based on organic solids.[1-11] Our analysis of the Au-merocyanine-TiO_2 cells is not dependent on there being actual energy bands present. For an analysis of the data we have presented the bands can be thought of as a way to represent the internal electric field in the merocyanine

Figure 30. Energy level representation of a Au-merocyanine-TiO_2 cell before (a) and after (b) contact respectively.

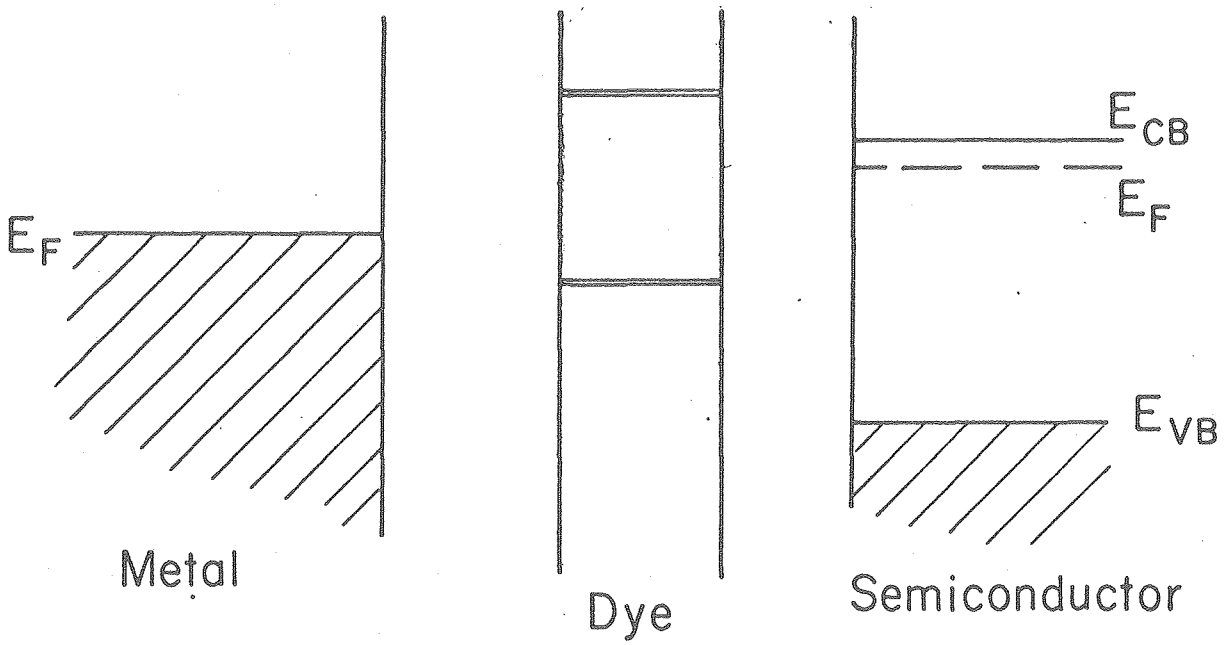

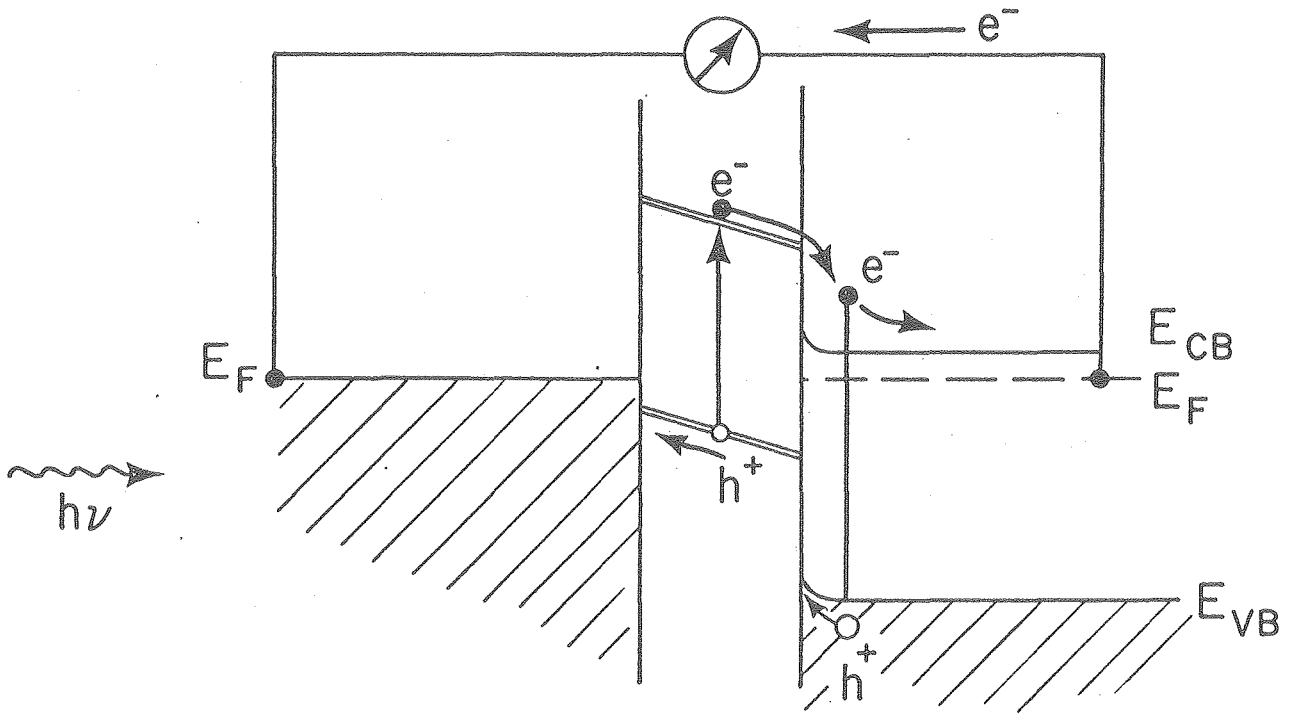

Energy levels under short circuit current condition

XBL 791-4616

phase.

The band widths of organic solids, where the overlap integrals are determined by Van der Waals interaction, are so small (of the order of kT) that when specimens are polycrystalline or amorphous the overall transport process will be that appropriate to a localized carrier treatment. A covalently bonded semiconductor can be viewed as one large "extended" molecule. A molecular solid represents almost the opposite limit of a small unit in a weakly interacting aggregate. The overlap integrals of the wavefunctions are small and the bands are consequently narrow and susceptible to internal potential fluctuations. The hopping model of conductivity considers carrier motion proceeding directly from one localized state to another based on the quantum mechanical transition rates between localized sites.[43] In molecular solids the excitation tends to remain localized. Therefore, the generation of free carriers involves both external electric fields and internal attractive coulomb fields.

The necessity for considering hopping as a mechanism for charge carrier motion arises from considerations of the mean free path in organic solids. A carrier of effective mass m and mobility μ has a mean free path L given, at ordinary temperatures, by the approximate relation[44]

$$L \cong 10^{-8}\mu(m/m_0)^{1/2}\text{cm}$$

where μ is the mobility in units of $cm^2volt^{-1}sec^{-1}$ and m_0 the free electron mass. In most molecular solids values of μ are generally less than 5 $cm^2volt^{-1}sec^{-1}$ so that the mean free path, calculated from mobility data, is then of the order of 0.1 to 1 angstrom. This is

appreciably less than the lattice spacing in a molecular crystal. It then becomes questionable whether the band theory notion of a mean velocity of the carriers can be applied.

The idea that band theory may be applied to organic materials in the form of pure single crystals is, however, supported by data presently available,[26] although its applicability to polycrystalline and amorphous molecular solids remains questionable.

Chapter 4

Doping of Merocyanine Films with Iodine

4.1. Introduction

The investigation into the effect of doping the merocyanine film with iodine, which is a strong electron acceptor, was initiated because of two considerations.

As the capacitance-voltage measurements show, the high resistance in the merocyanine film precludes any band bending in the semiconductor substrate. This is supported by data on photocarrier generation using UV light strongly absorbed by the TiO_2. The quantum yield for photocarrier generation, as measured by the number of charge carriers per incident photon, was about 1%. In a Schottky barrier configuration, with band bending in the semiconductor providing a charge separating field, the quantum yield can be expected to be close to 100%. This lack of an electric field inside the semiconductor can also be expected to adversely affect the charge separation in that the electron injected into the semiconductor conduction band has less probability of being swept away to prevent geminate recombination. In a device relying on charge carrier generation in the semiconductor as well, it becomes necessary to increase the conductivity of the dye phase so as to allow an electric field across a semiconductor depletion region.

The second source of motivation comes from numerous reports in the literature of sharp increases of photoconductivity as well as dark conductivity of organic solids doped with electron acceptors.[63-66] Intentionally doping semiconductor materials with trace impurities in order to alter photoelectronic properties is used extensively and is

well understood in inorganic solar cell technology. For organic systems, on the other hand, the complex relationships between dopant types and concentrations and photoelectronic properties are just beginning to be studied. Dramatic changes in the photoconductive properties of p-type organic solids have been reported. As much as four orders of magnitude increases in the photoconductivity of phthalocyanine surface cells with a layer of iodine added has been reported.[64]

The original work on doping with electron acceptors used a surface cell technique whereby the conductivity of a two-layer system with a layer of the acceptor species deposited on top of the material to be investigated, was measured along the film.[63-66] There was no attempt made to determine whether the acceptor species diffused into the substrate or whether the effect was purely a surface effect.

4.2. Experimental

Because of the high vapor pressure of iodine, its employment in high vacuum necessitates the deposition on cooled substrates. Iodine films deposited onto room temperature substrates come off under high vacuum in a matter of a few minutes. Since iodine doping of dye films is a reversible reaction, the iodine can be completely removed by pumping in vacuum, it becomes necessary to cool the dye film to prevent the iodine from escaping while the cell is being prepared.

The best results to date have been achieved with the following technique: prior to the sublimation of the iodine, the TiO_2 crystal is exposed to iodine vapor at room temperature and atmospheric pressure for about 15 minutes. This leaves a visibly brown film on the surface. The crystal is then quickly cooled to liquid nitrogen temperature with the substrate cooling system as the vacuum is being pumped

down to prevent moisture in the air from condensing on the surface. The brown iodine film will remain on the surface in a vacuum of 10^{-5} torr for as long as is necessary to prepare the cell. The merocyanine is then sublimed on top of the iodine film at at rate of about 2 angstroms per second from a crucible held at approximately 220°C. The substrate could then be heated to room temperature followed by deposition of the Au film or heated after the Au film was deposited. Standard photovoltaic measurements were then made on the cell. The cell was subsequently placed in vacuum and heated to 60°C for 30 minutes followed by photovoltaic measurements. This was repeated several times until a maximum value was reached for the photovoltaic response. The idea was to use the increased diffusivity of iodine at elevated temperatures to attempt to diffuse the I_2 throughout the dye film.

4.3. Results and Discussion

4.3.1. Transient Response. Fig. 31 shows the short circuit current and open circuit voltage transients for a typical iodine doped cell. The J_{sc} transient is dramatically different from that of the undoped cells. The rise time as well as the decay time are now limited solely by the response of the recorder whereas the rise time of undoped cells is typically of the order of tens of seconds reaching a steady state. This is sometimes followed by a slow decay to a level about 20% lower than the peak with a time constant of the order of an hour. The slow decay for doped cells is always present and has a time constant of the order of minutes also resulting in a level approximately 20% lower than the peak transient. The exact numbers vary slightly

Figure 31. Short-circuit current and open circuit voltage transients for a cell with a 500 angstrom merocyanine film doped with iodine. The light was incident through the TiO_2.

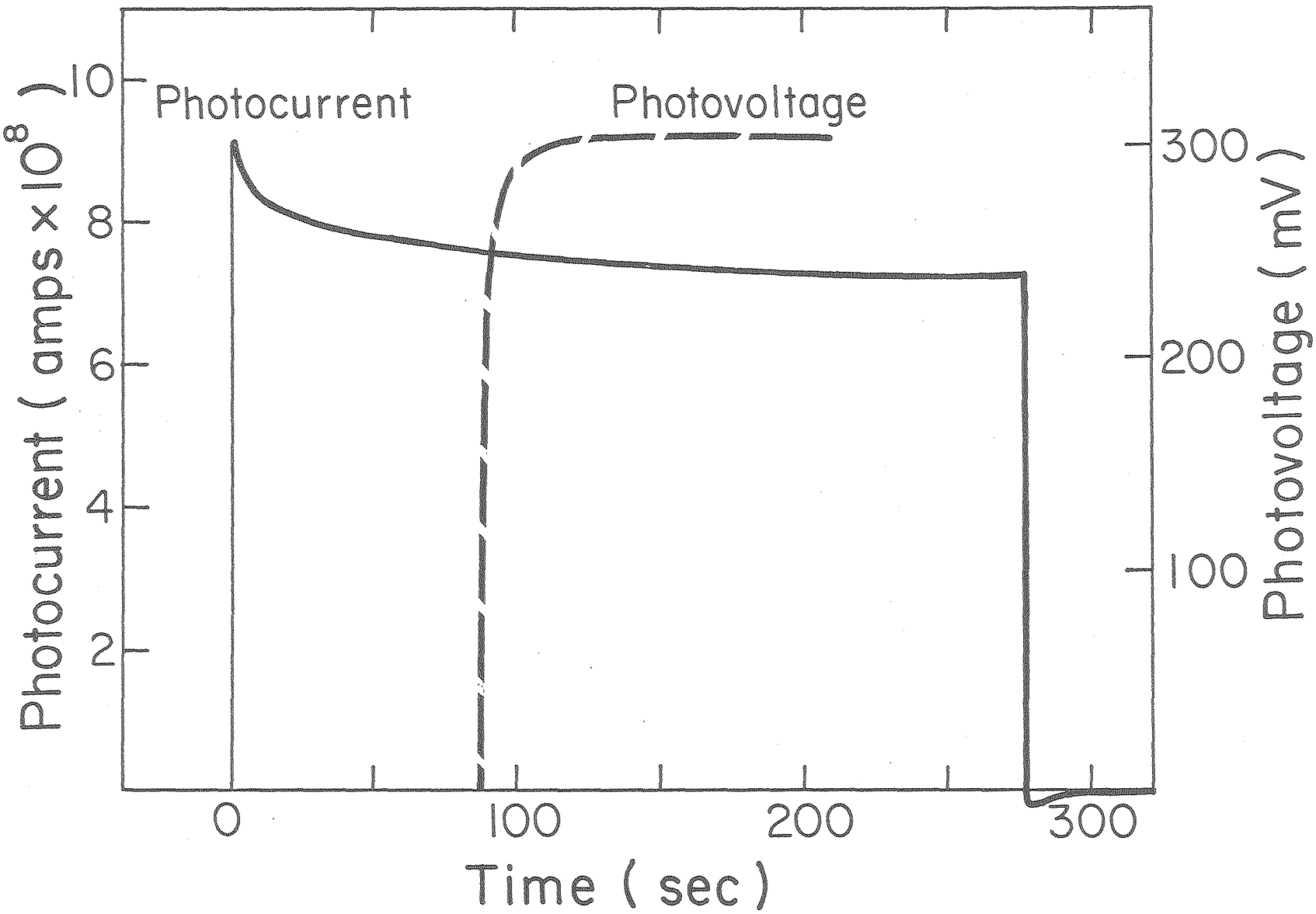
Photocurrent
Photovoltage
Photocurrent (amps x 10^8)
Photovoltage (mV)
Time (sec)
10
8
6
4
2
300
200
100
0
100
200
300

XBL797-4901

from cell to cell depending upon its history. On switching off the light the decay results in a small reverse current indicating the presence of capacitive charging effects.

The open circuit voltage also exhibits a faster rise and decay time for the doped cells, the change being less dramatic because the response in this case is limited by the large time constant of the measuring circuit, the resistance in the open circuit mode being about 10^{14} ohms.

4.3.2. Action Spectra. The action spectrum of the short circuit photocurrent is shown in Fig. 32 for a cell with a 500 angstrom thick merocyanine film doped with iodine with the technique described below. The cell had been heat treated in vacuum for 1 1/2 hours. With further heat treatment in vacuum the cell reverts to undoped behavior. This indicates that the vacuum treatment indeed does make the iodine diffuse through the merocyanine film and also through the 200 angstrom thick Au film.

As can be seen, the shape of the action spectrum changes only slightly upon doping. The quantum efficiency increased by approximately a factor of 3, from 4% to about 12%. Increases by as much as a factor of five have been noticed on some films. The open circuit voltage increased usually by much less; the best result represents an increase by a factor of 1.8 with a 500 angstrom merocyanine film. The effect of the doping was more pronounced for thinner films (500 angstroms and less) than for thicker films (1000 angstroms and thicker). The results, however, were difficult to reproduce better than to within a factor of two.

Figure 32. Short circuit photocurrent action spectrum for a cell with a 500 angstrom merocyanine film doped with iodine and a cell with a 500 angstrom undoped film. Also shown is the absorption spectrum of the undoped film.

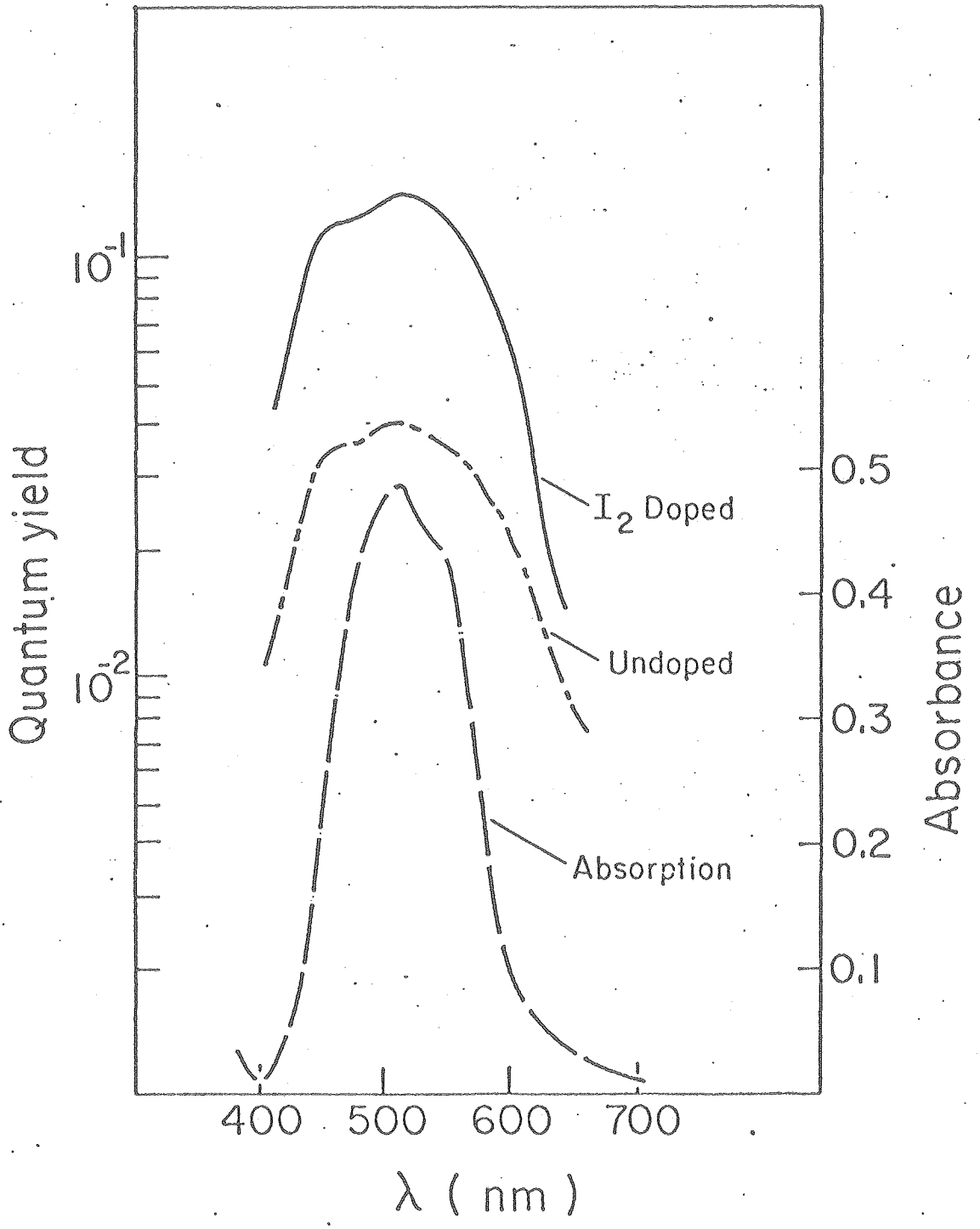
Quantum yield
10^{-1}
10^{-2}
I_2 Doped
Undoped
Absorption
0.5
0.4
0.3
0.2
0.1
Absorbance
400
500
600
700
λ (nm)

XBL796-4840

In order to investigate the hypothesis of charge carrier generation via exciton-surface processes, we have plotted the reciprocal short circuit photocurrent, normalized to incident photon flux, versus the reciprocal absorption constant for a cell with a 2000 angstrom thick merocyanine film in Fig. 33. On the same graph is also shown the results for an undoped cell. As can be seen, the values do not give a good fit to a striaght line. An attempt to obtain a least squares fit for a straight line yields an exciton diffusion length of 2300 angstroms. This is an unreasonable number, since the diffusion length in very pure anthracene crystals is about 600 angstroms.[28] This indicates that a different charge carrier mechanism may be operative.

The increased dark conductivity of doped films would be expected to result in a larger degree of band bending in the semiconductor substrate and therefore more efficient charge generation by intrinsic absorption of photons with energy larger than the band gap. This has indeed been noticed and increases by about a factor of three were observed on some cells.

The improved efficiency, however, degraded slowly with time. The doped films, on standing overnight under ambient atmospheric conditions, reverted to their undoped behavior.

The vacuum heat treatment shows that there is an optimum dopant concentration. When the cells are too heavily doped the photovoltaic properties were completely degraded. The exact amount of doping or the doping profile in the merocyanine films was not measureable.

4.3.3. Photovoltage-Photocurrent Characteristics. Fig. 34

Figure 33. $1/J$ versus $1/\alpha$ plot of short circuit photocurrent for a cell with a 2000 angstrom iodine doped merocyanine film. Also shown is the plot for an equivalent cell with an undoped film, retraced from Fig. 26.

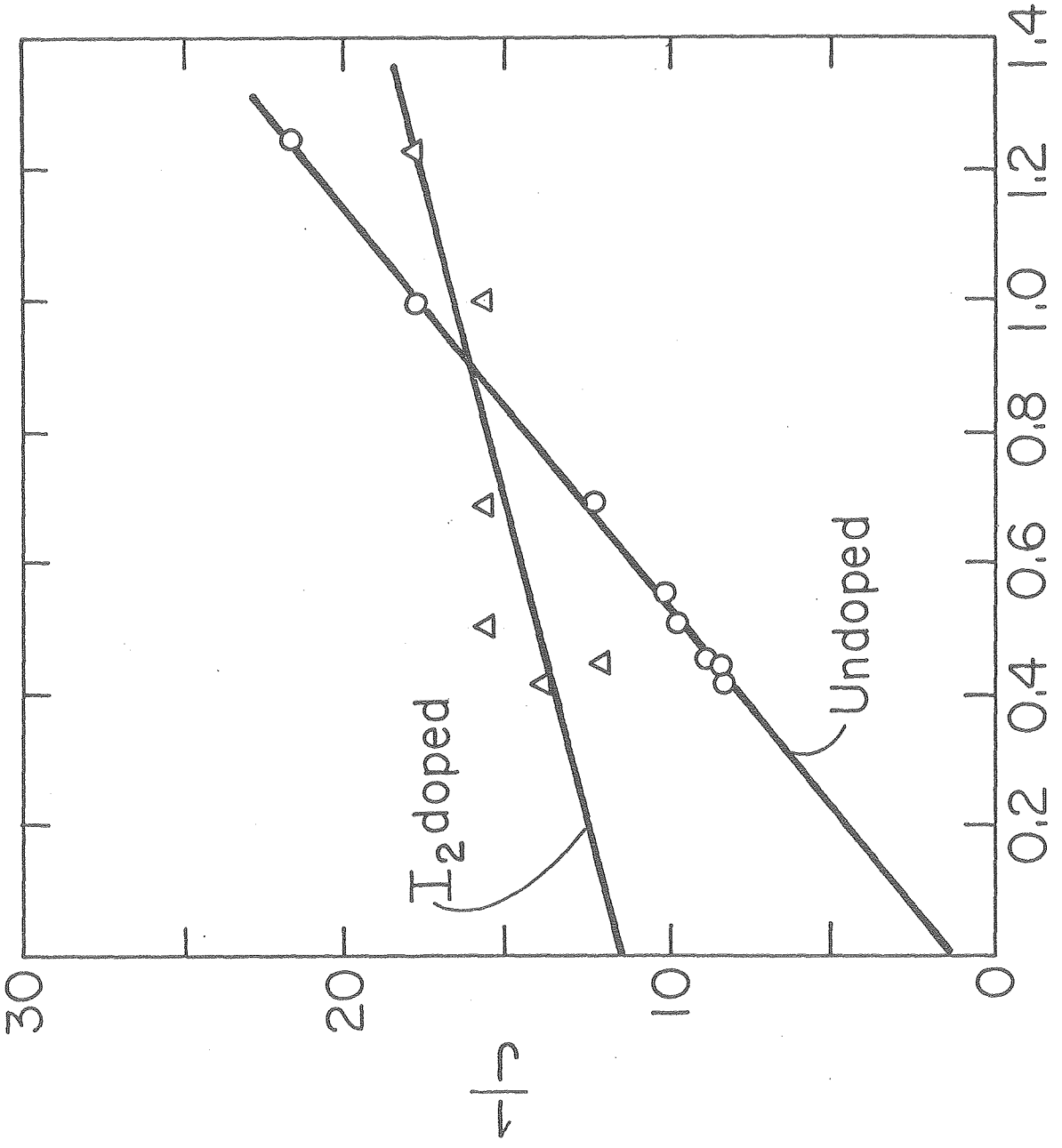

XBL797-4902

Figure 34. Photovoltage-photocurrent characteristics for a cell with a 500 angstrom merocyanine film doped with iodine and a cell with a 500 angstrom undoped film.

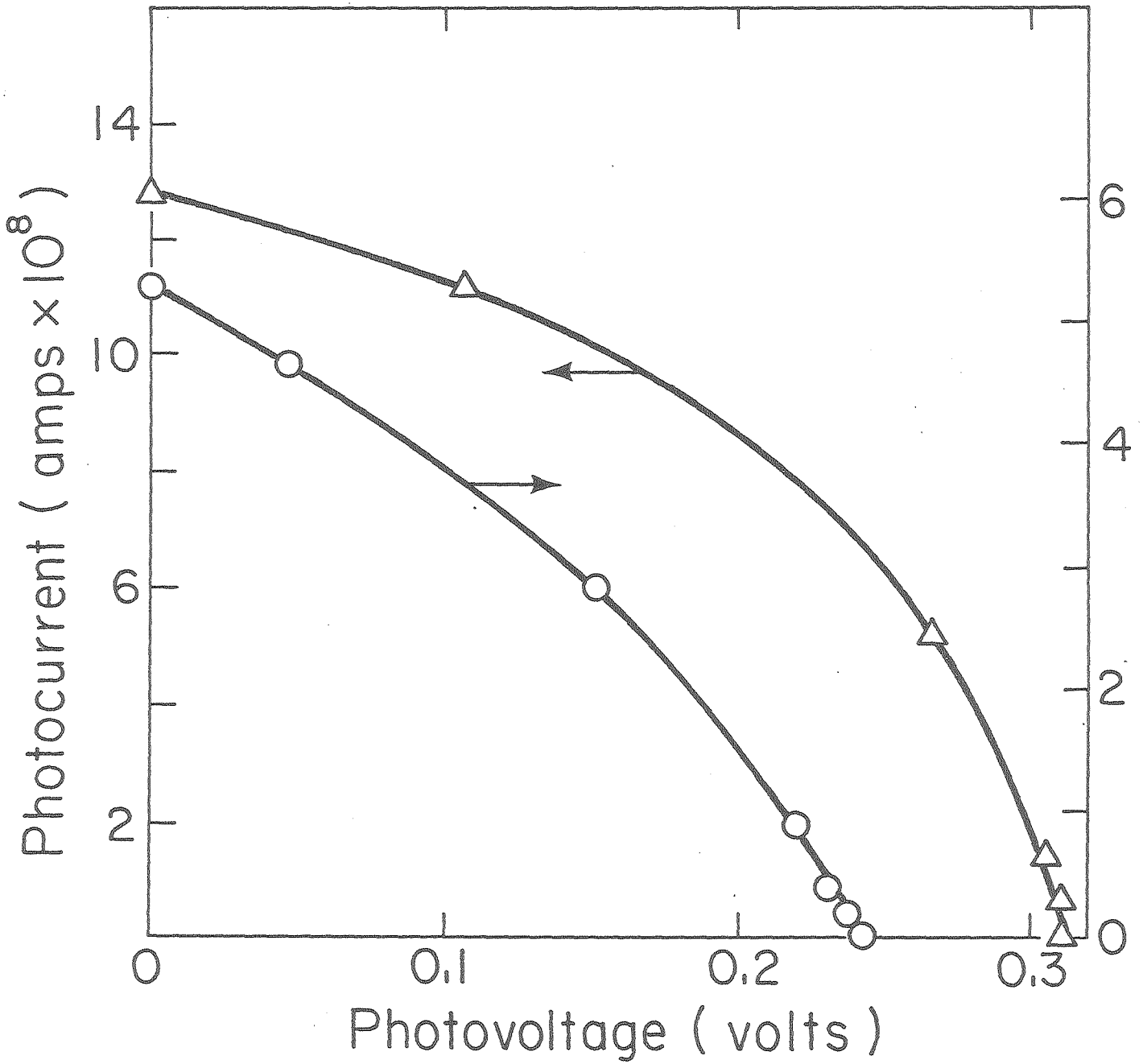
Photocurrent (amps x 10^{8})
14
10
6
2
6
4
2
0
0
0.1
0.2
0.3
Photovoltage (volts)

XBL797-4884

shows the J-V characteristics in the photovoltaic mode of a Au-merocyanine-TiO_2 cell with a 500 angstrom I_2 doped film. The J-V curve for an undoped film is also shown for comparison. The curve is obtained by varying the load resistance at a constant light intensity at 520nm.

Besides the increases in J_{sc} and V_{oc} the curvature of the cell also changes. This leads to an increase in the fill factor from 0.35 for an undoped cell to 0.44 for the I_2 doped cell. The maximum power output from this cell occurs with a load resistance of about 5×10^6 ohms and is about 2×10^{-8}W. The incident light power on the active cell area was about 5×10^{-6}W. This yields a monochromatic power conversion efficiency of about 0.4% which is an increase by a factor of four relative to undoped cells.

4.3.4. Discussion. The improved response of cells with better conducting merocyanine films was demonstrated with the iodine doping experiments. Increases in the photocurrent response by as much as a factor of five with monochromatic irradiation were observed. The doping with iodine had the potnetial for both enhancing the conductivity of the films by introducing partial charge transfer or mixed valence states and for providing favorable surface state band bending which could lead to higher output voltage. The concept of partial charge transfer has been used to explain doping effects in molecular conductors[65-69] and in conductive polymers.[70,71] Raman studies of iodine doped polyacetylene[70] and phthalocyanines[66] have identified the presence of I_3^- as the dominant species resulting in charge transfer from the organic state to the iodine as an acceptor. The charge transfer need not be complete. The resulting hole is weakly bound

to the acceptor ions by the coulombic potential, forming acceptor states in the gap. Thermal activation out of the bound states results in carriers for transport. PHotocarriers in doped films could result from collision of singlet excitons with acceptor-hole complexes resulting in activation out of the bound states and recombination of the exciton. The charge carrier generation therefore changes to a bulk process.

The greatly decreased rise and decay time constants of the photocurrent and photovoltage response indicate that the iodine presence fundamentally changes the nature and concentration of trapping states in the merocyanine. The continued presence of the slow decay with a decreased time constant of the photocurrent to a level about 20% lower than the peak value indicate that it may be a surface controlled capacitive charging effect. The absence of a reverse current upon turning off the light in the case of the undoped films can be explained by the large time constant of the decay dominating the reverse capacitive discharge, the two being separate processes.

Despite the preliminary nature of these experiments, it is clear that increases in efficiency of at least five fold can readily be obtained. It is hoped that a better understanding of donor-acceptor complexes and other dopants could result in even higher potential efficiency increases.

Chapter 5

Quenching of Dye Excitation at the Metal Surface

5.1. Introduction

In section 3.8. we discussed the quenching of an excited dye molecule in the immediate vicinity of a metal surface. We showed that the quantum efficiency for photocarrier generation drops for thicknesses of the merocyanine films less than about 350 angstroms (Fig. 28). We now proceed to investigate this effect in more detail.

The influence of a metalic mirror on an excited molecule in its vicinity has been extensively studied during the past few years. Drexhage et al.[72-74] performed extensive measurements of the lifetime of a molecular emitter as a function of its distance from the mirror. Using fatty-acid monolayer assembly techniques they measured the fluorescence lifetime of Europium complexes using Au, Cu, and Ag mirrors. Chance et al.[75] developed a general model for energy transfer between a molecular emitter and a metallic absorber which is exact within the classical framework. Based on Sommerfeld's early work on radio wave propagation near the surface of the earth,[76,77] they calculated the magnitude of the Poynting vector in the dielectric surrounding the dipole.

They found that for large distances (greater than about 2000 angstroms) from the metal surface the fluorescence lifetime oscillated as a function of the distance while for small distances (less than 200-300 angstroms) the lifetime went monotonically to zero. The oscillations are expressed quantitatively as arising from the interference between the reflected wave and the initial wave. The decrease

at small distances is due to non-radiative energy transfer to the metal. The states of the metal that accept the energy are the surface-plasmon modes of the metal-dielectric interface.[75,78] The nature of the oscillations and the energy transfer at intermediate distances vary from metal to metal. For Au the lifetime increases monotonically up to about 2000 angstroms. Killesreiter[81] studied the sensitized charge transfer efficiency of an excited oxacarbocyanine dye adsorbed on the surface of a molecular crystal of p-chloranil with Al as an evaporated counter electrode. By sandwiching arachidic acid monolayers between the dye and the aluminum electrode he was able to determine the photocurrent response as a function of the distance between the dye and the metal surface and found a quenching effect for separations less than about 200 angstroms.

We decided to investigate this quenching effect on the merocyanine film by introducing a "spacer" of varying thickness between the merocyanine and the Au electrode. The spacer would necessarily have to be a hold conductor for the photogenerated hole carriers in the merocyanine film. Perylene was chosen because it is known to be a p-type conductor with an ionization energy of 5.33 eV[82] which is sufficiently less than the ionization energy of the merocyanine, 5.6-5.8 eV.[45] A model of the energy level diagram can then be schematically represented as in Fig. 35.

If instead of perylene we substitute a dielectric with a high ionization energy, we would expect a blocking contact against the flow of charge carriers to result. Since the ionization energy increases with the decrease in the number of ring systems of the

Figure 35. Energy level representation of a Au-perylene-merocyanine-TiO_2 cell under short circuit current condition.

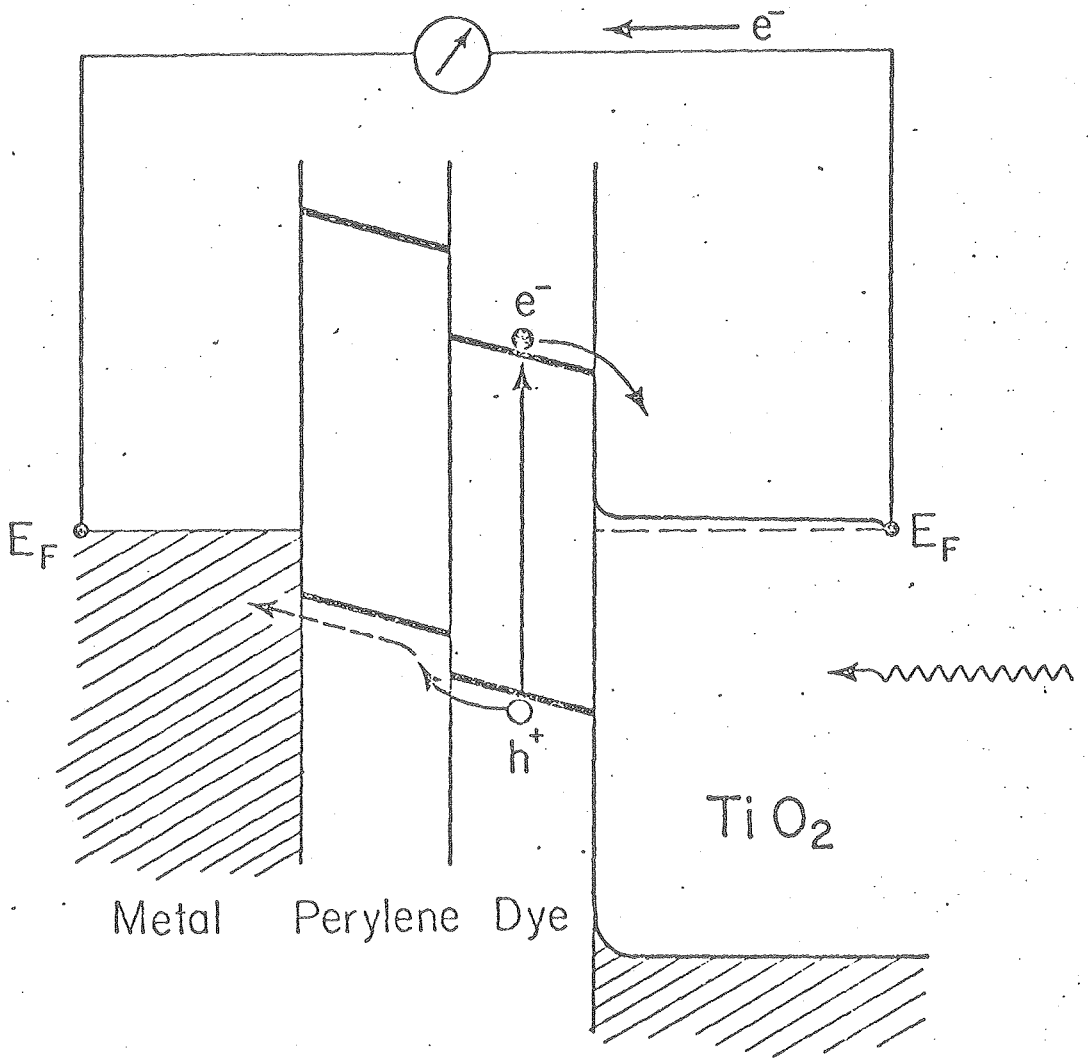

XBL 796-4833

molecule,[45] di-tert. Butyl Hydroquinone was chosen. A compound with hydrocarbon chains was chosen because of its lower vapor pressure as compared to the unsubstituted molecular species.

5.2. Experimental

Perylene was purchased from Aldrich Chemical Company and 2,5 di-tert. Butyl Hydroquinone (BQH) from Eastman Kodak Company. Both were used without further purification. The chemical structure of the two compounds is shown in Fig. 36. The cells were made by sequential sublimation from molybdenum boats in a vacuum of about 10^{-5}torr. The temperature of the perylene powder was held at about 180°C and the BQH at about 110°C. The deposition rates were 2 angstroms per second. BQH, because of its high vapor pressure, required the substrate to be cooled to liquid nitrogen temperatures. The perylene films were deposited onto room temperature substrates. The thicknesses of the films were measured with a quartz crystal monitor which was calibrated with a multiple interference microscope.

5.3. Results

The perylene films were smooth and glassy in appearance and were transparent in the visible when deposited onto room temperature substrates (Fig. 37). The characteristic absorption bands of the free molecule in solution disappears in the film. This was also observed by Kamura et al.[83] and attributed to a dichroism effect on microcrystals with a preferred orientation.

Fig. 38 shows the effect of the perylene layer on the photocurrent response for a cell with a 200 angstrom merocyanine film.

Figure 36. The chemical structure of perylene and 2,5 di-tert. Butyl Hydroquinone used in making the photovoltaic cells.

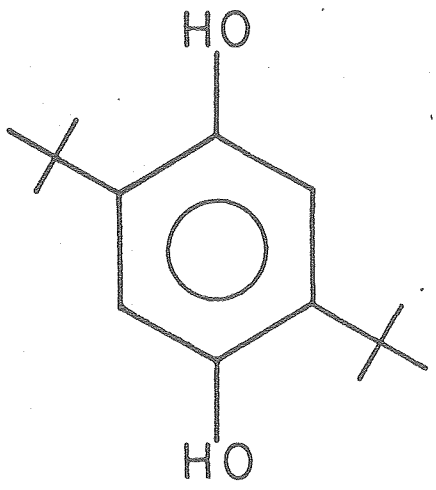

2,5 di-tert. Butyl Hydroquinone

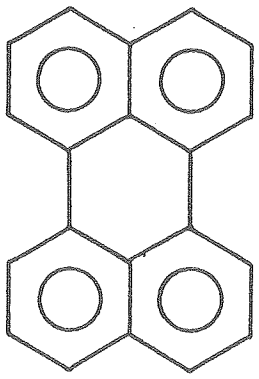

Perylene

XBL797-4894

Figure 37. Absorption spectrum of perylene in benzene solution and a perylene film on quartz.

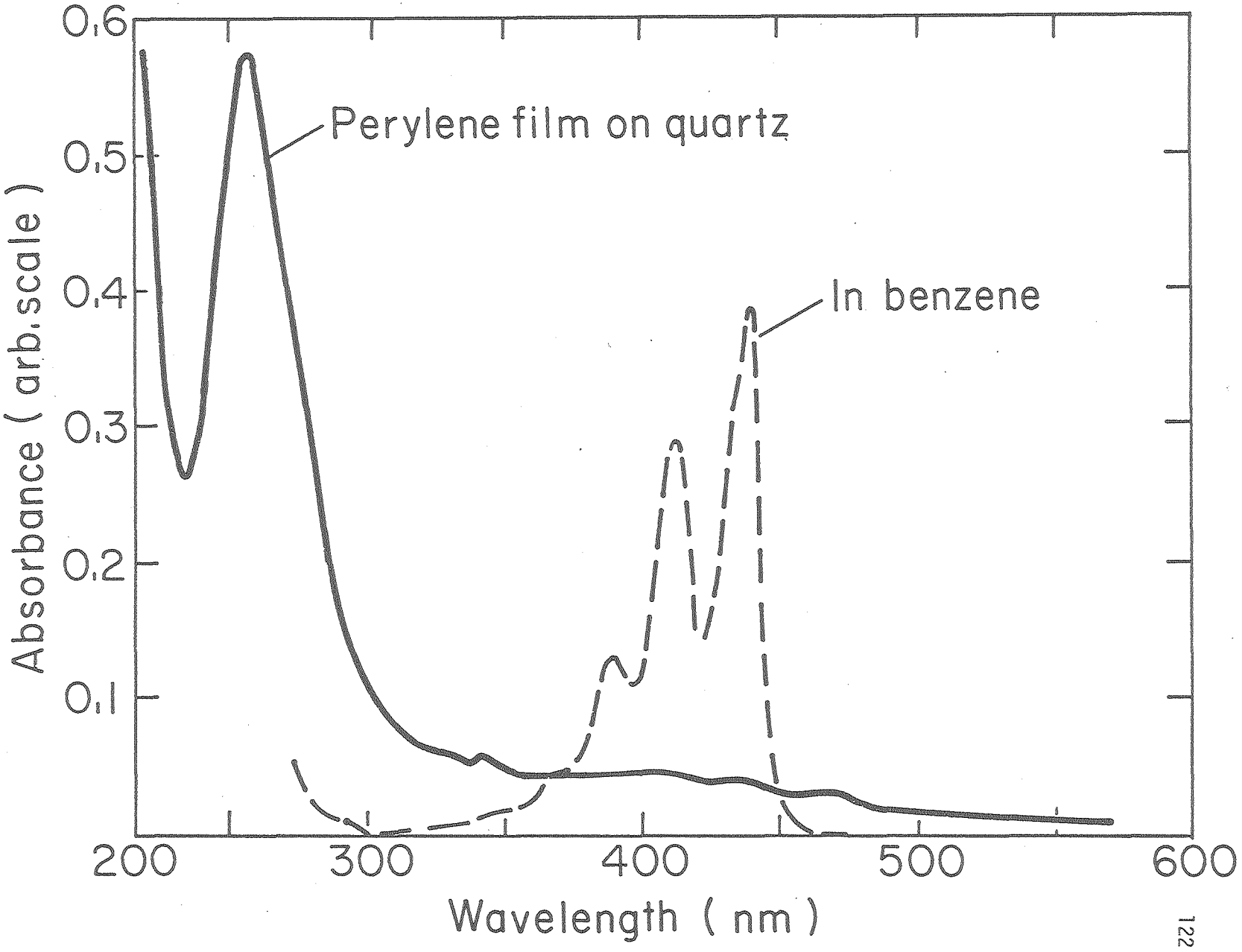

122

XBL797-4897

Figure 38. Quantum yield for a Au-perylene-merocyanine-TiO_2 cell plotted as a function of the thickness of the perylene layer. The thickness of the merocyanine was 200 angstroms.

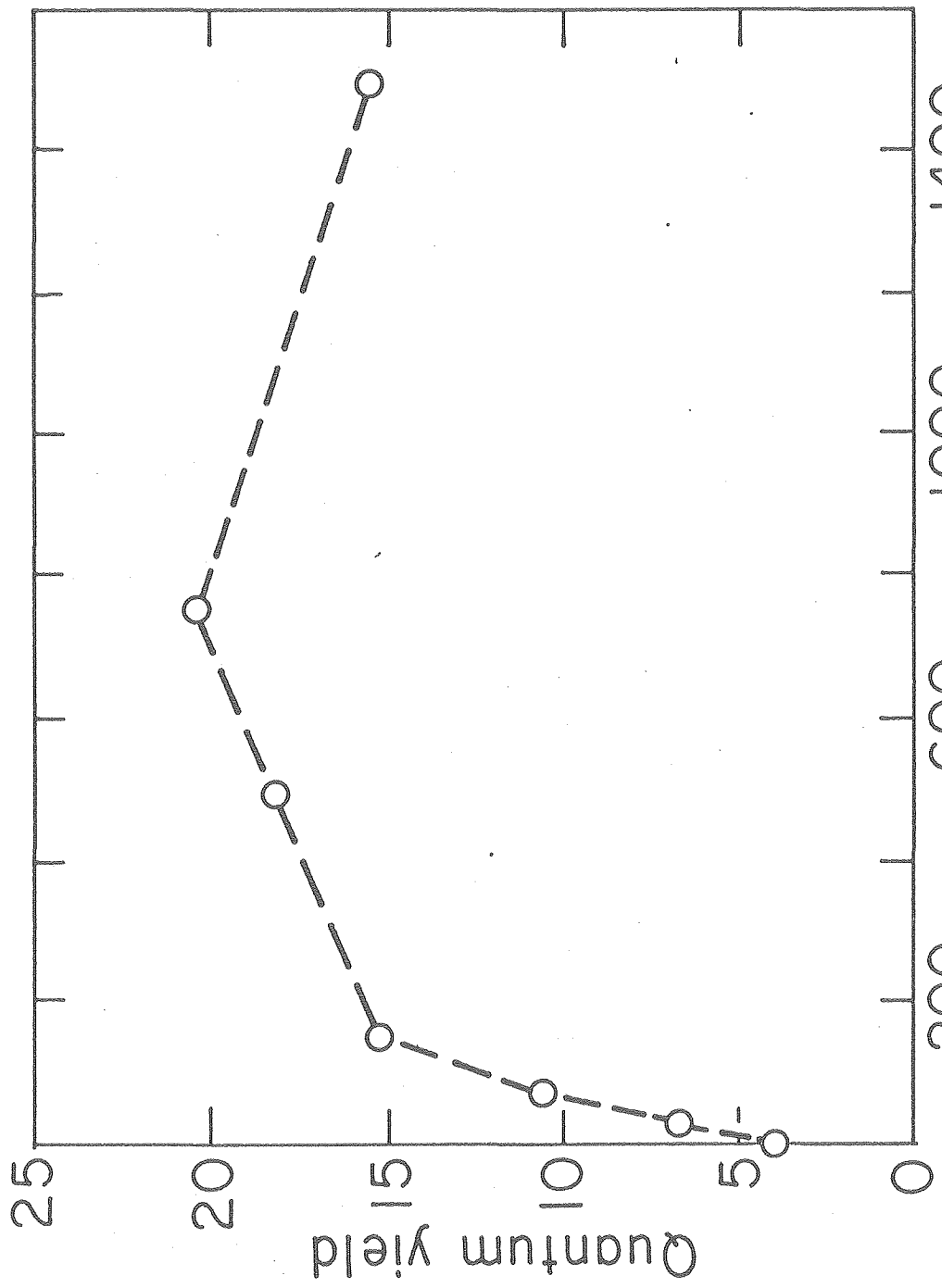
Quantum yield
25
20
15
10
5
0
200
600
1000
1400
Perylene thickness (angstroms)

XBL 797-4895

The quantum yield, measured as the number of electron per photon absorbed by the merocyanine, is plotted as a function of the thickness of the perylene layer for one particular TiO_2 crystal. As can be seen, the quantum yield increases approximately five fold to about 21% for a perylene layer of 750 angstroms. The slight decrease for a thickness of 1500 angstroms could perhaps be attributed to the oscillatory nature of the excitation lifetimes at larger distances or to the decreasing strength of the electric field across the dye layer with increasing thickness. The increases in quantum yield are even more striking considering the fact that the electric field at the junction decreases with increase in perylene thickness (see Fig. 28). If BQH is substituted for the perylene the efficiency drops dramatically and for a thickness of 600 angstroms is reduced by over two orders of magnitude, confirming the hypothesis of BQH being a blocking contact for holes from the merocyanine.

5.4. Properties of the Perylene-Merocyanine Junction

In order to determine the charge separating properties of the perylene-merocyanine interface we compared the action spectrum of a cell having a 1000 angstrom perylene film between a 2000 angstrom merocyanine film and the Au electrode with a similar cell without the perylene but with the same thickness of the merocyanine. With an absorbance of 2.0 and an exciton diffusion length of less than 100 angstroms, the charge carrier generation will be that due to exciton dissociation at the perylene-merocyanine interface. Fig. 39 shows the action spectra for the two cells recorded with light incident on the Au surface. Although the action spectra are similar in shape the local minimum near the peak of the absorption as well as the peaks on

Figure 39. Short circuit photocurrent action spectrum with light incident through the Au electrode for a cell with a 1000 angstrom perylene layer and a cell with no perylene. The action spectra were normalized to incident photon flux at each wavelength. The thickness of the merocyanine was 2000 angstroms.

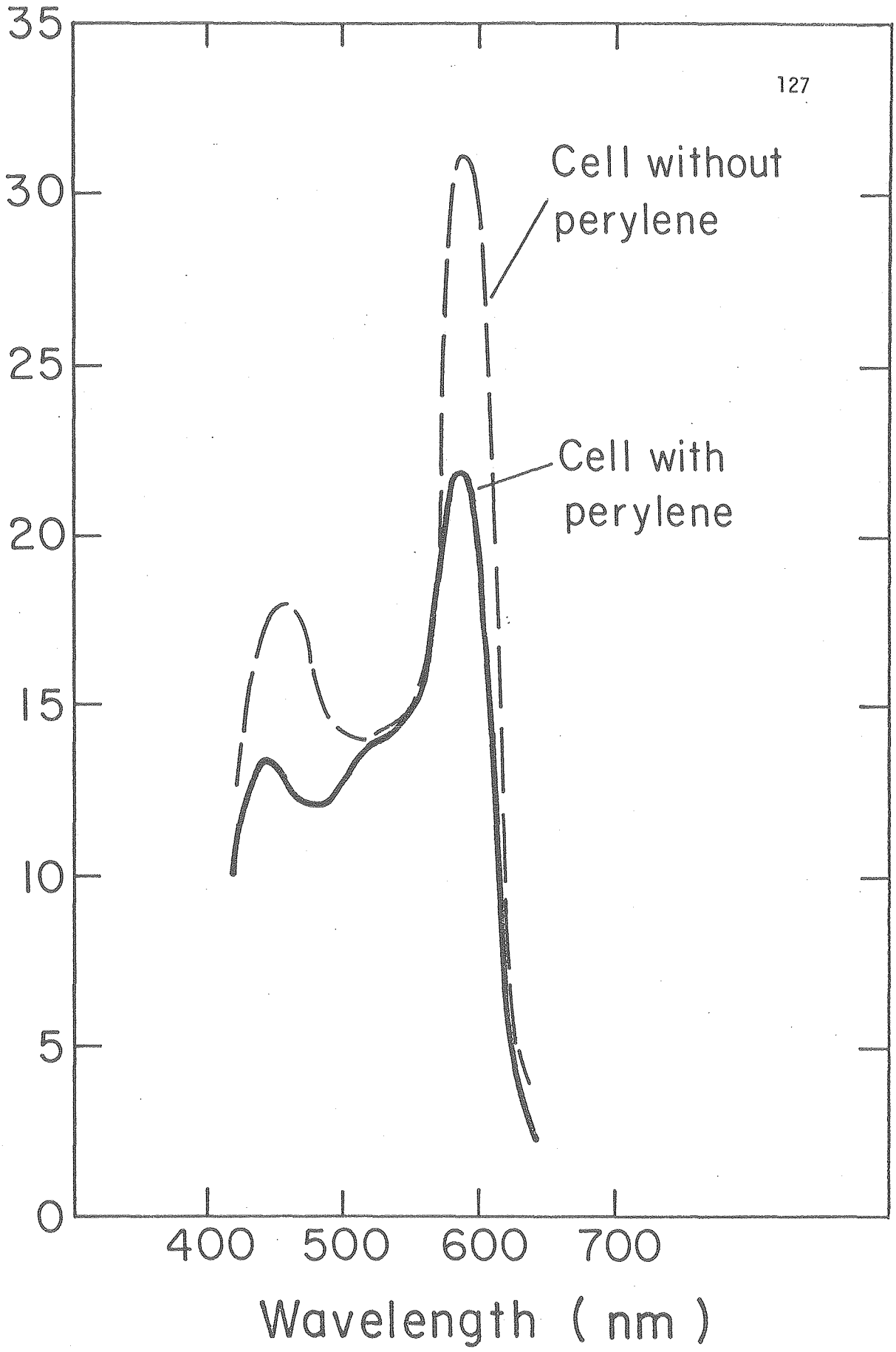
35
30
25
20
15
10
5
0
400
500
600
700
Wavelength (nm)
Cell without perylene
Cell with perylene

XBL797-4904

the shoulders are less pronounced in the cell with perylene. The local minimum was attributed to a quenching of the excitation near the Au-merocyanine interface. The quenching effect remaining at the perylene-merocyanine interface is probably due to the lack of an electric field at the interface strong enough to substantially overcome the coulombic forces resulting in geminate recombination. This effect appears to be independent of the ability of the interface to transmit photoproduced holes from the merocyanine phase.

This could have important implications for the concept of extending the absorption range of organic systems by employing multilayers of dye films. Unless by doping and other methods one is able to initiate charge separation in the bulk of the dye phase, the interfaces between the layers may well be too inefficient for serving that purpose. Dye mixing as well as doping may turn out to be the more fruitful approach.

Chapter 6

Conclusions

The experimental results presented in the preceding sections suggest that there are ways to utilize in photoelectric devices very thin films of organic pigments having a high electron transfer efficiency.

From the correspondence between the absorption spectra and the spectral response of photoconduction it is concluded that the primary step is the formation of singlet excitons by the absorption of light. This excitation energy may migrate through the film as an exciton, travelling an average distance of about 80 angstroms before it dissociates or is quenched. Only excitons reaching the merocyanine-TiO_2 interface actually result in charge carriers. The dissociation of the exciton leads to an electron being injected into the conduction band of the TiO_2 and a hole injected into the merocyanine. The hole then travels through the merocyanine to the Au electrode.

The charge carrier generation is presumed to result from a competition between the electric field at the interface and the coulombic attraction between the electron and the hole. The mechanism, we believe, is therefore the one described by Onsager's theory of geminate recombination adapted to the present one-dimensional system.

The Au-merocyanine interface is ineffective for charge carrier generation due to a quenching of the excitons in the immediate vicinity of the metal surface and possibly a reduced internal electric field near the interface.

As the current-voltage data and the temperature dependence of

the photoresponse and decay constant show, the films have a high density of both electron and hole traps in addition to recombination centers near the middle of the "band gap."

The capacitance-voltage data show that the junction region is depleted of mobile charge carriers. This implies that there is a virtual absence of band bending in the semiconductor and that the cell acts as a simple capacitor with the merocyanine as a dielectric.

If the semiconductor substrate is to be used as a separate absorber generating mobile charges by intrinsic excitation, the dark conductivity fo the dye phase must be increased to semiconductor conductivities in order to generate a depletion region in the semiconductor. This can be achieved by introducing the concepts of doping and charge transfer complexes. Our experiments with doping of the merocyanine with iodine show that in addition to this effect the photoconductivity of the merocyanine was increased as well. The accompanying increase in photovoltage is probably a result of larger photocurrent. Increases in photocurrent generation by as much as five fold relative to the undoped cells were recorded.

The mechanism of photocurrent generation appears to change upon doping with iodine. Analyses of the spectral response of photoconduction revealed a poor correspondence with the theory of exciton-surface processes. The concept of partial charge transfer has been used to explain doping effects in molecular solids and conductive polymers. Raman studies of iodine doped polyacetylene and phthalocyanines indicate the presence of I_3^- resulting in charge transfer. Photocarriers in doped films may result from collisions between

singlet excitons and the acceptor-hole complexes resulting in activation out of the bound states formed by the charge-transfer complex. Obviously, more thorough and controlled doping studies are necessary in order to establish the identity of the species and the nature of the mechanisms involved in doping of dye films.

Very thin films would be expected to be the most efficient for charge injection both because of the limitations on the exciton diffusion length in the case of undoped films and the increase in the electric field as the electrochemical potential difference is distributed over a shorter distance. For films of a few hundred angstroms, however, the excitation is partially quenched by the proximity of the metal surface. This quenching effect was investigated by sandwiching perylene layers of varying thickness between the merocyanine and the Au for cells with a 200 angstrom merocyanine film. We found a dramatic improvement in the photoconductive response as the merocyanine was removed from the metal surface resulting in increases of as much as five fold for a perylene thickness of 750 angstroms. This increase is even more remarkable as the electric field across the dye layer decreases sharply as the thickness of the perylene is increased.

What are the advantages of a cell of this type? The present goal of most attempts at overcoming the excessive costs of manufacturing solar cells is to convert to thin film processing. From a manufacturing point of view, organic materials seem to have a distinct advantage in that they are potentially cheap and relatively easy to apply in the form of thin films. They can have very high absorption coefficients, greater than $10^5 cm^{-1}$ for some pigments <u>versus</u> 10^3-10^4

cm^{-1} for silicon.[38] This allows the use of thinner films and therefore lower materials requirements.

A practical cell for solar energy conversion employing cells of the type discussed above would likely use as a substrate a semiconductor suitable for thin film production, e.g. CdS with intrinsic absorption in the high energy region of the solar spectrum. If this is coupled with a dye which absorbs in the red, one can cover essentially the whole solar spectrum. Since the dye will be transparent in the region where the semiconductor absorbs, light can be incident directly on the semiconductor depletion region without losses, resulting in highly efficient charge generation. Ring substitutions can produce dyes with wider absorption bands than the merocyanine centered any place in the spectrum that is required for optimum absorption. Some squarylium dyes are known to absorb as much as 50% of the solar spectrum.[10]

The advantages of a two- or multilevel system lie primarily in minimizing the thermal losses which inevitably result in one-band gap semiconductor junction devices. Additionally, as the above data show, there is also the possibility of manipulating energy levels in order to decrease the back current and thereby achieve higher output voltages. Open circuit voltages of as much as 1.1 volts have been achieved in some organic photovoltaic devices.[11]

There may also be other photoelectric device applications where narrow absorption and action spectra situated in various regions of the spectrum would be desirable.

Long term stability under ambient atmospheric conditions is an

important question which has to be addressed when constructing devices based on organic solids. Our research has not been concerned with long term stability beyond 2-3 days, although the merocyanine films did degrade over such a period. Careful encapsulation as well as employing polymerized compounds may be able to produce devices with the necessary longevity.

Our research to date shows that there are ways to utilize the optoelectronic properites of very thin organic films with a high probability of charge generation. It seems likely, therefore, that the low yields achieved to data for organic photovoltaic systems may be more due to device limitations that limitations intrinsic to organic materials as a class.

Appendix

Theory of Space-Charge-Limited Currents

Following Rose[46] and Mark and Helfrich[47] we derive the equations describing space-charge limited current flow in an insulator. When a sufficiently high voltage is applied across a specimen, the currents are no longer ohmic and no longer determined by carrier densities that were present in the absence of the applied voltage. The currents at sufficiently high fields are limited by a space charge of excess carriers injected by the electrode. We limit the present discussion to electron flow but the formalism is equally valid for hole currents.

We assume that the mobility of the electrons is independent of the electric field and that the density of trapping states per unit energy range below the conduction band can be described by a distribution of the following form,

$$h(E) = \left(\frac{H}{kT_c}\right)\exp(-E/kT_c) \qquad (A1)$$

where E is the energy measured downward from the bottom of the conduction band, H is the total trap density, and T_c is a characteristic temperature of the distribution. We assume for the moment that the temperature T = 0 and that all traps are filled to the quasi-fermi level E_f. We can then write for the negative space-charge at the position x from the cathode,

$$\zeta(x) = q\int_{E_f(x)}^{\infty}(H/kT_c)\exp(-E/kT_c) = qH\exp(-E_f(x)/kT_c) \qquad (A2)$$

where q is the elementary charge. The upper limit of the integral has been extended to infinity by assuming that the quasi-fermi level is sufficiently far removed from the fermi level of the neutral crys-

tal. If we now raise the temperature and assume a quasi-equilibrium for injected electrons has been established, then the new electron quasi-fermi level will not be significantly different from that defined by equation (A2) as long as $T_c > T$ and $\zeta(x) > \zeta_f(x)$, the density of free charge in the conduction band, i.e.

$$\zeta(x) = qN_c \exp(-E_f(x)/kT) \tag{A3}$$

where N_c is the effective density of states in the conduction band. From (A2) and (A3) we obtain

$$\zeta_f(x) = N_c q^{1-\ell} H^{-\ell} [\zeta(x)]^{\ell} \tag{A4}$$

where $\ell \equiv T_c/T$. The charge distribution is determined by Poisson's equation

$$\frac{d\xi(x)}{\ell x} = \frac{\zeta(x)}{\varepsilon\varepsilon_0} \tag{A5}$$

where ξ is the electric field strength and $\varepsilon\varepsilon_0$ the permittivity of the dielectric and free space respectively.

The total current density is given by

$$\mathcal{J}_t = \mu\zeta_f(x)\xi(x) \tag{A6}$$

where μ is the electron mobility. We show below that the diffusion current can be neglected in this case. Substituting (A4) and (A6) in (A5) we obtain

$$\frac{d\xi}{dx} = R[\xi(x)]^{-1/\ell} \tag{A7}$$

where $R \equiv (H/\varepsilon\varepsilon_0) q^{(\ell-1)/\ell} (\mathcal{J}_t/N_c\mu)^{1/\ell}$. With the boundary condition being $\xi(0) = 0$ at the cathode, the solution to (A7) is

$$\xi(x) = \left(\frac{\ell+1}{\ell} R\right)^{\ell/(\ell+1)} x^{\ell/(\ell+1)} \tag{A8}$$

Integrating (A8) from $x = 0$, the charge injecting electrode, to $x = d$, the thickness of the solid, we obtain for the potential across the

specimen

$$V = \left(\frac{\ell+1}{\ell}R\right)^{\ell/(\ell+1)}\left(\frac{\ell+1}{2\ell+1}\right)d^{(2\ell+1)/(\ell+1)} \tag{A9}$$

Substituting for R and solving for j_t, we have

$$\mathcal{J}_t = N_c\mu q^{1-\ell}\left(\frac{\varepsilon\varepsilon_0}{H(\ell+1)}\right)^{\ell}\left(\frac{2\ell+1}{\ell+1}\right)^{\ell+1}\frac{V^{\ell+1}}{d^{2\ell+1}} \tag{A10}$$

as given in the text. If no traps are present the problem is limited to solving

$$\frac{d\xi}{dx} = \frac{\zeta_f(x)}{\varepsilon\varepsilon_0} \tag{A11}$$

and

$$\mathcal{J}_t = \mu\zeta_f(x)\xi(x) \tag{A12}$$

which gives Child's Law for the current density in a trap free solid,

$$\mathcal{J}_c = (9/8)\mu\varepsilon\varepsilon_0\frac{V^2}{d^3} \tag{A13}$$

By setting $j_c = j_t$ we obtain the transition voltage where all the traps are filled and the current assumes the Child's Law behavior. Solving for the transition voltage we obtain

$$V_{t-c} = \frac{qd^2}{\varepsilon\varepsilon_0}\left[\frac{9}{8}\frac{H^{\ell}}{N_c}\left(\frac{\ell+1}{\ell}\right)^{\ell}\left(\frac{\ell+1}{2\ell+1}\right)^{\ell+1}\right]^{1/(\ell-1)} \tag{A14}$$

Diffusion Current

In deriving equation (A7) we ignored the diffusion current in writing equation (A6) for the total current. We now demonstrate that the assumption of negligible diffusion current is valid in our particular example. Consider the following expressions for the two current components,

$$\mathcal{J}_{field} = \mu\zeta_f\xi$$

$$\mathcal{J}_{diff.} = -D\frac{d\zeta_f}{dx}$$

where j_{field} is the field driven current, $j_{diff.}$ the diffusion controlled current, and D the diffusivity for electron. Using the Einstein relation, $D = \mu kT/q$ we obtain the ratio:

$$\frac{\mathcal{J}_{diff.}}{\mathcal{J}_{field}} = \frac{kT}{q\xi}\frac{1}{\zeta_f}\frac{d\zeta_f}{dx}$$

From equations (A4), (A5), (A7), and (A8) we find that

$$\zeta_f(x) \sim x^{-\ell/(\ell+1)}$$

We then have

$$\frac{1}{\zeta_f(x)}\frac{d\zeta_f}{dx} = -\frac{\ell}{\ell+1}\frac{1}{x}$$

and $$\frac{\mathcal{J}_{diff.}}{\mathcal{J}_{field}} = \frac{kT}{q\xi}\frac{\ell}{\ell+1}\frac{1}{x}$$

We see that the diffusion current dominates in the vicinity of the cathode. Using our data from the dark current-voltage measurements, we can get an estimate of the range of the diffusion dominated current. For an applied voltage of 1 volt over 1000 angstroms, or a field strength of $\xi \sim 10^{-3}\text{V-Å}^{-1}$ or about 10^{5}V-cm^{-1}, we find

$$\frac{\mathcal{J}_{diff.}}{\mathcal{J}_{field}} \sim \frac{25}{x(\text{Å})}$$

i.e. beyond about 25 angstroms from the cathode the current is field dominated and neglecting the diffusion current is justified.

REFERENCES

1. A. K. Ghosh and T. Feng, J. Appl. Phys. 44, 2781 (1973).
2. C. W. Tang and A. C. Albrecht, (a) Mol. Cryst. Liq. Cryst. 25, 53 (1974); (b) J. Chem. Phys. 62, 2139 (1975); (c) J. Chem. Phys. 63, 953 (1975); (d) Nature 254, 507 (1975).
3. L. E. Lyons and O. M. G. Newman, Aust. J. Chem. 24, 13 (1971).
4. A. K. Ghosh, D. L. Morel, T. Feng, R. S. Shaw, and C. A. Rowe, J. Appl. Phys. 45, 239 (1974).
5. M. I. Fedorov and V. A. Benderskii, (a) Sov. Phys. Semicond. 2, 580 (1968); (b) Sov. Phys. Semicond. 4, 1198 (1971); (c) Sov. Phys. Semicond. 4, 1720 (1971).
6. V. Y. Merritt and H. J. Hovel, Appl. Phys. Lett. 29, 414 (1976).
7. V. Y. Merritt, IBM J. Res. Develop. 22, 353 (1978).
8. F. J. Kampas and M. Gouterman, J. Phys. Chem. 81, 690 (1977).
9. F. R. Fan and L. R. Faulkner, (a) J. Chem. Phys. 69, 3334 (1978); (b) J. Chem. Phys. 69, 3341 (1978).
10. D. L. Morel, A. K. Ghosh, T. Feng, E. L. Stogryn, P. E. Purwin, and C. Fishman, Appl. Phys. Lett. 32, 495 (1978).
11. A. K. Ghosh and T. Feng, J. Appl. Phys. 49, 5982 (1978).
12. C. Mees and T. James, eds., The Theory of the Photographic Process (Macmillan: New York, 1966).
13. R. C. Nelson, J. Phys. Chem. 71, 2517 (1967).
14. R. C. Nelson, J. Opt. Soc. Am. 51, 1182 (1961).
15. E. Inoue, H. Kokado, and U. Yamaguchi, J. Phys. Chem. 67, 767 (1965).

16. H. Meier, Spectral Sensitization (The Focal Press, Ltd.: London: 1968).

17. H. Tributsch and H. Gerischer, Ber. Bunsenges. Phys. Chem. 73, 850 (1969).

18. H. Gerischer, Surface Sci. 13, 265 (1969).

19. L. W. James, Proceedings of the International Electron Devices Meeting, Washington, D. C., 1975.

20. R. T. Ross and T. L. Hsiao, J. Appl. Phys. 48, 4783 (1977).

21. J. R. Bolton, Science 202, 705 (1978).

22. D. Cronemeyer, Phys. Rev. 113, 1222 (1959).

23. E. C. Dutoit, R. L. Van Meirhaeghe, F. Cardon, and W. P. Gomes, Ber. Bunsenges. Phys. Chem. 79, 1206 (1975).

24. C. Kittel, Introduction to Solid State Physics, 4th ed. (John Wiley & Sons: New York, 1971).

25. R. S. Knox, Theory of Excitons, Solid State Physics Series, Supplement 5, F. Seitz and D. Turnbull, eds. (Academic Press: New York, 1963).

26. H. Inokuchi and Y. Maruyama, Photoconductivity and Related Phenomena, J. Mort and D. M. Pai, eds. (Elsevier Scientific: New York, 1976).

27. J. W. Stekette and J. de Jonge, Philips Res. Rep. 17, 363 (1962).

28. B. J. Mulder, Philips Res. Rep. Supplement 4 (1968).

29. M. Silver, D. Olness, M. Swicord, and R. C. Jarnagin, Phys. Rev. Lett. 10, 12 (1963).

30. V. A. Benderskii, M. I. Fedorov, and N. N. Usov, Doklady Akad. Nauk. SSSR 183, 1117 (1968).

31. J. Sworakowski, Mol. Cryst. Liq. Cryst. 11, 1 (1970).

32. H. Meier, Die Photochemie der Organischen Farbstoffe (Springer Verlag: Berlin, 1963).

33. F. J. Kampas, K. Yamashita, C. K. Chang, and J. Fajer, Proceedings of the Third Solar Photochemistry Research Conference, Asilomar, 1979.

34. J. Singh and H. Baessler, Phys. Stat. Sol. (b) 63, 425 (1974).

35. L. Onsager, Phys. Rev. 54, 554 (1938).

36. M. A. Butler and D. S. Ginley, J. Electrochem. Soc. 125, 228 (1978).

37. CRC Handbook of Chemistry and Physics, 52nd edition (1971).

38. H. J. Hovel, Solar Cells, Vol. 11 in the series Semiconductors and Semimetals, R. K. Willardson and A. C. Beer, eds. (Academic Press: New York, 1975).

39. J. J. Wysocki, RCA Review 22, 57 (1961).

40. S. M. Sze, Physics of Semiconductor Devices (Wiley: New York, 1969).

41. A. J. Twarowski and A. C. Albrecht, J. Chem. Phys. 70, 2255 (1979).

42. M. Pope and H. Kallmann, Disc. of the Faraday Soc. 51, 7 (1971).

43. H. Scher, Photoconductivity and Related Phenomena, J. Mort and D. M. Pai, eds. (Elsevier Scientific: New York, 1976), p. 72.

44. F. Gutman and L. E. Lyons, Organic Semiconductors (John Wiley & Sons: New York, 1967).

45. H. Meier, Organic Semiconductors (Verlag Chemie: Weinheim, 1974).

46. A. Rose, Concepts in Photoconductivity and Allied Problems (Interscience: New York, 1963).

47. P. Mark and W. Helfrich, J. Appl. Phys. 33, 205 (1962).

48. H. Baessler, G. Hermann, N. Riehl, and G. Vaubel, J. Phys. Chem.

Solids 30, 1579 (1969).

49. A. Sussman, J. Appl. Phys. 38, 2738 (1967).

50. J. M. Thomas, J. O. Williams, and L. M. Turyon, Trans. Faraday Soc. 64, 2505 (1968).

51. W. E. Dahlke and S. M. Sze, Solid State Electronics 10, 865 (1967).

52. H. K. Henisch, Electroluminescence (Macmillan: New York, 1962).

53. A. Goetzberger, B. McDonale, R. H. Haitz, and R. M. Scarlet, J. Appl. Phys, 34, 1591 (1963).

54. B. Rosenberg, Disc. Faraday Soc. 51, 190 (1971).

55. R. H. Bube, W. M. Grove, and R. K. Murchinson, J. Appl. Phys. 38, 3515 (1967).

56. G. Tollin, D. R. Kearns, and M. Calvin, J. Chem. Phys. 32, 1013 (1960).

57. G. N. Meshkova, Sov. Phys. Semicond. 2, 1244 (1969).

58. R. H. Bube, Physical Chemistry: An Advanced Treatise, Vol. 10, H. Eyring, D. Henderson, and W. Jost eds. (Academic Press: New York, 1970), p. 515.

59. A. Rose, RCA Review 12, 362 (1951).

60. H. E. Fritsch and J. R. Huber, Ber. Bunsenges. Phys. Chem. 83, 64 (1979).

61. H. Meier, Z. Phys. Chem. 208, 340 (1958).

62. H. R. Bube, J. Appl. Phys. 34, 3309 (1963).

63. D. R. Kearns and M. Calvin, J. Chem. Phys. 29, 950 (1958).

64. D. R. Kearns, G. Tollin, and M. Calvin, J. Chem. Phys. 32, 1020 (1960).

65. H. Akamatu, H. Inokuchi, and Y. Matsunaga, (a) Nature 173, 108 (1954); (b) Bull. Chem. Soc. Japan 29, 213 (1956).

66. J. L. Peterson, C. S. Schramm, D. R. Stojakovic, B. M. Hoffmann, and T. J. Marks, J. Am. Chem. Soc. 99, 286 (1977).

67. W. Mehl and N. E. Wolff, J. Phys. Chem. Solids 25, 1221 (1964).

68. L. B. Coleman, M. J. Cohen, D. J. Sandman, F. G. Yamagishi, A. F. Garito, and A. J. Heeger, Solid State Commun. 12, 1125 (1973).

69. E. M. Engler, R. A. Craven, Y. Tomkiewicz, and B. A. Scott, J. Chem. Soc. Chem. Commun., 337 (1976).

70. C. K. Chiang, Y. W. Park, A. J. Heeger, H. Shirakawa, E. J. Louis, and A. G. MacDiarmid, J. Chem. Phys. 69, 5098 (1978).

71. I. B. Goldberg, H. R. Crowe, P. R. Newman, A. J. Heeger, and A. G. MacDiarmid, J. Chem. Phys. 70, 1132 (1979).

72. K. H. Drexhage, H. Kuhn, and F. P. Schafer, Ber. Bunsenges. Phys. Chem. 72, 329 (1968).

73. K. H. Drexhage, H. Fleck, H. Kuhn, F. P. Schafer, and W. Sperling, Ber. Bunsenges. Phys. Chem. 20, 1179 (1966).

74. K. H. Drexhage, J. Luminescence 1/2, 693 (1970).

75. R. R. Chance, A. Prock, and R. Silbey, (a) J. Chem. Phys. 62, 2245 (1975); (b) Ibid. 65, 2527 (1976); (c) Adv. Chem. Phys. 37, 1 (1978).

76. A. Sommerfeld, (a) Ann. Phys. Leipz. 28, 665 (1909); (b) Ibid. 81, 1135 (1926).

77. A. Sommerfeld, Partial Differential Equations of Physics (Academic Press: New York, 1949).

78. H. Morawitz and M. R. Philpott, Phys. Rev. B10, 4863 (1974).

79. M. R. Philpott, J. Chem. Phys. 62, 1812 (1975).

80. H. Killesreiter and H. Baessler, Phys. Stat. Sol. (b) 51, 657 (1972).

81. H. Killesreiter, J. Luminscence 12/13, 857 (1976).

82. B. Korsch, F. Illig, H. J. Gaehrs, and B. Tesche, Phys. Stat. Sol. (a) 33, 461 (1976).

83. Y. Kamura, I. Shirotani, K. Ohno, K. Seki, H. Inokuchi, Bull. Chem. Soc. Japan 49, 418 (1976).

TECHNICAL INFORMATION DEPARTMENT
LAWRENCE BERKELEY LABORATORY
UNIVERSITY OF CALIFORNIA
BERKELEY, CALIFORNIA 94720